



CHALMERS
UNIVERSITY OF TECHNOLOGY



Analyzing the Simplified Model of the DFIG Wind Turbine Under Short Circuit Faults

Master's Thesis in M.Sc. of Electric Power Engineering

KASRA HEIDARZAD PAHLAVIANI

Department of Electrical Engineering
CHALMERS UNIVERSITY OF TECHNOLOGY
Gothenburg, Sweden 2018

MASTER'S THESIS 2018:09:07

Analyzing the Simplified Model of the DFIG Wind Turbine Under Short Circuit Faults

KASRA HEIDARZAD PAHLAVIANI



Department of Electrical Engineering
Division of Electric Power Engineering
KASRA HEIDARZAD PAHLAVIANI
CHALMERS UNIVERSITY OF TECHNOLOGY
Gothenburg, Sweden 2018

Analyzing the Simplified Model of the DFIG Wind Turbine Under Short Circuit Faults

KASRA HEIDARZAD PAHLAVIANI

© KASRA HEIDARZAD PAHLAVIANI, 2018.

Supervisor: Assistant Professor Tarik Abdulahovic
Examiner: Professor Ola Carlson

Master's Thesis 2018:08:07
Department of Electrical Engineering
Division of Electric Power Engineering
Chalmers University of Technology
SE-412 96 Gothenburg
Telephone +46 31 772 1000

Cover: <https://pcs-instruments.com/wp-content/uploads/2016/07/Wind-Medium1.jpg>.

Typeset in L^AT_EX
Printed by Chalmers Reproservice
Gothenburg, Sweden 2018

Dedicated to my dear family.

Analyzing the Simplified Model of the DFIG Wind Turbine Under Short Circuit Faults

KASRA HEIDARZAD PAHLAVIANI

Department of Electrical Engineering

Chalmers University of Technology

Abstract

The Doubly Fed Induction Generator Wind Turbine is one of the most popular types of WT in order to convert wind's kinetic energy into electricity. The ability to use it when the wind speed is variable as well as having high efficiency and control can be considered as the main advantages of the Doubly Fed Induction Generator Wind Turbine. On the other hand, demanding higher costs and more complexity, specifically in terms of the control systems, in comparison with the fixed-speed model will be the disadvantages of the Doubly Fed Induction Generator Wind Turbine.

The objective of this thesis is to investigate the behavior of the simplified model of the Doubly Fed Induction Generator Wind Turbine under different types of the SC faults. The other vital factor that plays a key role in the model's behavior is the amplitude of the fault impedance. As a result, the behavior's of the detailed and simplified Doubly Fed Induction Generator Wind Turbine under same fault conditions, when the fault time and the amplitude of the fault impedance are equal, will be compared with each other.

Sequentially, some improved models for simplified types will be executed in order to use in some specific cases that the behavior of the simple model is not acceptable. The main object in the comparison process is the I_{fmax} value of the simplified model that should be close to its values in the detailed Doubly Fed Induction Generator model during fault analysis.

As a result, the behaviors' of the different types of the simplified models can be compared with the main detailed model and the best one during different fault conditions can be found.

Finally, the result of this thesis can be used to propagate to the wind park with many radials. The analysis of fault stability in the huge wind farm can be done much faster in comparison with the detailed model which consists of more controller components. The main important point that should be considered is that this simplified model cannot be implemented in reality and only can be used for stability analysis.

Keywords: Wind power, Wind turbine, Doubly-Fed Induction Generator (DFIG), Wind turbine, Short circuit fault.

Acknowledgements

My sincere gratitude goes to my dear supervisor Assistant Prof. Tarik Abdulahovic for his invaluable guidance and support throughout the course of this project. Thank you very much for your constant support and endless effort through the challenging times encountered.

Also, I want to address my gratitude examiner Prof. Ola Carlson for the fruitful discussions that provided substance to this thesis.

Special thanks go to my lecturers Prof. Massimo Bongiorno, Associate Prof. Peiyuan Chen, Dr. Ehsan Behrouzian and my dear friend Dr. Amir Parastar for their great guidance and supports during this time.

Ultimately, I would like to thank my dear family for always being my side and believing in me.

KASRA HEIDARZAD PAHLAVIANI,
Gothenburg, Sweden
September 2018

List of Abbreviations

MW : Mega Watt
GW : Giga Watt
EU : the European Union
WPP : Wind Power Plant
WT : Wind Turbine
DFIG : Doubly Fed Induction Generator
SC : Short Circuit
SLG : Single Line to Ground
DLG : Double Line to Ground
IG : Induction Generator
IM : Induction Machine
SG : Synchronous Generator
AM : Asynchronous Machine
PF : Power Factor
OC : Over Current
LLL : Line to Line to Line
LLLG : Line to Line to Line to Ground
LL : Line to Line
LLG : Line to Line to Ground

Contents

List of Figures	xv
List of Tables	xvii
1 Introduction	1
1.1 Background	1
1.2 Aim	2
1.3 Problem Description	2
2 Wind Energy	5
2.1 Properties of the Wind	5
2.2 Conversion of the Wind Energy	5
2.3 Types of WT	5
2.3.1 Fixed-Speed WT	6
2.3.2 Variable Speed WT	6
2.3.2.1 DFIG WT	7
2.3.2.2 Full-Converter WT	8
3 Induction Machine	9
3.1 Overview	9
3.2 Constructional Features of the IM	10
3.2.1 Squirrel-cage Rotor Winding	10
3.2.2 Wound Rotor Winding	10
3.3 External Variable Resistance Circuit in the Wound Rotor IM	10
3.4 Equivalent Circuit of the IM	11
3.5 Dynamic Models and Equations of the IM	12
4 Doubly Fed Induction Generator Wind Turbine	15
4.1 Overview	15
4.2 Principle Operation	16
4.3 Protective Circuit	16
5 The Simplified DFIG WT Model	19
5.1 Designing the Simplified Model	19
5.2 Calculating the Parameters	19
5.3 The Simplified Model	19
5.4 The Phasor Diagram Method	20

6	Short Circuit Fault	23
6.1	Fault Definition	23
6.2	SC Fault	23
6.2.0.1	Symmetrical SC Fault	23
6.2.0.2	Unsymmetrical SC Fault	24
7	Simulation of Detailed and Simplified Models	27
7.1	The DFIG WT behaviors Under SC Faults	27
7.1.1	Models in Steady-State Conditions	27
7.1.2	Models Under Symmetrical SC Faults	28
7.1.2.1	Under LLLG SC Fault	29
7.1.3	Models Under Unsymmetrical SC Faults	31
7.1.3.1	Under SLG SC Fault	31
7.1.3.2	Under LL SC Fault	34
7.1.3.3	Under LLG SC Fault	37
8	Simulation of the Detailed and Improved Simplified Models of the DFIG WT, Under SC Faults	43
8.0.1	Improved Simplified Model	43
8.0.2	Models Under Symmetrical SC Faults	44
8.0.2.1	Under LLLG SC Fault	44
8.0.3	Models Under Unsymmetrical SC Faults	50
8.0.3.1	Under SLG SC Fault	50
8.0.3.2	Under LL SC Fault	56
8.0.3.3	Under LLG SC Fault	62
9	Result	69
9.1	Comparing Detailed and Simplified Models of DFIG WT	69
9.2	Improved Simplified Type 1 with Different Values of R_{ex}	70
9.3	Improved Simplified Type 2 with Different Values of R_{ex}	70
9.4	Ultimate Results	71
9.4.1	Case 1 : for low value impedance, like $Z_f = 10^{-15} \Omega$	71
9.4.2	Case 2 : for medium value impedance, like $Z_f = 10^{-5} \Omega$	71
9.4.3	Case 2 : for high value impedance, like $Z_f = 10^{-2} \Omega$	71
9.5	Summary of the Results	72
10	Conclusion	73
11	Future Work	75
	Bibliography	77
A	Appendix	I
A.1	The Per Unit System	I
B	Appendix	III
B.1	Transformations for three-phase Systems	III
B.1.1	Introduction	III

B.1.2	Transformation of three-phase quantities to vectors	III
B.1.2.1	Transformation between fixed and rotating coordi- nate systems	IV
C	Appendix	VII
C.1	MATLAB Files	VII
C.1.1	m-file	VII
C.1.2	Simulink	VIII

List of Figures

2.1	Fixed-Speed WT schematic.	6
2.2	DFIG WT schematic.	7
2.3	Full Converter WT schematic.	8
3.1	The torque-speed characteristics of the IM [10].	9
3.2	The torque-speed characteristics of the induction motor with the external variable resistance circuit in both motor and generator modes. [9].	11
3.3	The per-phase equivalent circuit of the IM.	12
3.4	The dynamic equivalent circuit of the T-model of IM.	12
3.5	The dynamic equivalent circuit of the Inverse- Γ -model of IM.	13
4.1	DFIG WT schematic.	15
4.2	The Detailed type of the DFIG WT in PSCAD.	16
5.1	The Simplified type of the DFIG WT in the PSCAD/EMTDC.	20
5.2	The circuit diagram of the Simplified type of the DFIG WT.	20
5.3	The Phasor Diagram of the IM with extra resistance and capacitor on the rotor side.	21
5.4	The Phasor Diagram of the IM with extra resistance and capacitor on the rotor side after increasing the capacitor value.	21
5.5	The Phasor Diagram of the IM with extra resistance and capacitor on the rotor side after increasing the resistance value.	22
6.1	LLLG and LLL SC fault.	24
6.2	SLG, LL and LLG SC fault.	25
7.1	The blue curves belong to the detailed and the red ones belong to the simplified type during the steady-state.	28
7.2	Case 1 : $Z_f = 10^{-15} \Omega$	29
7.3	Case 2 : $Z_f = 10^{-5} \Omega$	30
7.4	Case 3 : $Z_f = 10^{-2} \Omega$	31
7.5	Case 1 : $Z_f = 10^{-15} \Omega$	32
7.6	Case 2 : $Z_f = 10^{-5} \Omega$	33
7.7	Case 3 : $Z_f = 10^{-2} \Omega$	34
7.8	Case 1 : $Z_f = 10^{-15} \Omega$	35
7.9	Case 2 : $Z_f = 10^{-5} \Omega$	36
7.10	Case 3 : $Z_f = 10^{-2} \Omega$	37

7.11	Case 1 : $Z_f = 10^{-15} \Omega$	38
7.12	Case 2 : $Z_f = 10^{-5} \Omega$	39
7.13	Case 3 : $Z_f = 10^{-2} \Omega$	40
8.1	Improved Simplified Model Type 1	43
8.2	Improved Simplified Model Type 2	44
8.3	Improved type 1 & 2, Case 1 : $Z_f = 10^{-15} \Omega$ & $R_{ex} = 0.125 \Omega$	45
8.4	Improved type 1 & 2, Case 2 : $Z_f = 10^{-15} \Omega$ & $R_{ex} = 1.25 \Omega$	45
8.5	Improved type 1 & 2, Case 3 : $Z_f = 10^{-15} \Omega$ & $R_{ex} = 0.00125 \Omega$. . .	46
8.6	Improved type 1 & 2, Case 4 : $Z_f = 10^{-5} \Omega$ & $R_{ex} = 0.125 \Omega$	47
8.7	Improved type 1 & 2, Case 5 : $Z_f = 10^{-5} \Omega$ & $R_{ex} = 1.25 \Omega$	47
8.8	Improved type 1 & 2, Case 6 : $Z_f = 10^{-5} \Omega$ & $R_{ex} = 0.00125 \Omega$. . .	48
8.9	Improved type 1 & 2, Case 7 : $Z_f = 10^{-2} \Omega$ & $R_{ex} = 0.125 \Omega$	49
8.10	Improved type 1 & 2, Case 8 : $Z_f = 10^{-2} \Omega$ & $R_{ex} = 1.25 \Omega$	49
8.11	Improved type 1 & 2, Case 9 : $Z_f = 10^{-2} \Omega$ & $R_{ex} = 0.00125 \Omega$. . .	50
8.12	Improved type 1 & 2, Case 1 : $Z_f = 10^{-15} \Omega$ & $R_{ex} = 0.125 \Omega$	51
8.13	Improved type 1 & 2, Case 2 : $Z_f = 10^{-15} \Omega$ & $R_{ex} = 1.25 \Omega$	51
8.14	Improved type 1 & 2, Case 3 : $Z_f = 10^{-15} \Omega$ & $R_{ex} = 0.00125 \Omega$. . .	52
8.15	Improved type 1 & 2, Case 4 : $Z_f = 10^{-5} \Omega$ & $R_{ex} = 0.125 \Omega$	53
8.16	Improved type 1 & 2, Case 5 : $Z_f = 10^{-5} \Omega$ & $R_{ex} = 1.25 \Omega$	53
8.17	Improved type 1 & 2, Case 6 : $Z_f = 10^{-5} \Omega$ & $R_{ex} = 0.00125 \Omega$	54
8.18	Improved type 1 & 2, Case 7 : $Z_f = 10^{-2} \Omega$ & $R_{ex} = 0.125 \Omega$	54
8.19	Improved type 1 & 2, Case 8 : $Z_f = 10^{-2} \Omega$ & $R_{ex} = 1.25 \Omega$	55
8.20	Improved type 1 & 2, Case 9 : $Z_f = 10^{-2} \Omega$ & $R_{ex} = 0.00125 \Omega$. . .	55
8.21	Improved type 1 & 2, Case 1 : $Z_f = 10^{-15} \Omega$ & $R_{ex} = 0.125 \Omega$	56
8.22	Improved type 1 & 2, Case 2 : $Z_f = 10^{-15} \Omega$ & $R_{ex} = 1.25 \Omega$	57
8.23	Improved type 1 & 2, Case 3 : $Z_f = 10^{-15} \Omega$ & $R_{ex} = 0.00125 \Omega$. . .	57
8.24	Improved type 1 & 2, Case 4 : $Z_f = 10^{-5} \Omega$ & $R_{ex} = 0.125 \Omega$	58
8.25	Improved type 1 & 2, Case 5 : $Z_f = 10^{-5} \Omega$ & $R_{ex} = 1.25 \Omega$	59
8.26	Improved type 1 & 2, Case 6 : $Z_f = 10^{-5} \Omega$ & $R_{ex} = 0.00125 \Omega$	59
8.27	Improved type 1 & 2, Case 7 : $Z_f = 10^{-2} \Omega$ & $R_{ex} = 0.125 \Omega$	60
8.28	Improved type 1 & 2, Case 8 : $Z_f = 10^{-2} \Omega$ & $R_{ex} = 1.25 \Omega$	61
8.29	Improved type 1 & 2, Case 9 : $Z_f = 10^{-2} \Omega$ & $R_{ex} = 0.00125 \Omega$. . .	61
8.30	Improved type 1 & 2, Case 1 : $Z_f = 10^{-15} \Omega$ & $R_{ex} = 0.125 \Omega$	62
8.31	Improved type 2 & 2, Case 1 : $Z_f = 10^{-15} \Omega$ & $R_{ex} = 1.25 \Omega$	63
8.32	Improved type 1 & 2, Case 3 : $Z_f = 10^{-15} \Omega$ & $R_{ex} = 0.00125 \Omega$. . .	63
8.33	Improved type 1 & 2, Case 4 : $Z_f = 10^{-5} \Omega$ & $R_{ex} = 0.125 \Omega$	64
8.34	Improved type 1 & 2, Case 5 : $Z_f = 10^{-5} \Omega$ & $R_{ex} = 1.25 \Omega$	65
8.35	Improved type 1 & 2, Case 6 : $Z_f = 10^{-5} \Omega$ & $R_{ex} = 0.00125 \Omega$. . .	65
8.36	Improved type 1 & 2, Case 7 : $Z_f = 10^{-2} \Omega$ & $R_{ex} = 0.125 \Omega$	66
8.37	Improved type 1 & 2, Case 8 : $Z_f = 10^{-2} \Omega$ & $R_{ex} = 1.25 \Omega$	67
8.38	Improved type 1 & 2, Case 9 : $Z_f = 10^{-2} \Omega$ & $R_{ex} = 0.00125 \Omega$. . .	67
B.1	$\alpha\beta$ and dq vectors frame.	IV
C.1	VII
C.2	VIII

List of Tables

7.1	The simplified type behaviors	41
9.1	Detailed Model of DFIG WT.	69
9.2	Simplified Model of DFIG WT.	69
9.3	Improved Simplified Type 1 with $R_{ex} = 0.125 \Omega$	70
9.4	Improved Simplified Type 1 with $R_{ex} = 1.25 \Omega$	70
9.5	Improved Simplified Type 1 with $R_{ex} = 0.00125 \Omega$	70
9.6	Improved Simplified Type 2 with $R_{ex} = 0.125 \Omega$	70
9.7	Improved Simplified Type 2 with $R_{ex} = 1.25 \Omega$	71
9.8	Improved Simplified Type 2 with $R_{ex} = 0.00125 \Omega$	71

1

Introduction

In recent decades, sustainable power production systems have been developed significantly and begun to supersede fossil fuel power plants for electricity generating as a certain replacement in some countries. The great feature of sustainable energies is being environmentally friendly. Undoubtedly, one of the main renewable energy resources that can be used to generate electricity in the large dimensions is the wind power. For instance, in 2017 in Europe has been installed 16.8 GW (15.6 GW in the EU) of gross additional wind power capacity which is the highest record on installations, annually. The a total net capacity which was installed made the wind energy the second largest type of power generation in Europe with of 168.7 GW. This form of energy is ranked after the gas installations [1]. So, today a massive expansion of wind parks are going around the world.

Obviously, as same as the other power systems, Wind Power Plants demanded specific protection systems in order to guarantee their safe and reliable operations. Besides, surviving them from inevitable phenomena, such as different types of fault. The possibility of damaging the systems seriously and cause interruptions in the transmitted power as long as happening blackout in the worst case which will have huge economical losses will be results of these events.

As a result, in the WPPs like the other components in a power system, the ability to predict and model the sources of different faults is required to have the best and safe operation of the system.

1.1 Background

WTs are categorized into different models, such as Fixed Speed, Doubly Fed Induction Generator and Full Power Converter, that each of them has different characteristics specially in terms of responding to the fault in the grid. Also, faults can be classified as several kinds like Short Circuit fault. The fault severity is depending on various factors, like one or three phase of the fault, its location and the amplitude of the fault impedance.

In insulation coordination studies it is required to perform analysis of the SC power inside a wind park as well as unexpected disconnection of radials under production. Since the number of WTs in the modern onshore and offshore wind farm is getting high, the simulation time of insulation coordination studies becoming too long and

not practical. Therefore, it is required to develop a computationally efficient simplified/ aggregated WT model with a satisfactory accuracy for insulation coordination studies.

1.2 Aim

In this project, the DFIG WT will be tested under different types of SC faults, like symmetrical or asymmetrical, in order to analyze its responses and behaviors during different kinds of fault. For achieving this goal, the detailed model of DFIG WT should be simulated in the PSCAD/EMTDC and MATLAB & Simulink software, initially. Then, different types of the SC fault, like Single Line Ground, Double Line Ground, etc. will be added to the system with several values of fault impedance. Finally, the obtained result will be compared with each other to find the simplest and optimal one. The models used for SC analysis is a simplified/ aggregated model that gives acceptable results under SC analysis but is much more computationally efficient in comparison with a detailed model. This simple model can be achieved by exchanging the power electronic components (Converters, Crowbar, DC Chopper, etc.) in the rotor side with the external varistor circuit in order to control and limit the rotor current to protect the DFIG.

Ultimately, the main purpose of this project is to investigate how the DFIG WT will operate with the external variable rotor resistance circuit in a WT during fault occasions.

The major aim of this paper is finding that "How will the behavior of the system's generator change by replacing the converter with the resistance in the rotor side?". As a result, the main focus of this paper is modeling the DFIG WT under different types of SC fault to find the best response and recognizing the simplest and optimal one in order to extend that model into a wind farm.

1.3 Problem Description

This section can be divided into different categories, such as studying existing detailed models of DFIG WT as well as proposing and developing several simplified simulated models of DFIG WT in PSCAD/EMTDC and MATLAB & Simulink software during the SC faults. Also, implementing them in order to find the fine tune of parameters and comparing the results among the models which are used in PSCAD/EMTDC and MATLAB & Simulink software for several of different cases.

Replacing the power electronic parts with the external variable resistance circuit in the rotor part of the IG with the suitable external resistance circuit and capacitor bank to correct the PF in the stator side will be the main target of this project. Besides, challenging with the simpler control system can be considered as the main benefits of the aggregate model. The possibility of absorbing the incoming power variation by changing the value of the variable rotor resistance circuit, to control the

rotor speed, faster than the pitch controller will be available to reach better power quality.

2

Wind Energy

In the following section, some basic concepts like wind properties, wind energy conversion as long as a brief overview of the usual models of WT will be discussed.

2.1 Properties of the Wind

The wind can be defined as a movement of air masses with different velocity in all areas of the atmosphere. Some specific factors such as general climate or geographical aspects will affect the wind behavior, directly. The building, trees, seas, etc, are the other parameters that will be effective in the character's of the wind, especially during the short period time that can be seen as the wind fluctuations.

2.2 Conversion of the Wind Energy

A WT mechanism is based on achieving the input wind's kinetic energy and converting it into the electrical energy. Some of the available wind's kinetic energy will be converted into to the mechanical power via the turbine blades. This process is called aerodynamic conversion and completely depends on the wind speed (V), the rotor swept area (A_r), the pitch angle of the blade, air density (ρ). Besides, the power coefficient ($C_p(\lambda, \beta)$) which is the function of the pitch angle (β) and the tip speed ratio (λ) which has a key role. Actually, the power coefficient ($C_p(\lambda, \beta)$) represents how much of the available wind's kinetic energy could be converted into the mechanical power.

During the steady-state condition the mechanical power can be calculated:

$$P_{mech} = \frac{1}{2} \rho A_r C_p(\lambda, \beta) V^3 \quad (2.1)$$

The above formula indicates the theoretical optimum for utilizing the power in the wind by reducing its velocity. It was discovered by Betz, in 1926, firstly [2].

2.3 Types of WT

Generally, WTs divided into two types, fixed-speed and variable speed.

2.3.1 Fixed-Speed WT

The fixed-speed model is the most basic utility-scale WT in operation, known as the Danish concept popularly. Operating at constant speed regardless of the wind speed as long as being simple, robust and reliable can be considered as its merits.

In this model the stator of the IG, with the squirrel-cage rotor, and the soft starter as well as the capacitor bank will be connected to the grid, directly to draw the magnetizing current from the line thereby reducing stator power factor. Also, at a fixed-speed, higher mechanical stress should be tolerated by the IG [3], [4].

Eventhough, when the wind's speed is low, the active power generation will also be low. Then, the machine will draw reactive power from the grid, mainly and the stator PF will be extremely poor [3]. The wind turbine rotor speed is fixed and determined by the grid frequency [4]. The rotor will vary with small speed variation from the nominal value (synchronous speed). Besides, the low speed range of its operation that might cause torque spikes which can damage the mechanical subsystems of the turbine. Causing the transients in the electrical circuits and demanding external reactive power support, which is essential in order to compensate for the reactive power consumption by the IM, is the other limiting factor of this type of WT.

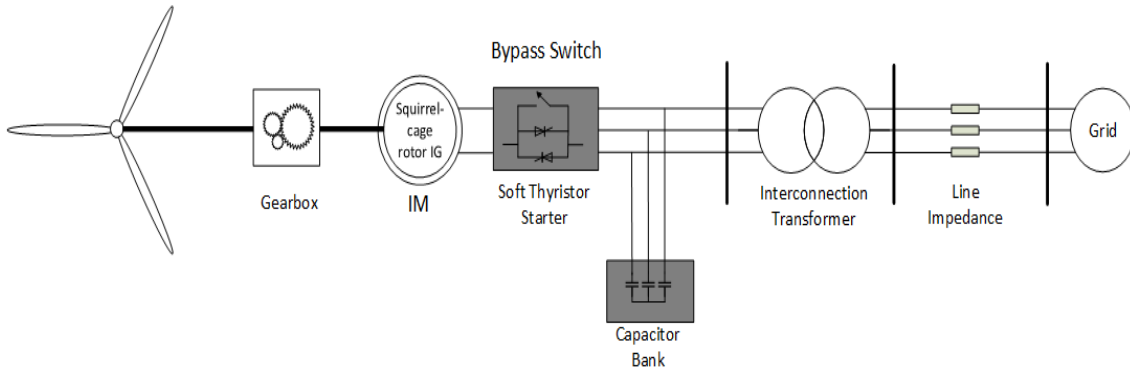


Figure 2.1: Fixed-Speed WT schematic.

2.3.2 Variable Speed WT

The main aim of designing variable speed WT is operating in the wider range of the rotor speed. By using the power electronics components, like converters, the possibility of controlling the torque via controlling the current as well as rotor speed of the IG with gearbox and emergency braking systems can be used to maximize the achieved kinetic energy of the wind. Eventhough, reducing the mechanical stresses by better torque and power fluctuations control.

As a result, the possibility of matching the rotor and wind speed to achieve the maximum efficiency as well as connecting the rotor to the grid at low speed when

the wind is low can be considered as the main advantages of the variable speed WT [5].

Eventhough, additional cost and power losses of converters besides implementing of the extra filters for the output current in order to remove harmonics of the power electronics equipment can be taken into account as disadvantages of the variable speed WT.

Variable speed WT will be classified into two main models, DFIG WT and Full-converter WT according to the difference in generation technology.

2.3.2.1 DFIG WT

Generally, in the DFIG model of the WT, the stator of the IG, will be connected to the grid, directly. The rotor winding will be connected via slip rings to the back-to-back power electronics converter. The ability to control the rotor current in order to extract the maximum wind's kinetic energy as well as lower losses of the power electronics converter, due to handling approximately 30 percent of the total power fraction, are the main benefits of DFIG WT.

The ability to control active and reactive power, completely. Besides, limited speed range, at around -30 % to 30 % of synchronous speed and less expensive PWM inverter capacity can be considered as the main pros of the DFIG WT [6].

On the other hand, demanding gearbox and full scale power converters will be the drawback of DFIG WT [7].

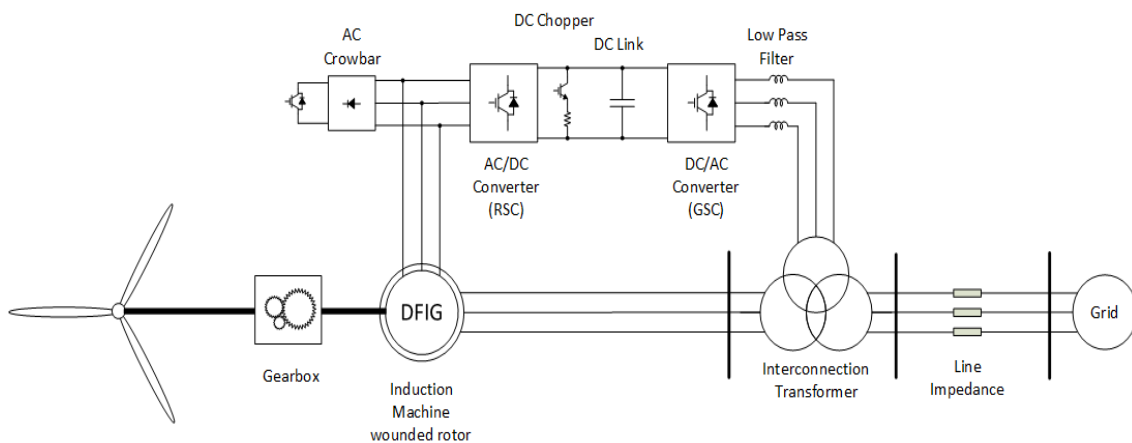


Figure 2.2: DFIG WT schematic.

In chapter 4, the DFIG WT will be examined with further details like its protection and control systems.

2.3.2.2 Full-Converter WT

In the full-converter WT, the power flow from the WT to the grid is through back-to-back power electronics converter. There is no direct connection from the WT to the grid and the converter must be rated to the entire output power. The ability to use high-pole-count, permanent magnet, Synchronous Generator in order to let low-speed operation. Besides, the possibility of eliminating the gearbox to increase reliability and reduce the total costs of the system are the main features of the full-converter WT. Nonetheless, IG can be used in this type. Also, full-converter WT offers an independent active and reactive power control.

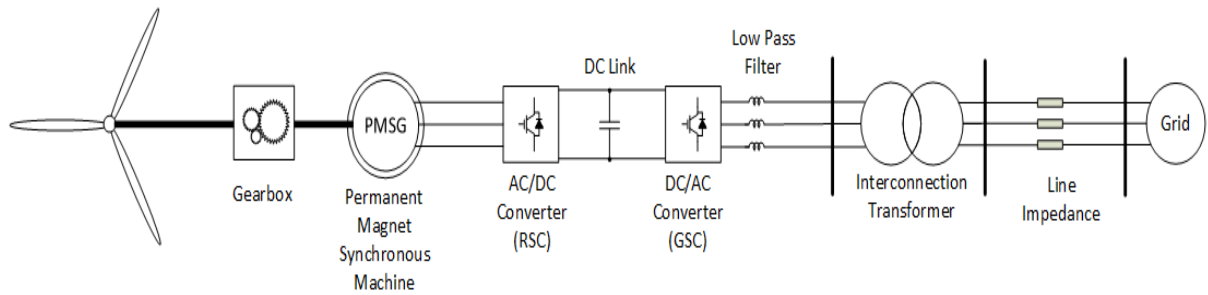


Figure 2.3: Full Converter WT schematic.

The main focus of this thesis is simplifying the DFIG WT model in order to find the aggregated type that can be controlled with the external variable rotor resistance circuit instead of using power electronics components as long as the different control methods.

3

Induction Machine

Initially, in this chapter the brief description of the IM, its operational performance will be presented. Then, the equivalent circuit, the dynamic models and equations of the IM which will be discussed.

3.1 Overview

One of the most popular types of the electrical machine in the industry is IM or Asynchronous Machine that consists of stator and rotor, both of them are carrying the AC currents. The rotor is mounted on the bearings and separated from the stator by an air gap from each other. The reason of why it has been known as IM is, the voltage of the rotor which produces the current and the flux of the rotor will be produced by the electromagnetic induction in the rotor winding. This is the main feature of the IM [8], [9].

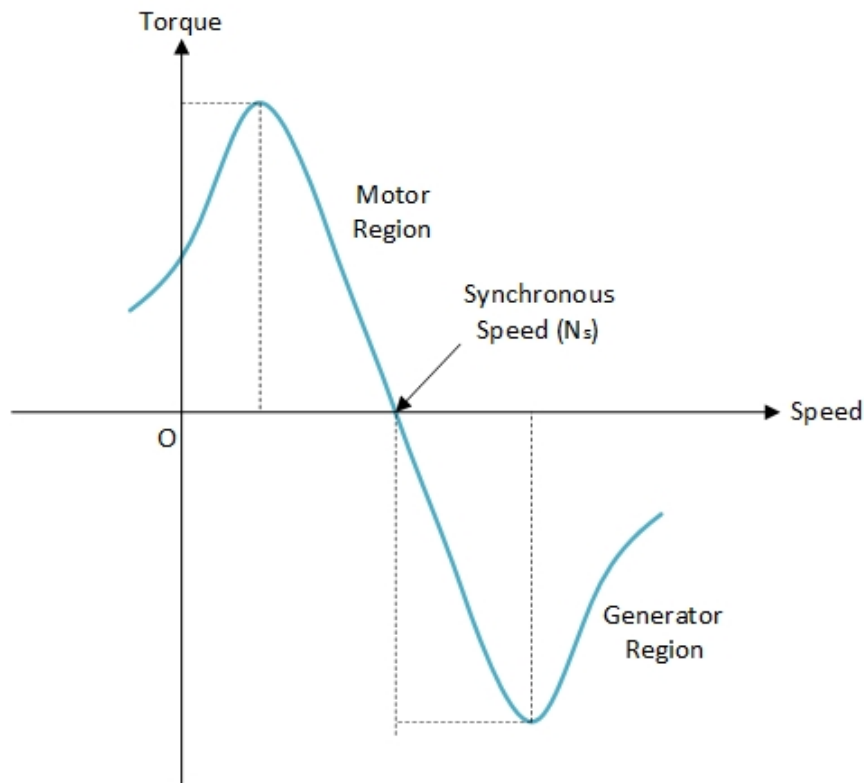


Figure 3.1: The torque-speed characteristics of the IM [10].

3.2 Constructional Features of the IM

IM can be used as a motor or generator and based on the rotor structure divided into two main type, squirrel-cage winding and wound rotor winding. The main focus of this chapter is analyzing the wound rotor winding due to its usage in the DFIG WT.

3.2.1 Squirrel-cage Rotor Winding

The squirrel-cage winding rotor is simpler, cheaper, more economical and stronger than wound rotor winding. It consists of a series of conducting bars, usually made from aluminum or copper, which are laid into the carved rotor slots and shorted at both ends by the end rings.

3.2.2 Wound Rotor Winding

The second type of the IM is wound rotor winding which has a complete Y-connected set of three-phase windings. Also, the rotor's shaft has been tied up to the slip rings which is connected to the three-phase rotor wires. The possibility of connecting to an external circuit via using stationary brushes pressing against the slip rings, is the major benefit of the wound rotor winding IM. The rotor winding can be connected to an external three-phase variable resistance circuit or connection in order to control the speed of the rotor [8]. The rotor winding can be also be connected to the frequency converter that controls the frequency and current in the same time.

3.3 External Variable Resistance Circuit in the Wound Rotor IM

The maximum torque that can be produced by the IM is not dependent on the rotor resistance but by adjusting the value of the rotor resistance, via external variable resistance circuit, it will be possible to achieve this maximum torque at different speeds. As a result, by adding the external resistance circuit, the highest torque can be at standstill situation. There is a high starting torque accomplished.

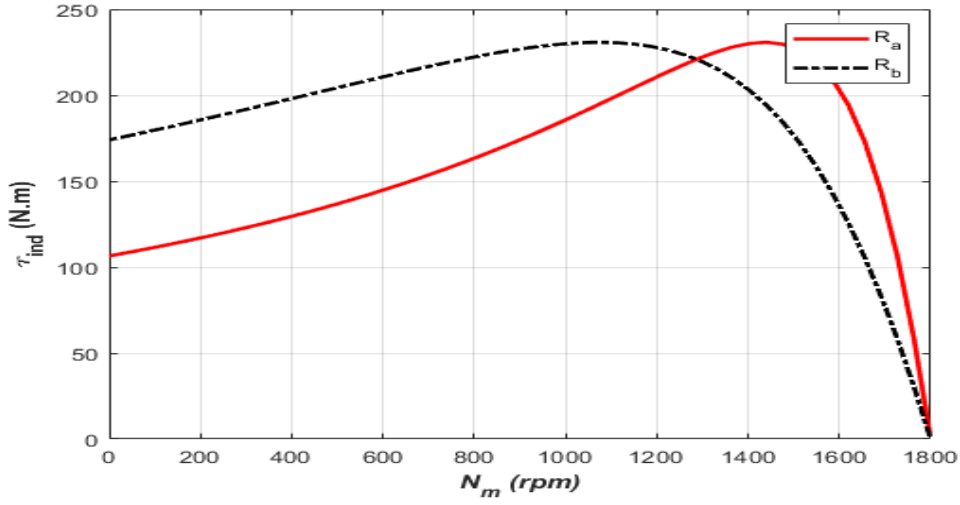


Figure 3.2: The torque-speed characteristics of the induction motor with the external variable resistance circuit in both motor and generator modes. [9].

As can be noticed in figure 3.2, $R_a \succ R_b$. The external resistance circuit will be connected to the rotor winding through the slip rings. The point that should be considered is the slip that the highest torque happens is proportional to the rotor circuit resistance, completely in IM [8].

$$S_{Tmax} \propto (R_{w2} + R_{ext}) \quad (3.1)$$

where:

R_{w2} is the per-phase resistance of the rotor winding.

R_{ext} is the per-phase external resistance that connected to the rotor winding.

The serious disadvantage of this method is the losses in the rotor side based on adding the external resistance circuit will be increased, significantly.

$$P_{loss} = R_{total} I^2 \quad (3.2)$$

where:

R_{total} is the sum of the R_{w2} and R_{ext} ($R_{total} = R_{w2} + R_{ext}$).

3.4 Equivalent Circuit of the IM

The equivalent circuit of the IM which can be represented like the diagram. Also, the point that should be considered is that an IM is a single excited machine [9].

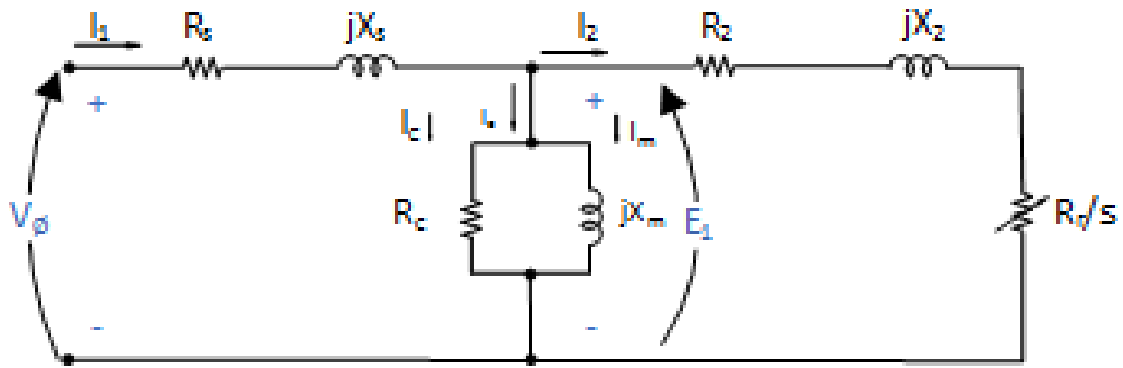


Figure 3.3: The per-phase equivalent circuit of the IM.

3.5 Dynamic Models and Equations of the IM

The IM can be represented in two different dynamic models, the T and the Inverse-T models.

The T-model of the IM usually used in terms of variable speed drives in electro-mechanics charges [11].

The T-model is the usual equivalent circuit for the IM in the most electrical machines references, with some exceptions. Likewise, in the rotor side, the R_r/s with the R_r , which is the series rotor resistance with the voltage source and the rotor shaft that is sticking out of the rotor-emf symbol [12].

In the T-model, the stator winding losses and leakage inductance represented by R_s and L_{ls} , respectively, while R_r and L_{lr} indicate the rotor winding losses and leakage inductance, respectively. Also, the other parameters, such as, L_m , $j\omega_r\phi_r^{(s)}$ and ω_r are representing, the machine's magnetizing inductance, the back-EMF and the rotor angular speed, respectively.

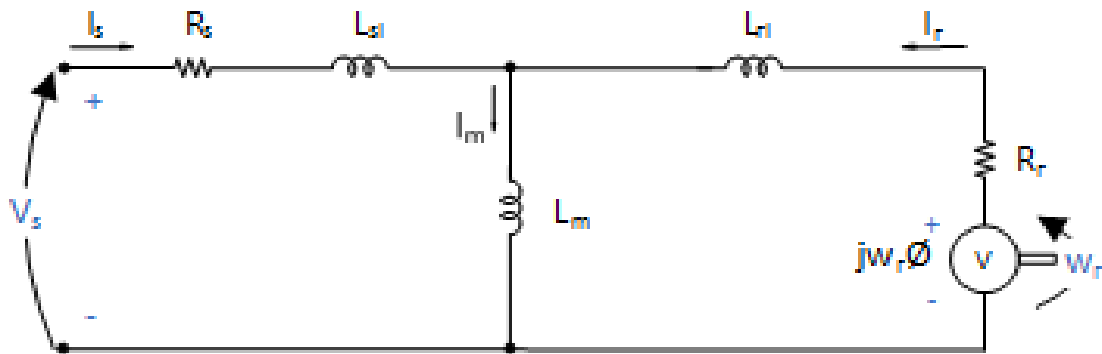


Figure 3.4: The dynamic equivalent circuit of the T-model of IM.

On the other hand, the Inverse- Γ -model of the IM that uses more in comparison with T-model because of being simpler, specifically in the control laws area, and consisting of the rotor and stator inductance into one equivalent inductance to the stator side (L_σ) which are the main differences between two model [13], [14].

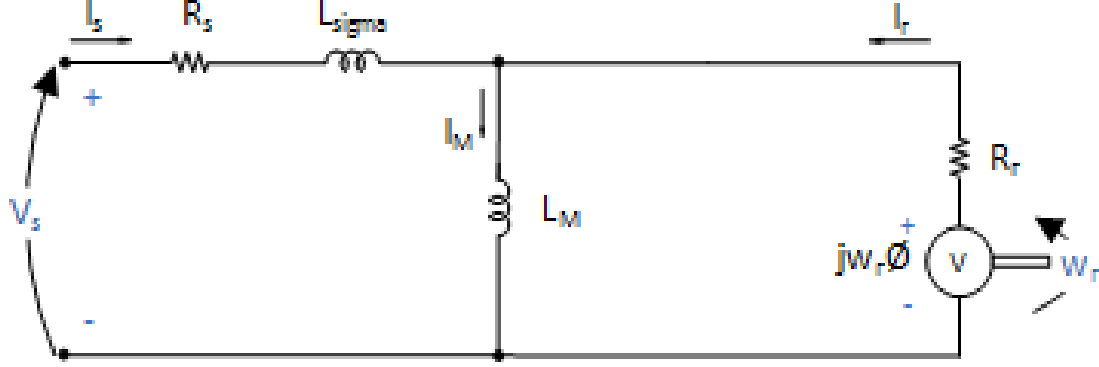


Figure 3.5: The dynamic equivalent circuit of the Inverse- Γ -model of IM.

When shifting from the T-model to the Inverse- Γ -model, the new relationship between some parameters should be defined like this. Eventhough, the significant point that must be considered is that the expressions and parameters with the subscript "R" represents the Inverse- Γ -model and the subscript "r" indicates the T-model of the IM [13], [14].

$$L_r = L_{lr} + L_m \quad (3.3)$$

$$b = \frac{L_m}{L_r} \quad (3.4)$$

$$\phi_R^s = b\phi_r^s \quad (3.5)$$

$$i_R^s = \frac{i_r^s}{b} \quad (3.6)$$

$$L_M = \frac{L_m^2}{L_r} \quad (3.7)$$

$$L_\sigma = L_s - L_M = L_s - \frac{L_m^2}{L_r} = \frac{L_m(L_{sl} + L_{rl}) + L_{sl}L_{rl}}{L_m + L_{rl}} \approx L_{sl} + L_{rl} \quad (3.8)$$

$$i_M^s = i_s^s + i_R^s \quad (3.9)$$

$$R_R = b^2 R_r \quad (3.10)$$

Based on the parameters that have been defined as the references in Figure 3.6, the dynamic electrical equations of the IM in the stationary coordinate frame can be written like ($V_r^r = 0$) :

$$V_s^s = R_s i_s^s + \frac{d\phi_s^s}{dt} \quad (3.11)$$

$$0 = R_R i_R^s - j\omega_r \phi_R^s + \frac{d\phi_R^s}{dt} \quad (3.12)$$

By using the Park's transformation which is described in Appendix B, the above equations can be converted into the rotating dq -coordinate frame. So, the results of the converted equations can be written as:

$$V_s^{(dq)} = R_s i_s^{(dq)} + j\omega_s \phi_s^{(dq)} + \frac{d\phi_s^{(dq)}}{dt} \quad (3.13)$$

$$0 = R_R i_R^{(dq)} + j\omega_{slip} \phi_R^{(dq)} + \frac{d\phi_R^{(dq)}}{dt} \quad (3.14)$$

whereas ω_s is the synchronous angular speed, ω_r is the rotor angular speed and $\omega_{slip} = \omega_s - \omega_r = s\omega_s$. Furthermore, the fluxes of the stator and rotor can be expressed as:

$$\phi_s^s = L_s i_s^s + bL_m i_R^s = L_s i_s^s + \frac{L_m^2}{L_r} i_R^s = L_\sigma i_s^s + L_M i_M^s \quad (3.15)$$

$$\phi_R^s = bL_m i_s^s + b^2 L_r i_R^s = \frac{L_m^2}{L_r} (i_s^s + i_R^s) = L_M i_M^s \quad (3.16)$$

$$\phi_s^{(dq)} = L_\sigma i_s^{(dq)} + L_M i_M^{(dq)} \quad (3.17)$$

$$\phi_R^{(dq)} = L_M i_M^{(dq)} \quad (3.18)$$

4

Doubly Fed Induction Generator Wind Turbine

This chapter includes the explanation of the DFIG WT. Also, the protective elements that should be used in this model will be illustrated in a detailed way.

4.1 Overview

The fundamental operation and function of the DFIG WT which is one of the most popular type of WTs that is used even in large power ranges (MW) will be analyzed. The main important aspect of the DFIG is its ability and flexibility in terms of working with variable speed.

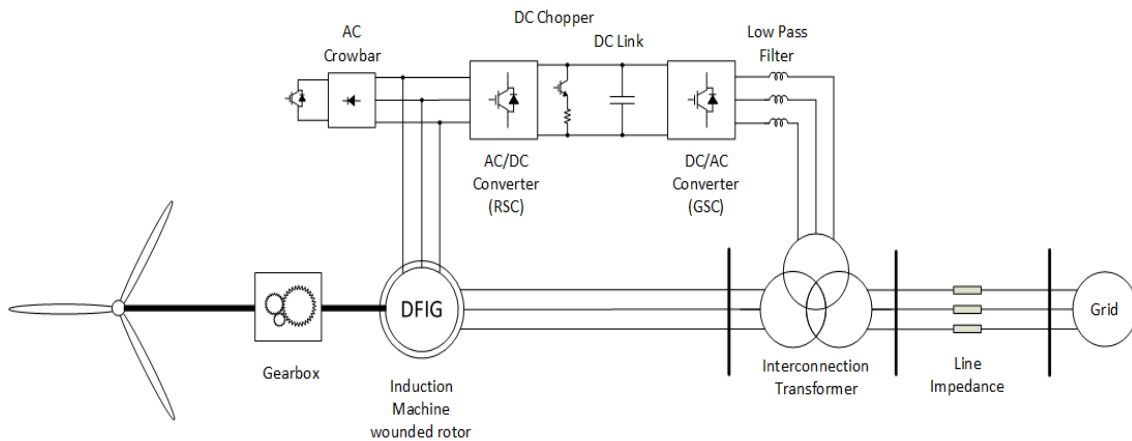


Figure 4.1: DFIG WT schematic.

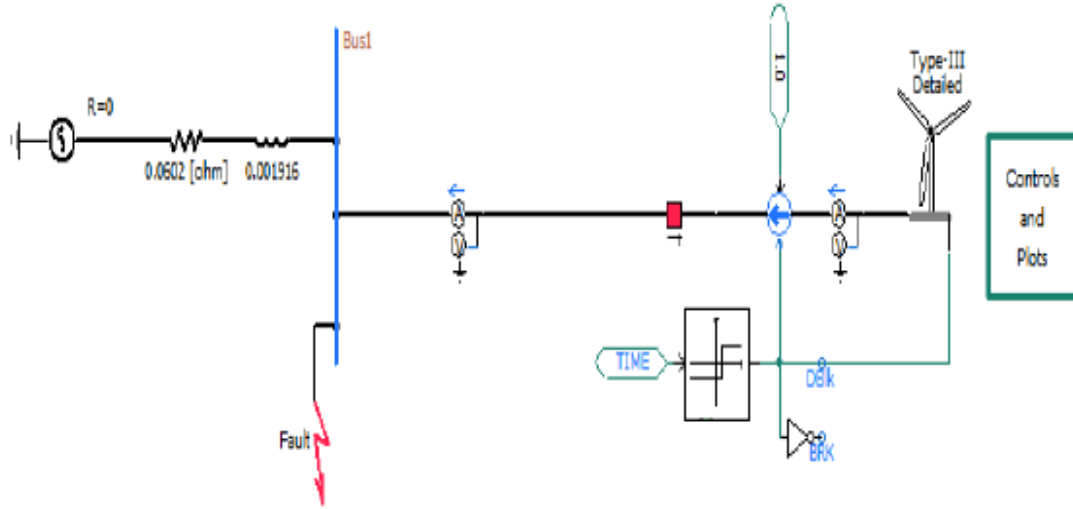


Figure 4.2: The Detailed type of the DFIG WT in PSCAD.

The values of the resistance and inductor that are connected to the Bus 1 are 0.0602 Ω and 0.001916 H, respectively.

4.2 Principle Operation

The main technology of the DFIG is converting wind energy with variable speed into electric energy [14], [15]. This type of WT requires specific protective circuit, which is called crowbar, on the rotor side in order to provide safe operation during severe and rush voltage dip [16].

4.3 Protective Circuit

As it mentioned above, the protective circuit in DFIG is called an AC crowbar circuit and DC chopper. The possibility of dumping the machine's flux as well as bringing down the induced voltage, on the rotor side, to the standard and acceptable level for the rotor converter is the main duty of the rotor crowbar circuit. Also, the great point that should be noticed is the power converter must be disconnected when the crowbar is running.

Consequently, when the permanent and momentous imbalance of grid voltage happens, on the rotor side, the negative sequence of the induced voltage might be higher than the acceptable value for the rotor power converter. At this time, the IG should be disconnected from the power grid till the grid voltage recovers to the standard

situations [17], [18].

On the other hand, during the low asymmetry factor of the grid voltage, it will be possible for IG to operate continuously to provide high quality energy.

5

The Simplified DFIG WT Model

5.1 Designing the Simplified Model

Using external resistance in the rotor circuit of the IM to control the speed of it as long as using external capacitor bank to inject reactive power in the rotor side for achieving unity PF is the main idea of the simplified model. The point that should be considered is that the fault time is very short like micro seconds.

5.2 Calculating the Parameters

In order to calculate the parameters values in the simplified model, using MATLAB Simulink model as long as phasor diagram method can be helpful. Also, the point that should be noticed is these amplitudes have been estimated based on try and error way to make the PF on the stator side unity.

5.3 The Simplified Model

The below illustrations represent the structures of the simplified model of the DFIG WT in the PSCAD/EMTDC software and its circuit diagram.

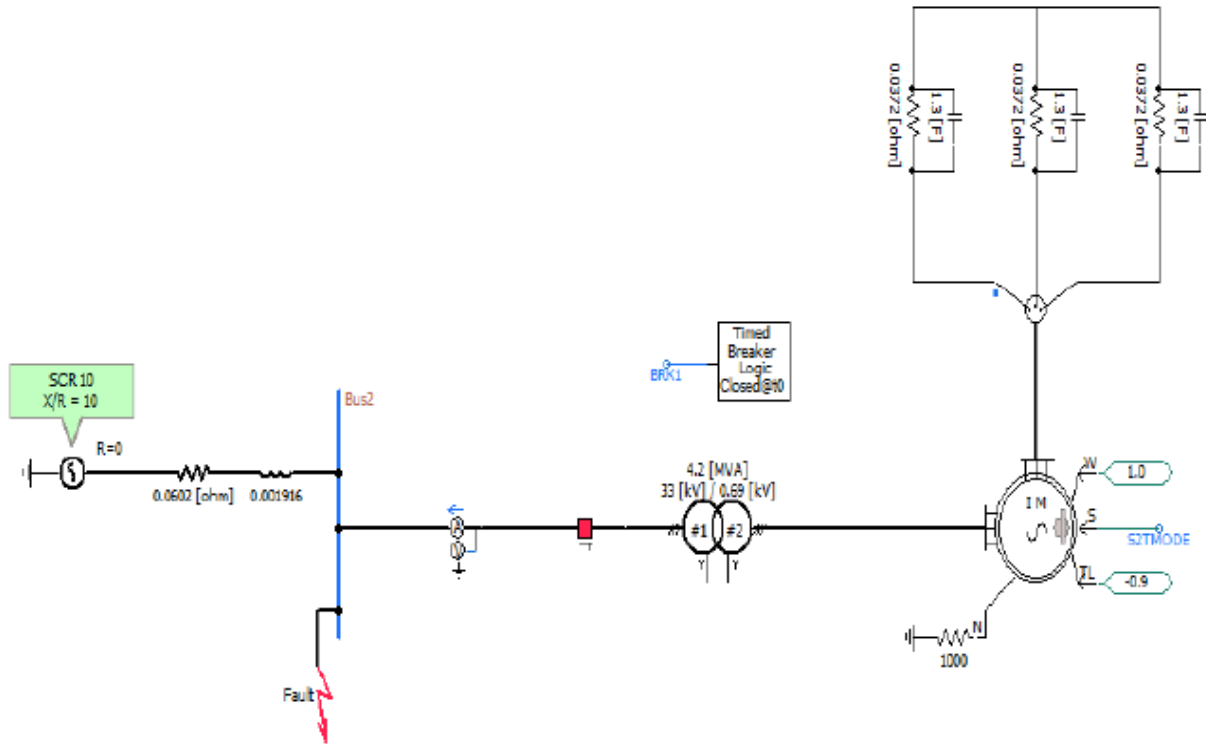


Figure 5.1: The Simplified type of the DFIG WT in the PSCAD/EMTDC.

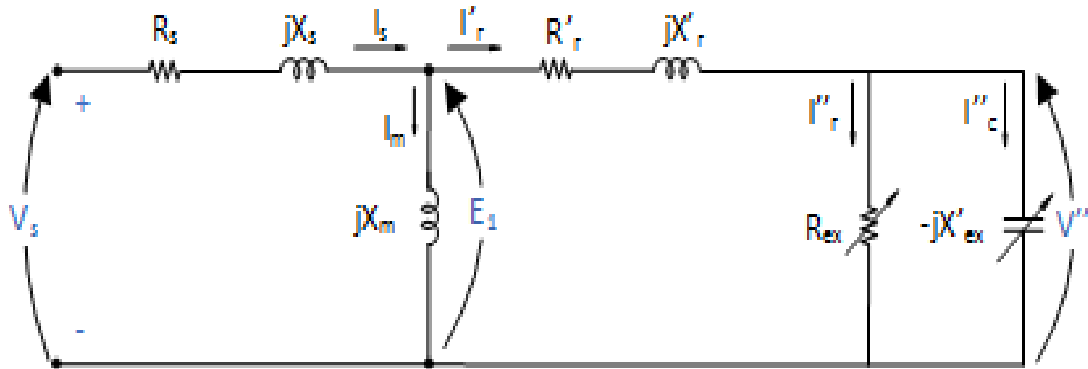


Figure 5.2: The circuit diagram of the Simplified type of the DFIG WT.

As can be noticed, the capacitor bank, on the rotor side, used to make the PF unity on the stator side.

5.4 The Phasor Diagram Method

By using the phasor diagram method, the improved results to reach the unity PF can be seen. Two different methods can be implemented in the IM to increase the stator PF to become unity. Initially, increasing the value of the capacitor bank in

the rotor side. Secondly, increasing the amplitude of the external resistance in the rotor circuit. The result of both methods can be noticed in the below figures.

ϕ_1 = the angle between V_s and I_s

ϕ_2 = the angle between V'' and I'_r

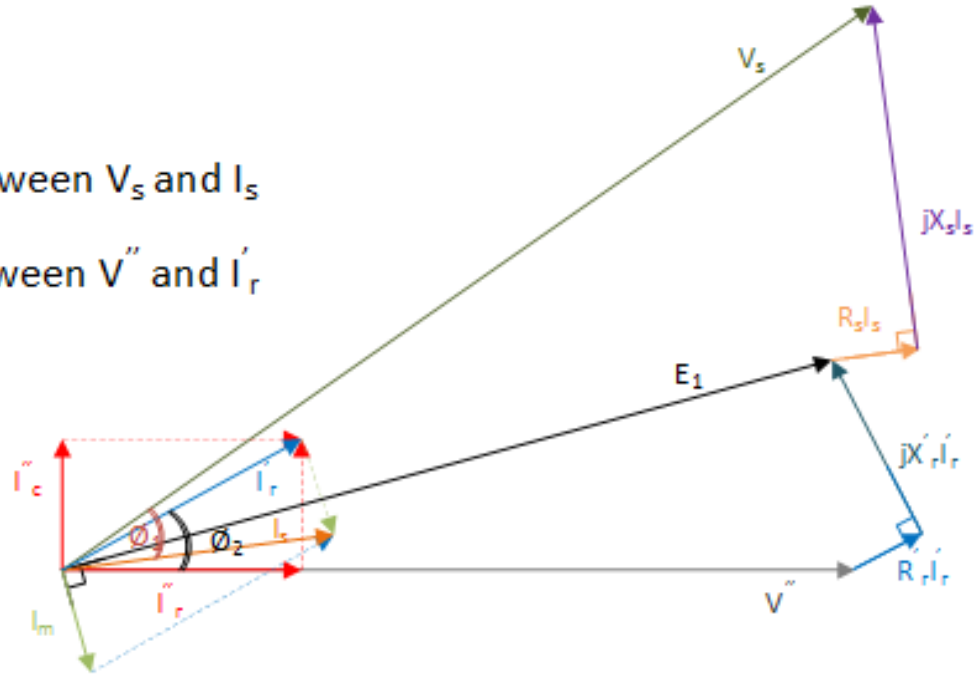


Figure 5.3: The Phasor Diagram of the IM with extra resistance and capacitor on the rotor side.

$\phi_1 = 0$, the angle between V_s and I_s

ϕ_2 = the angle between V'' and I'_r

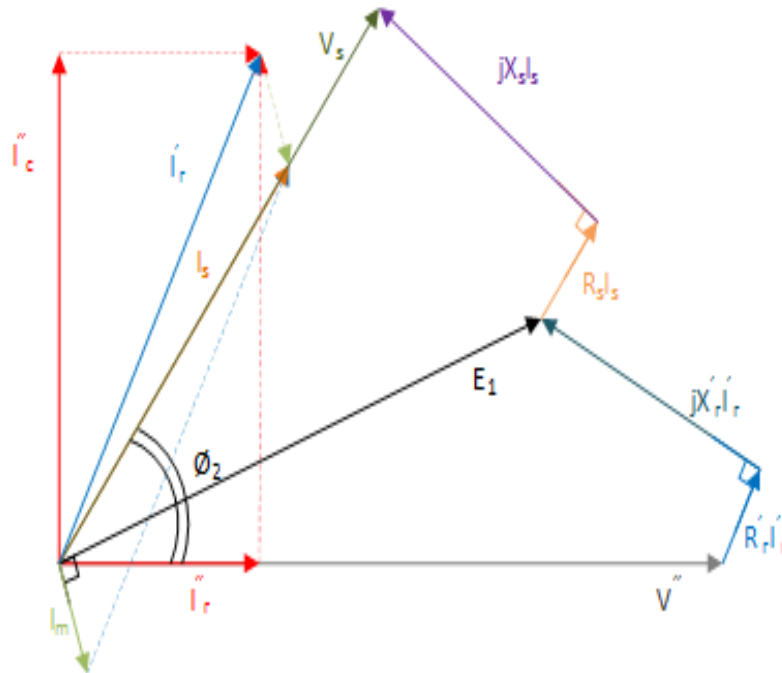


Figure 5.4: The Phasor Diagram of the IM with extra resistance and capacitor on the rotor side after increasing the capacitor value.

ϕ_1 = the angle between V_s and I_s

ϕ_2 = the angle between V'' and I_r'

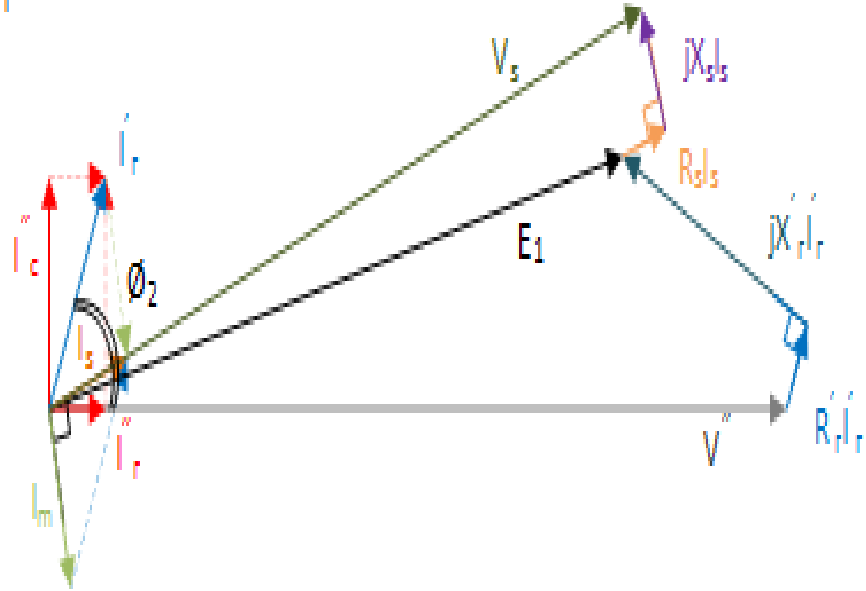


Figure 5.5: The Phasor Diagram of the IM with extra resistance and capacitor on the rotor side after increasing the resistance value.

6

Short Circuit Fault

6.1 Fault Definition

During the steady-state situations a power system will operate under balanced conditions and all pieces of power equipment will carry normal currents besides the voltage of busses will be on the limited prescribed values. Any kinds of failure that causes disruption to this normal conditions is called a fault. Generally, a fault (fault current) in electrical power systems can be defined as any abnormal electric current in the system that might be caused by equipment failures, like rotating machines or transformers, or environmental conditions and human errors. Faults will be divided into different types, such as SC fault, OC fault, transient fault, arcing fault, etc. [19], [20].

Some specific parameters, like the impedance of the intervening circuit and the internal impedance of the generators will affect the magnitude of the fault currents. Analyzing of the faults is one of the main parts of the power systems analysis and the achieved data of this part can be used in terms of proper setting of the relays, making assessments for the rating of the protective switchgears and insulation co-ordination process in order to prevent huge economical losses and fatal disastrous events [21], [22]. In this chapter, the SC fault will be illustrated.

6.2 SC Fault

Initially, the definition of the SC should be considered which is an abnormal condition in a connection between two nodes, in an electrical circuit, that makes them to be at the same voltage amplitude. SC provides a path with a zero ohm or a very low impedance for an electrical current which excessively high amplitude and damages the rest parts of the circuit or the other electrical components by causing overheating, fire, explosion, etc. SC faults will be categorized into two major types, symmetrical and unsymmetrical SC fault.

6.2.0.1 Symmetrical SC Fault

Due to affecting all three phases of the system simultaneously, this type of fault ,which is the most severe type, is called symmetrical or (three phase) balanced fault

that occurs so infrequently in the power systems at around 5 % of the total faults [21], [22]. Actually, during this type of fault, the network does not lose its balanced conditions but the electrical components of the power system will be faced with serious damages. Because the network still is balanced, the fault can be solved on a per-phase basis and the other two phases will see the identical SC current but with 120 degree phase shift. The reached data from the symmetrical SC fault can be used in order to select and set the phase relays, the capacity of the circuit breakers and rating of the protective switchgear in the systems [21], [22]. The symmetrical SC fault might be grounded or not, LLL and LLLG that can be clearly noticed in the figure 6.1. In the below figures, the fault impedance represented by Z_f .

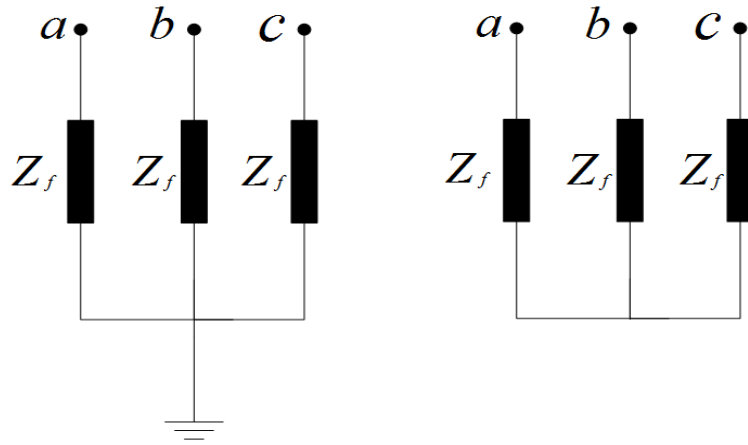


Figure 6.1: LLLG and LLL SC fault.

6.2.0.2 Unsymmetrical SC Fault

In direct contrast to the symmetrical SC fault, unsymmetrical or unbalanced SC fault exists that the network losses its balanced conditions and becomes unbalanced which means the impedance values are different in each phase causing unbalance current to flow in the phases. Unsymmetrical SC fault does not affect each of the three phases, equally besides being so common and significantly less severe than symmetrical type. It can be categorized into various types, like SLG, LL and LLG that can be seen in the below figures. The information that will be got from LG SC Fault can be used to select and set the ground relays [21], [22].

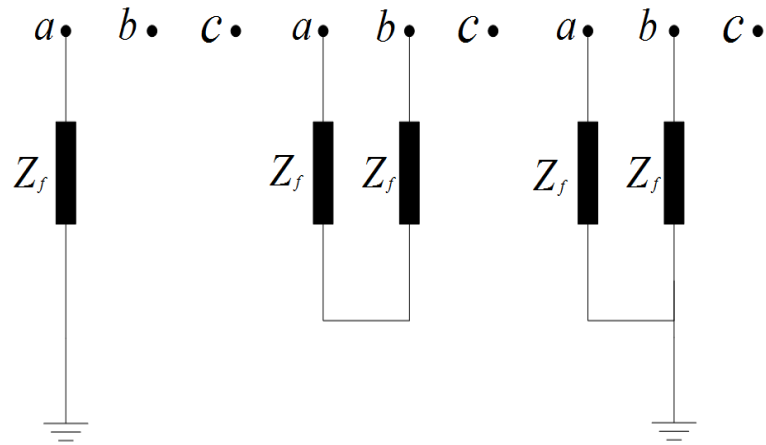


Figure 6.2: SLG, LL and LLG SC fault.

The most common type of the unbalanced SC fault is LG roughly 65-70 %. Then, LLG and LL are located in the sequential ranks with 15-20 % and 5-10 %, respectively [19], [20].

7

Simulation of Detailed and Simplified Models

In this chapter the detailed and simplified models of the DFIG WT which had been simulated in the PSCAD/EMTDC software will be analyzed under different types of SC faults.

In order to analyze different types of faults and achieve their results, three different values for fault impedance will be considered. The values of Z_f which can be categorized as case 1, 2 and 3 are 10^{-15} , 10^{-5} and 10^{-2} ohm, respectively.

7.1 The DFIG WT behaviors Under SC Faults

After modifying the detailed DFIG WT model, that has been built in the PSCAD/EMTDC software, with the given parameters, it should be analyzed under a different type of SC faults. In the all below figures, blue lines represent the detailed model and the red ones indicate the simplified types.

7.1.1 Models in Steady-State Conditions

Firstly, the behaviors of both types will be considered during steady-state, which can be shown in figure 7.1.

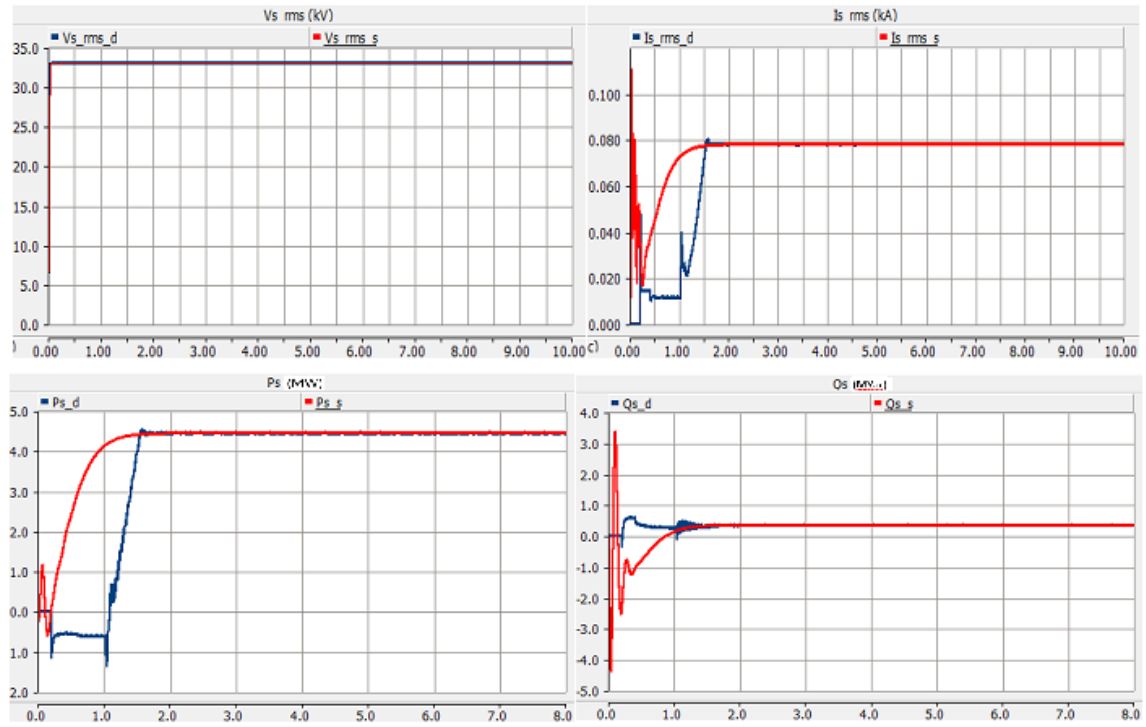


Figure 7.1: The blue curves belong to the detailed and the red ones belong to the simplified type during the steady-state.

The figure 7.1 depicts the measured outputs of the detailed and simplified types of the DFIG, on the stator side, the high side of the transformer that can be seen in the figure 5.1. It represents V_{rms} (kV), I_{rms} (kA), P_{rms} (MW) and Q_{rms} (MVar), respectively.

The figure 7.1 demonstrates, at the zero seconds when the switch will be on, the transient current can be noticed obviously. Starting from the zero amperes is the result of this phenomenon and some seconds will be taken to reach at steady-state condition.

In the PSCAD/EMTDC software, four different types of faults can be simulated. Fault type 1, represents SLG SC fault. Fault type 2, illustrates LLG SC fault. Fault type 3, indicated LL SC fault. Finally, fault type 4, describes LLLG SC fault.

7.1.2 Models Under Symmetrical SC Faults

Initially, the symmetrical SC Fault will be added into the detailed and improved simplified models, which is categorized into types 1 and 2, of the DFIG WT in order to examine it. In order to reach this goal, the voltage dip (kV) and the fault current (kA) for both detailed and simplified models will be shown for each fault types. Besides, the enlarged pictures of the I_{fmax} (kA) types.

7.1.2.1 Under LLLG SC Fault

The results of fault type 4, in the PSCAD/EMTDC software.

The significant point that should be noticed is that the fault time considered 0.3 seconds due to the typical value of the relay protection in the power system in Sweden. Each country has specific grid codes that defined based on that country's power systems.

The voltage dip and fault current changes during the LLLG SC fault, which took 0.3 second for different values of fault impedance 10^{-15} , 10^{-5} and 10^{-2} ohm, can be seen in figures 7.2, 7.3 and 7.4, respectively.

The fault impedance (Z_f) causes overcurrent, which represent as I_f . Consequently, the voltage dip is the result of this phenomenon that can be seen in the below figures.

Sequentially, the other element that is effective in the value of the overcurrent and voltage dip during the fault process is the amplitude of the Z_f . Besides, the fault type that is another effective factor in therms of the amplitude of the voltage dip.

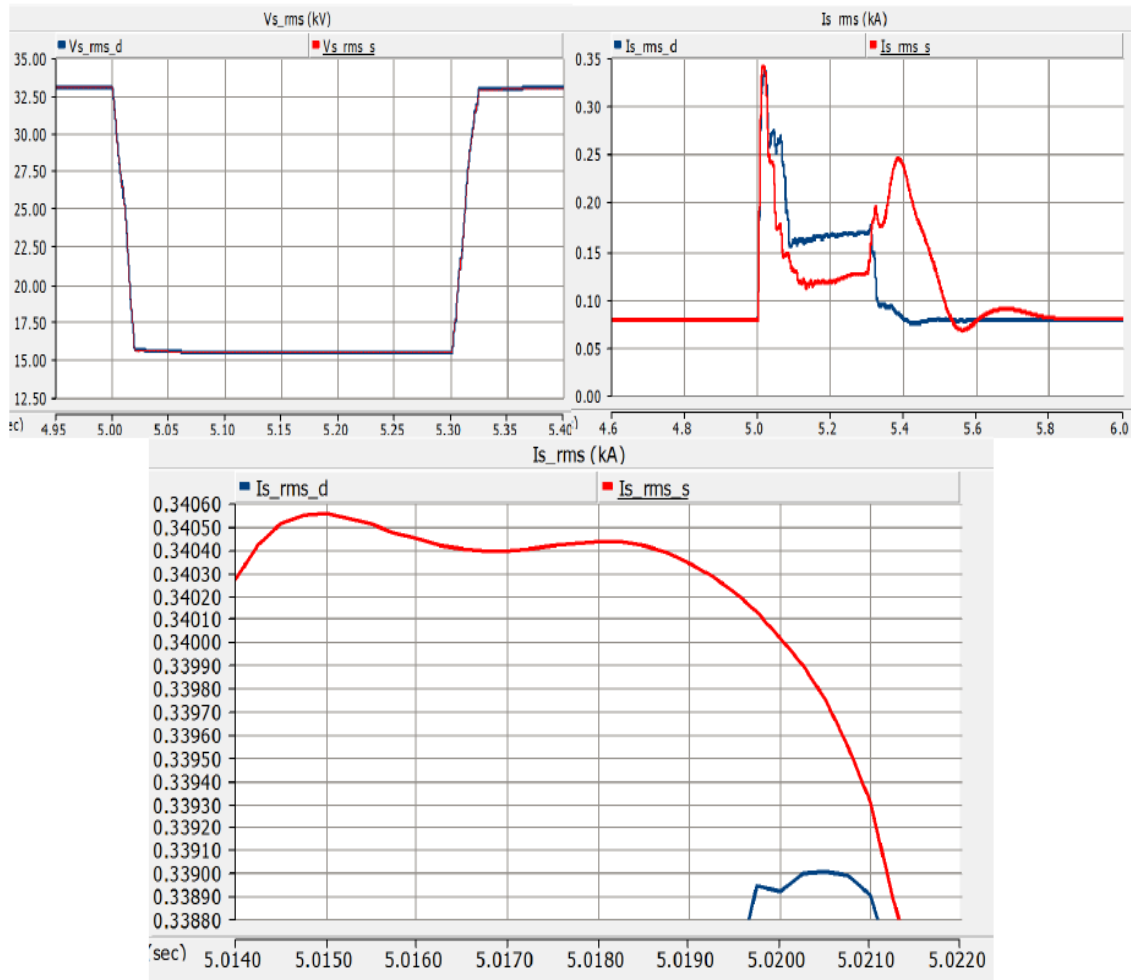


Figure 7.2: Case 1 : $Z_f = 10^{-15} \Omega$

7. Simulation of Detailed and Simplified Models

As can be seen in the figure 7.2, the I_{fmax} of the detailed and simplified types are 0.3392 and 0.3455 kA, respectively.

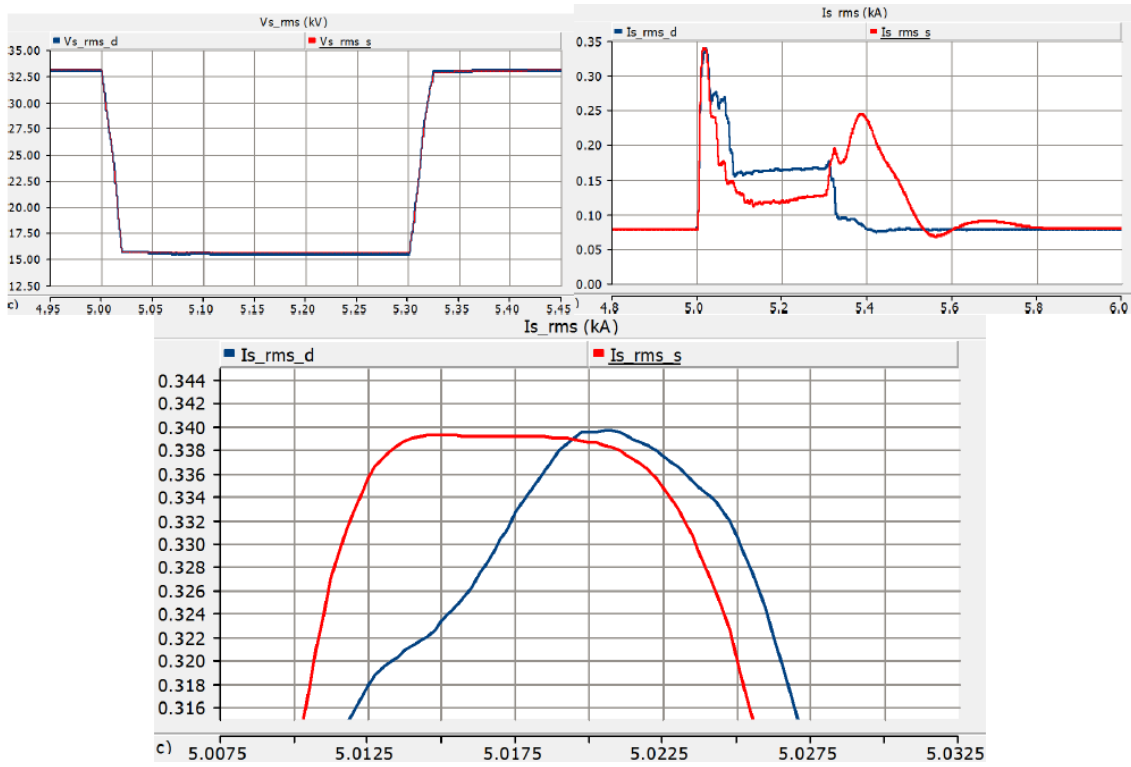


Figure 7.3: Case 2 : $Z_f = 10^{-5} \Omega$

In the figure 7.3, the I_{fmax} of the detailed and simplified types are 0.339 and 0.399 kA, respectively.

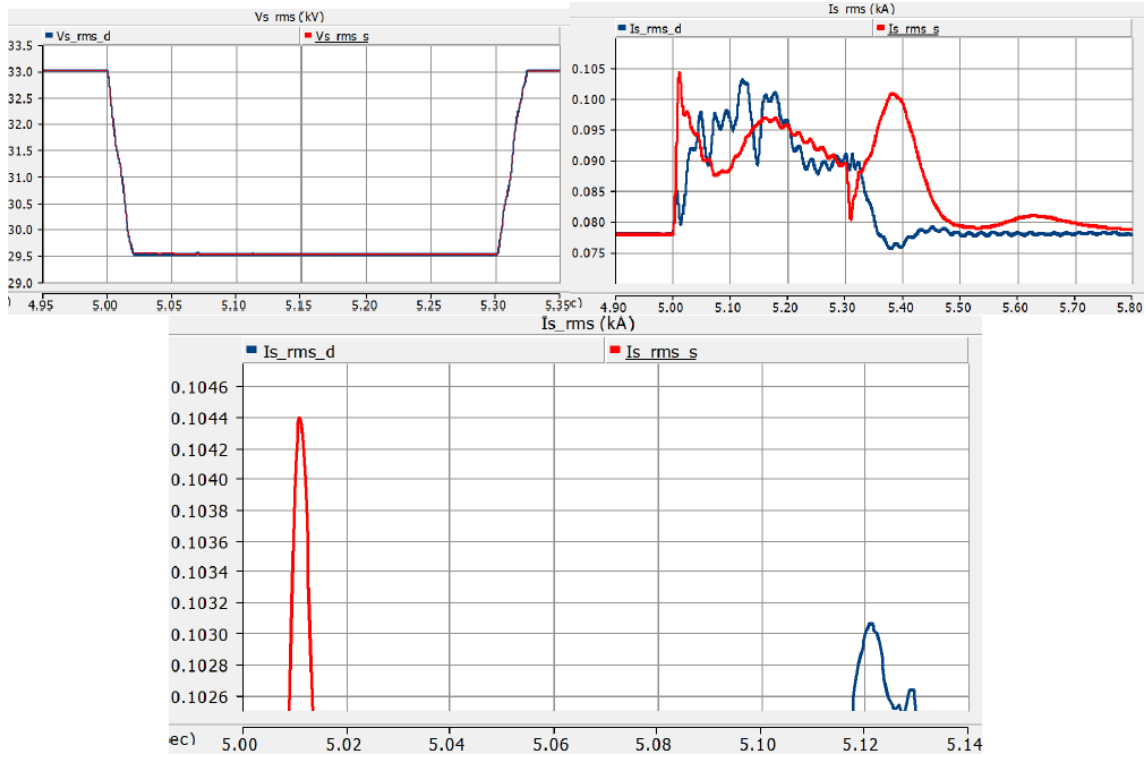


Figure 7.4: Case 3 : $Z_f = 10^{-2} \Omega$

In the figure 7.4, the I_{fmax} of the detailed and simplified types are 0.1031 and 0.1044 kA, respectively.

7.1.3 Models Under Unsymmetrical SC Faults

Now, the unsymmetrical SC Fault will be added into the detailed and improved simplified models, which is categorized into types 1 and 2, models of the DFIG WT.

7.1.3.1 Under SLG SC Fault

The results of fault type 1, in the PSCAD/EMTDC software.

Also, the voltage dip and fault current behaviors during the SLG SC fault, which took 0.3 seconds for the same values of fault impedance, can be seen in figures 7.5, 7.6 and 7.7, respectively.

The significant point that is obvious is that is the amplitude of voltage dip under SLG SC fault is 24.5 kV which is different from LLLG SC fault that was 15 kV. The reason of this issue is different amplitude of Z_f and type of the fault. This phenomenon can be seen in the other cases like LL SC and LLG SC fault.

7. Simulation of Detailed and Simplified Models

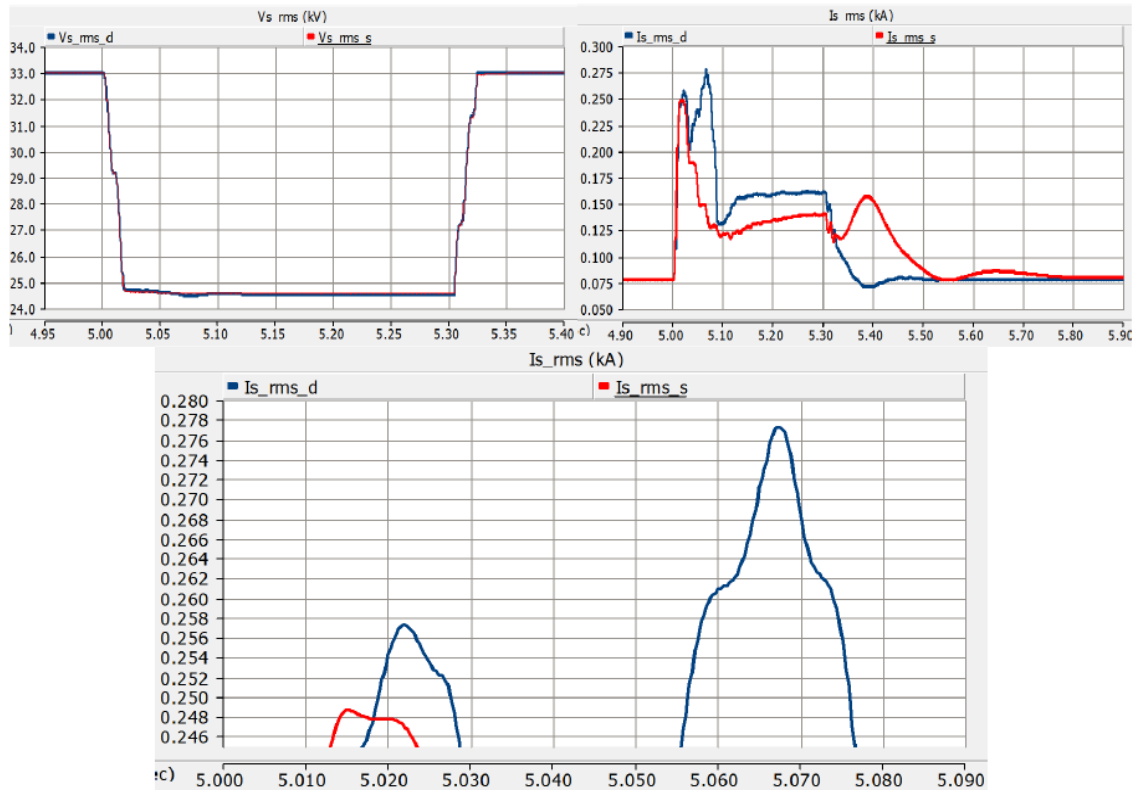


Figure 7.5: Case 1 : $Z_f = 10^{-15} \Omega$

As can be noticed in the figure 7.5, the I_{fmax} of the detailed and simplified types are 0.279 and 0.249 kA, respectively.

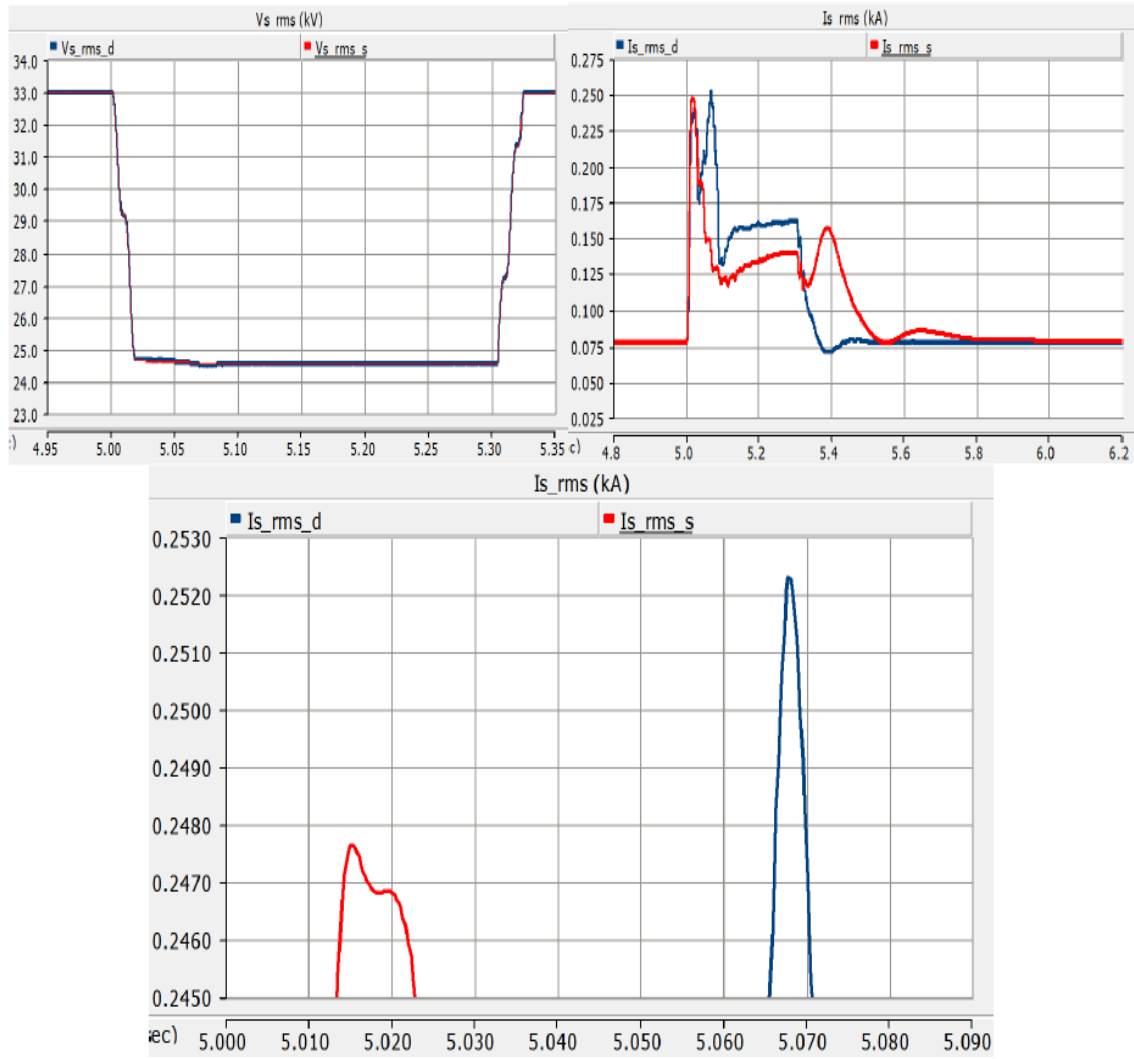


Figure 7.6: Case 2 : $Z_f = 10^{-5} \Omega$

In figure 7.6, the I_{fmax} of the detailed and simplified types are 0.2525 and 0.2478 kA, respectively.

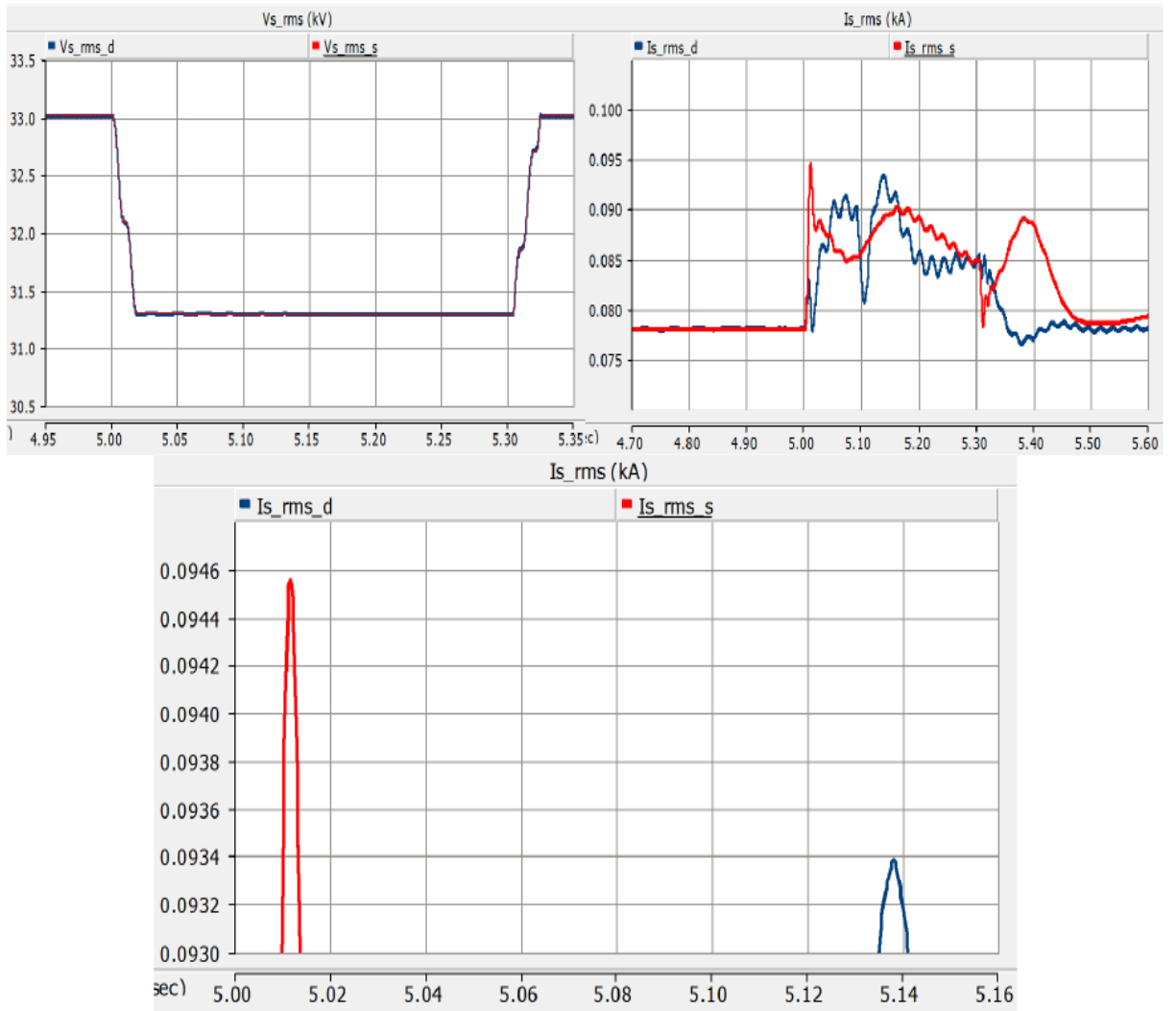


Figure 7.7: Case 3 : $Z_f = 10^{-2} \Omega$

In figure 7.7, the I_{f_max} of the detailed and simplified types are 0.09340 and 0.09455 kA, respectively.

7.1.3.2 Under LL SC Fault

The results of fault type 3, in the PSCAD/EMTDC software.

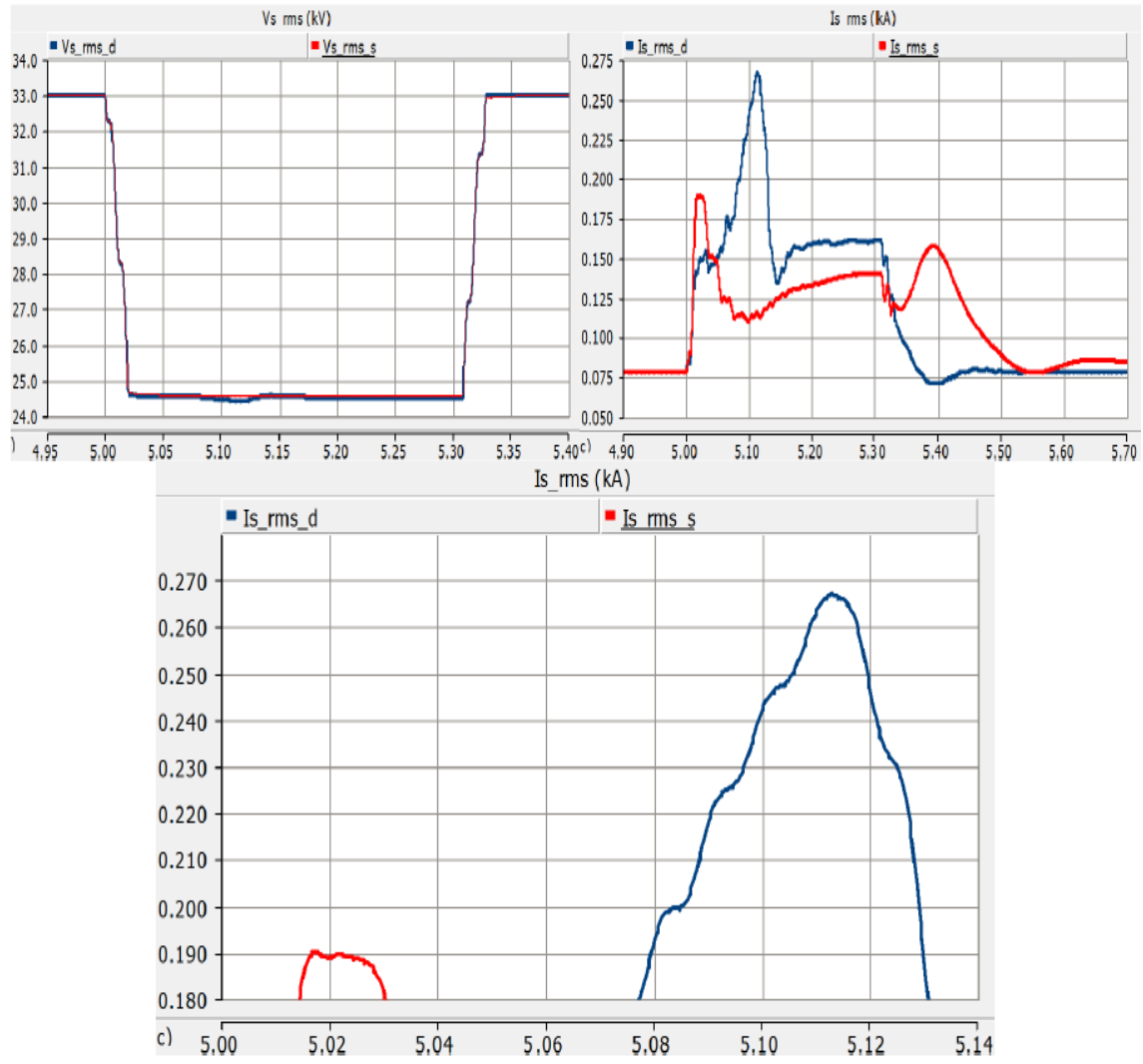


Figure 7.8: Case 1 : $Z_f = 10^{-15} \Omega$

As can be shown in the figure 7.8, the I_{fmax} of the detailed and simplified types are 0.267 and 0.191 kA, respectively.

7. Simulation of Detailed and Simplified Models

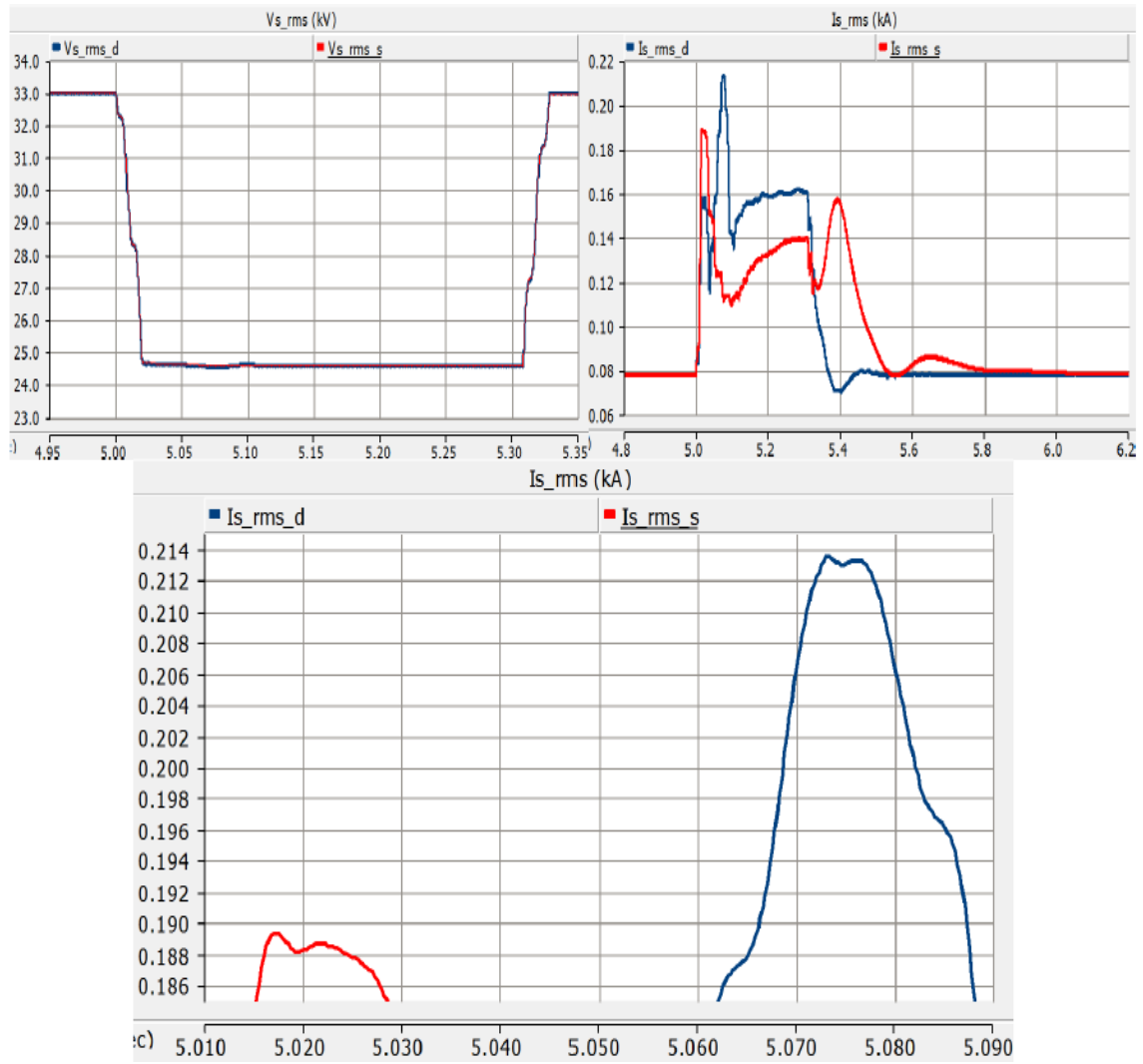


Figure 7.9: Case 2 : $Z_f = 10^{-5} \Omega$

In the figure 7.9, the I_{f_max} of the detailed and simplified types are 0.2135 and 0.189 kA, respectively.

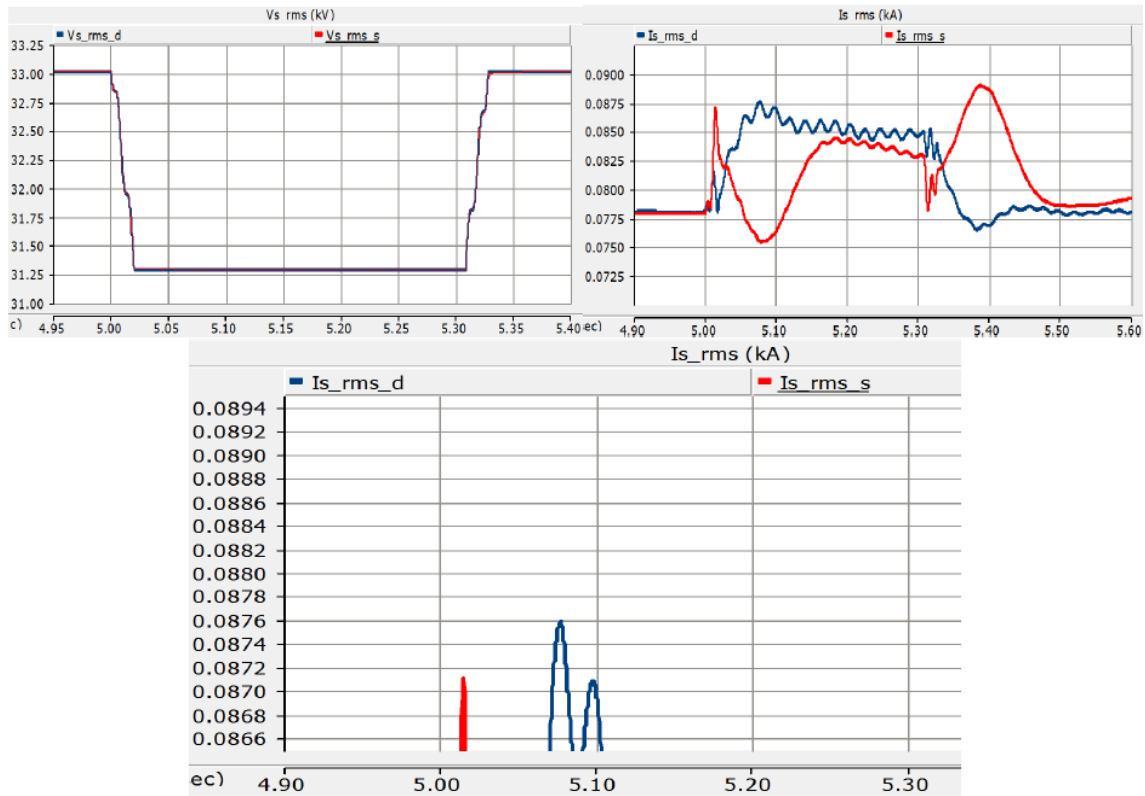


Figure 7.10: Case 3 : $Z_f = 10^{-2} \Omega$

In the figure 7.10, the I_{fmax} of the detailed and simplified types are 0.0876 and 0.0871 kA, respectively.

The voltage dip and fault current changes during the LL SC fault, which took 0.3 seconds for same values of fault impedance, can be noticed in figures 7.8, 7.9 and 7.10, respectively.

7.1.3.3 Under LLG SC Fault

The results of fault type 2, in the PSCAD/EMTDC software.

7. Simulation of Detailed and Simplified Models

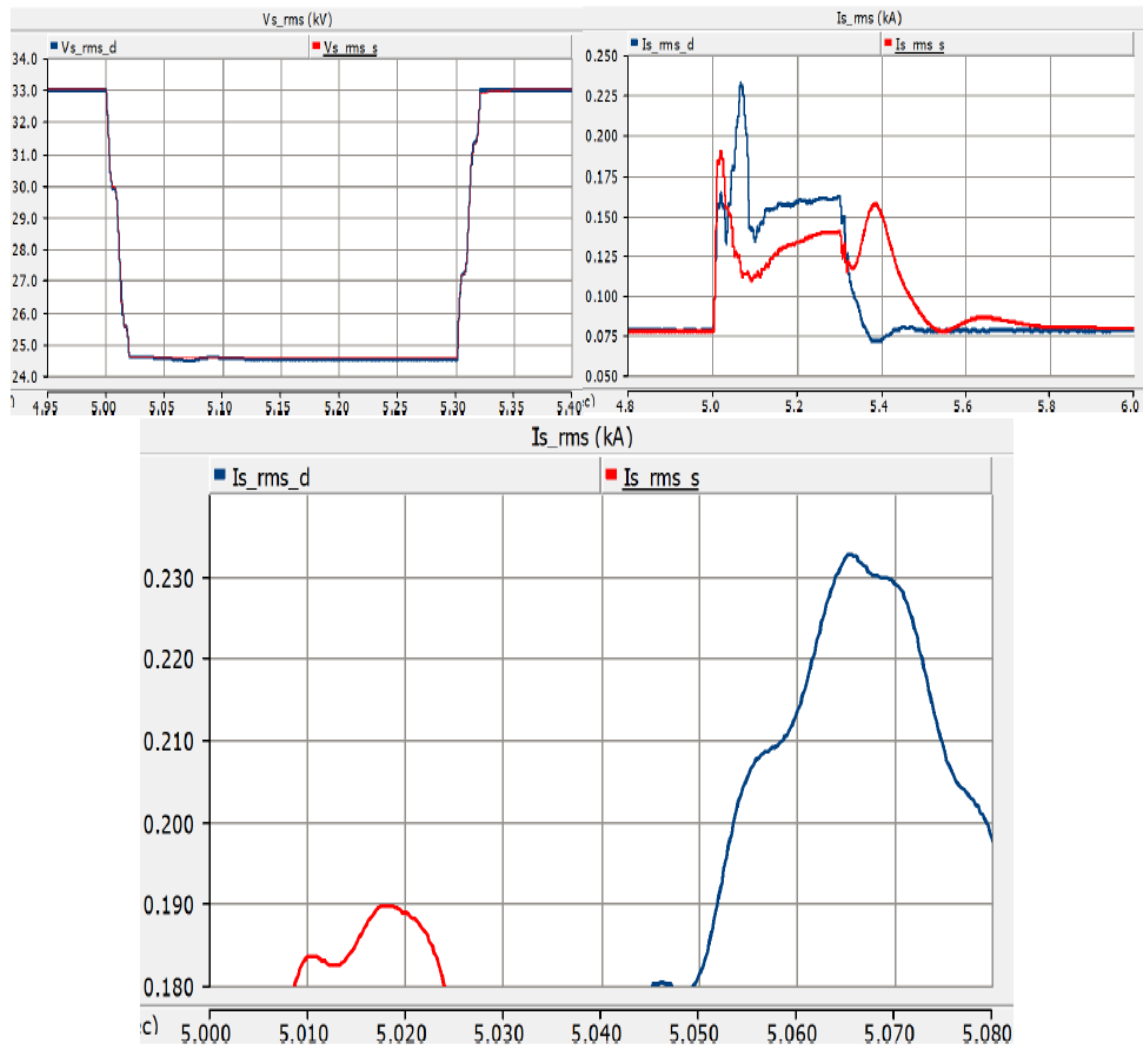


Figure 7.11: Case 1 : $Z_f = 10^{-15} \Omega$

As can be demonstrated in the figure 7.11, the I_{fmax} of the detailed and simplified types are 0.234 and 0.190 kA, respectively.

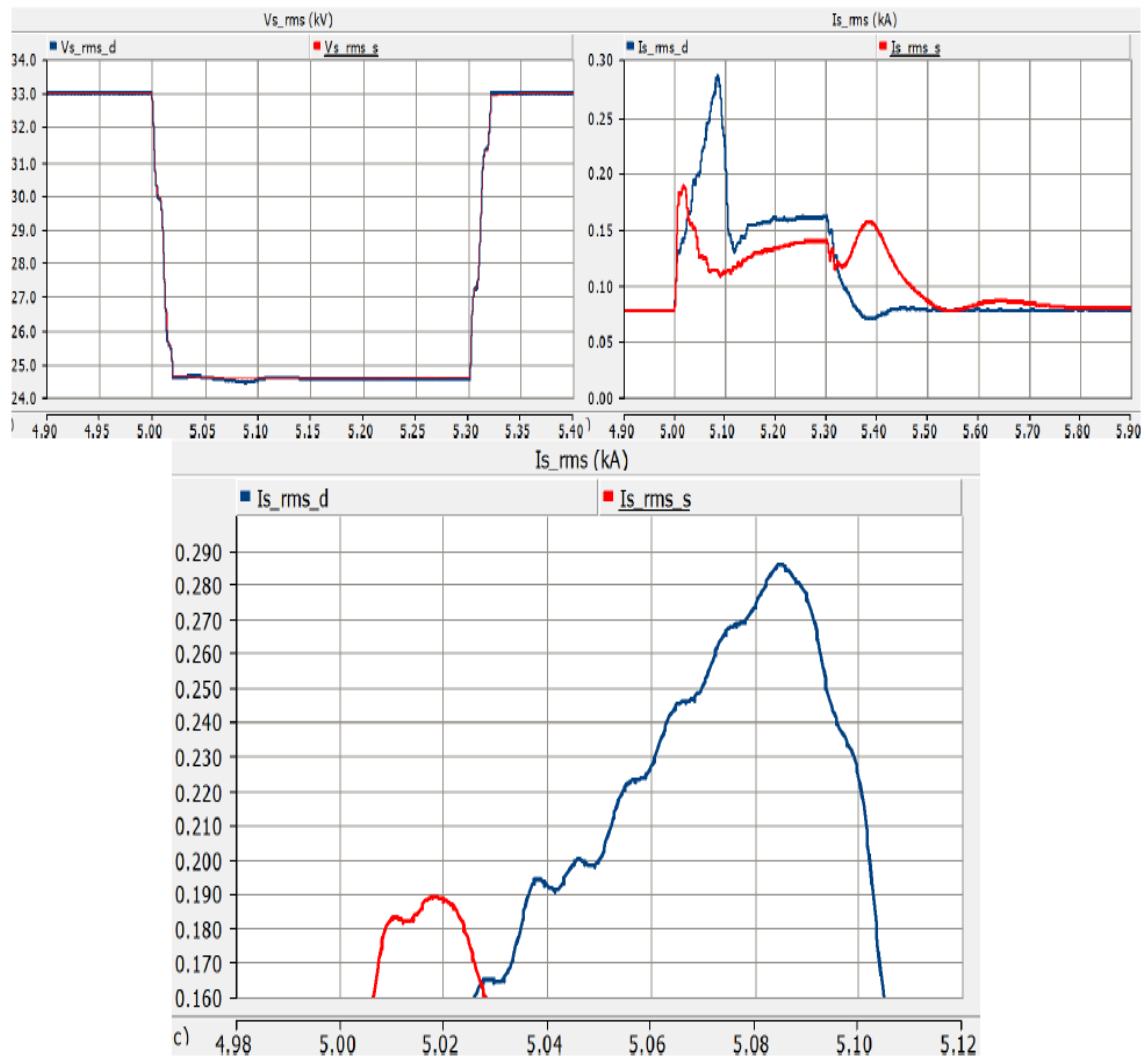


Figure 7.12: Case 2 : $Z_f = 10^{-5} \Omega$

In the figure 7.12, the I_{fmax} of the detailed and simplified types are 0.286 and 0.190 kA, respectively.

7. Simulation of Detailed and Simplified Models

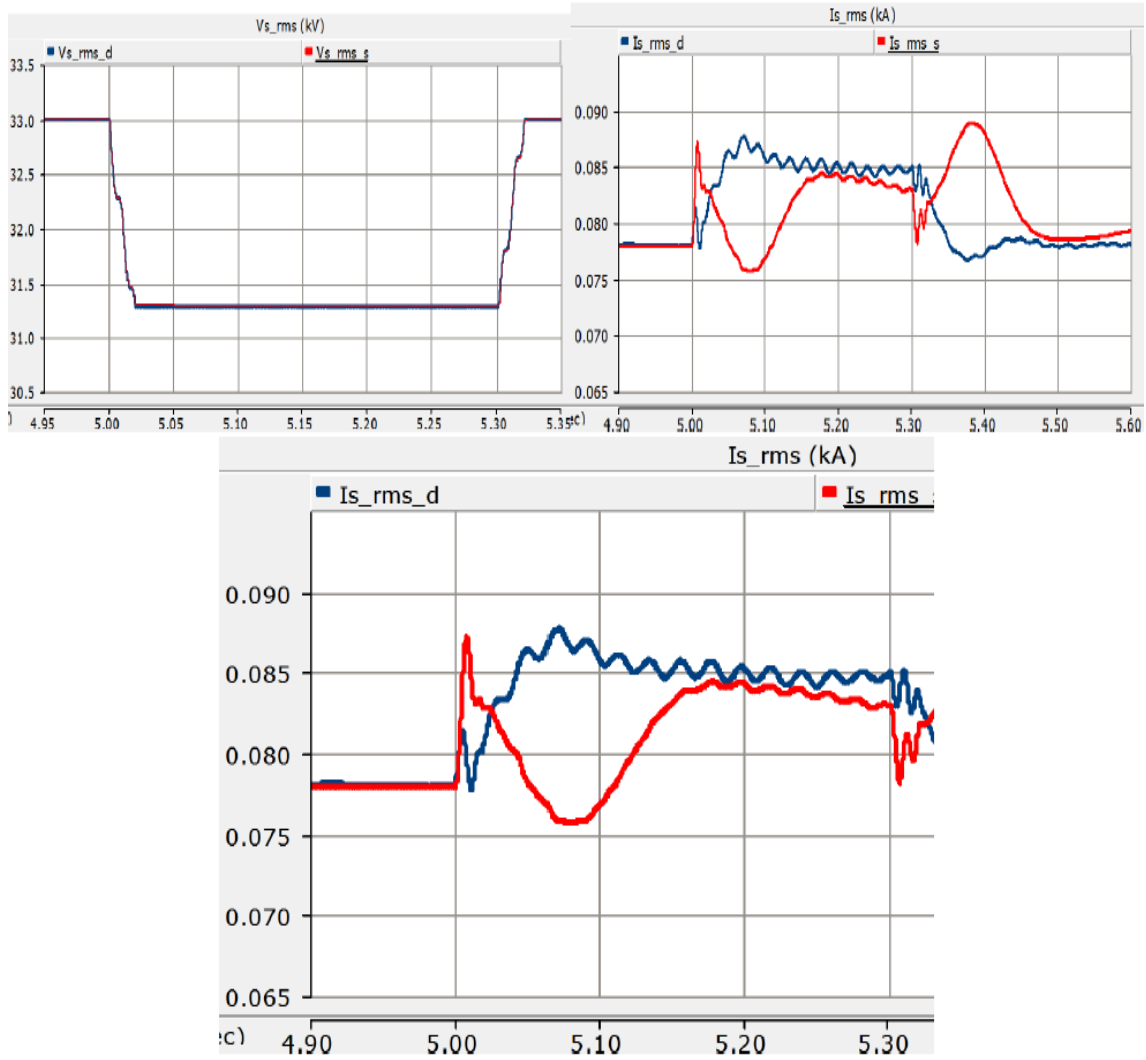


Figure 7.13: Case 3 : $Z_f = 10^{-2} \Omega$

In the figure 7.13, the I_{fmax} of the detailed and simplified types are 0.08885 and 0.0877 kA, respectively.

Finally, the voltage dip and fault current changes during the LLG SC fault, with same conditions as the previous cases, can be seen in figures 7.11, 7.12 and 7.13, respectively.

Sequentially, the below table can be used to summarize, the behavior of the simplified model in terms of different fault types and impedance.

As can be noticed, the acceptable and unacceptable cases have been indicated in the table 7.1. These results achieved by comparing the I_{fmax} of the detailed model and the simplified one.

Obviously, in the most cases the results are acceptable, by comparing the results of the detailed model with the simplified ones, except during faults 1 and 2 when the

fault impedance is too low and medium , 10^{-15} and 10^{-5} , respectively. In order to find the acceptable results for these cases the two improved models for the simplified type will be analyzed in the next chapter.

Table 7.1: The simplified type behaviors

Simplified Type	Fault 1	Fault 2	Fault 3	Fault 4
$Z_f = 10^{-15} \Omega$	Acceptable	Unacceptable	*Acceptable	Acceptable
$Z_f = 10^{-5} \Omega$	Acceptable	Unacceptable	Unacceptable	Acceptable
$Z_f = 10^{-2} \Omega$	Acceptable	Acceptable	Acceptable	Acceptable

* It is not completely close to the detailed value but is the best one that can be achieved.

The acceptable range for difference between the pick values of the overcurrent between detailed model and simplified one considered at around 10 %.

8

Simulation of the Detailed and Improved Simplified Models of the DFIG WT, Under SC Faults

This chapter includes the two different improved simplified models of DFIG WT, which will be controlled with other passive elements in the rotor circuit, will be analyzed under different types of SC faults with as same fault conditions as detailed model.

8.0.1 Improved Simplified Model

To reach this aim, two different model can be executed. Initially, using an extra resistance branch in parallel with the previous branch, which included parallel resistance and capacitor, on the rotor side. This extra branch that is open during steady-state and will be closed when fault happens.

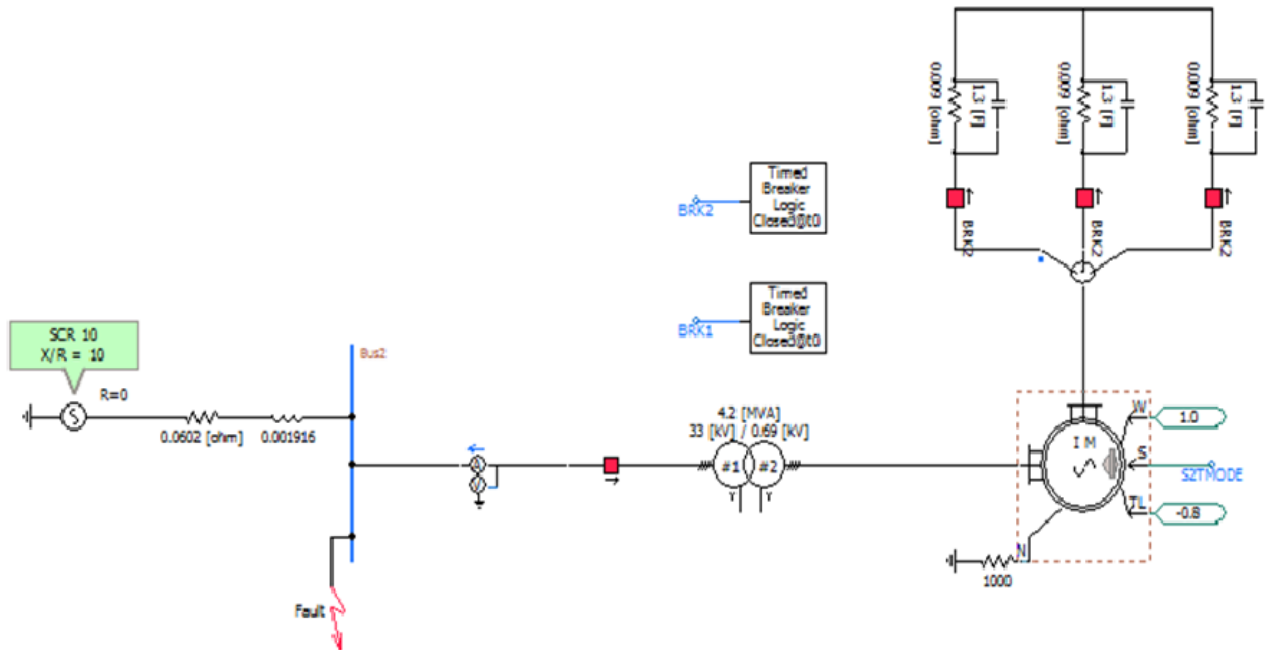


Figure 8.1: Improved Simplified Model Type 1

8. Simulation of the Detailed and Improved Simplified Models of the DFIG WT, Under SC Faults

Sequentially, the second improved type is as same as previous one, but the parallel resistance and capacitor branch has breaker that will open it during the fault.

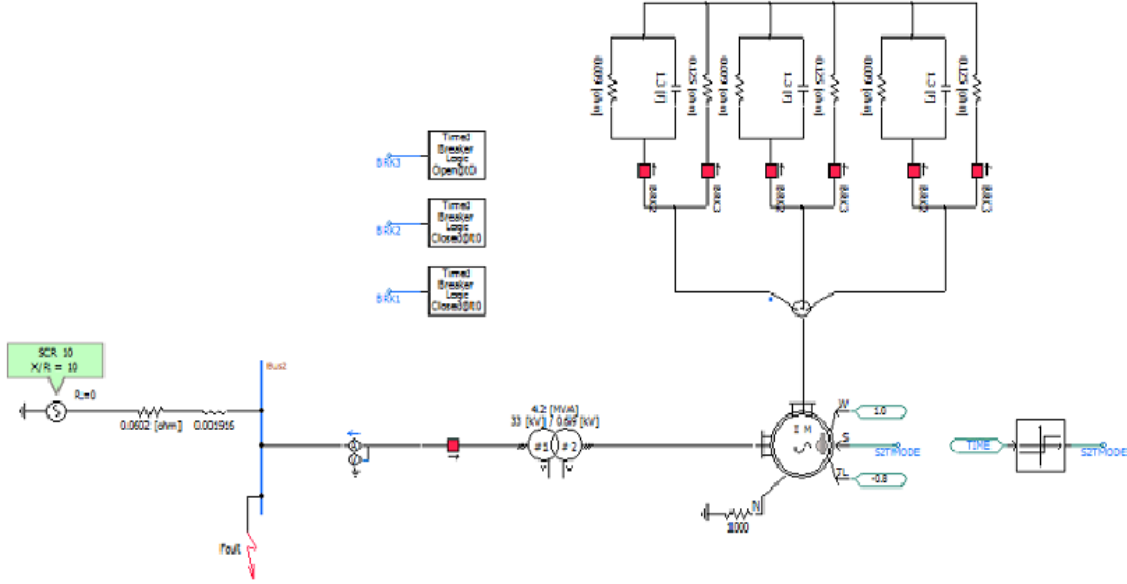


Figure 8.2: Improved Simplified Model Type 2

In order to choose the amplitude of the extra resistance, the value of the chopper resistance in the detailed model can be helpful. Firstly, for extra resistance 0.125Ω and then two different values like 1.25 and 0.00125Ω will be tested.

In below figures, the detailed model behaviors will be compared with the improved simplified models types 1 and 2 (The blue curves represent the detailed model and the red ones indicate the simplified types). Note, the left columns belong to type 1 and the right columns belong to type 2.

The main focus of these below results is on the models with $Z_f = 10^{-15}$ and $10^{-2} \Omega$ during faults 2 and 3.

8.0.2 Models Under Symmetrical SC Faults

Initially, the symmetrical SC Fault will be added into the detailed and improved simplified models, which is categorized into types 1 and 2, of the DFIG WT in order to examined it.

8.0.2.1 Under LLLG SC Fault

The results of fault type 4, in the PSCAD/EMTDC software.

Figures 8.3, 8.4 and 8.5 represent the voltage dip and fault current of improved simplified DFIG types 1 and 2 when fault impedance is so low (10^{-15} ohm) with different values of R_{ex} under LLLG SC fault.

8. Simulation of the Detailed and Improved Simplified Models of the DFIG WT,
Under SC Faults

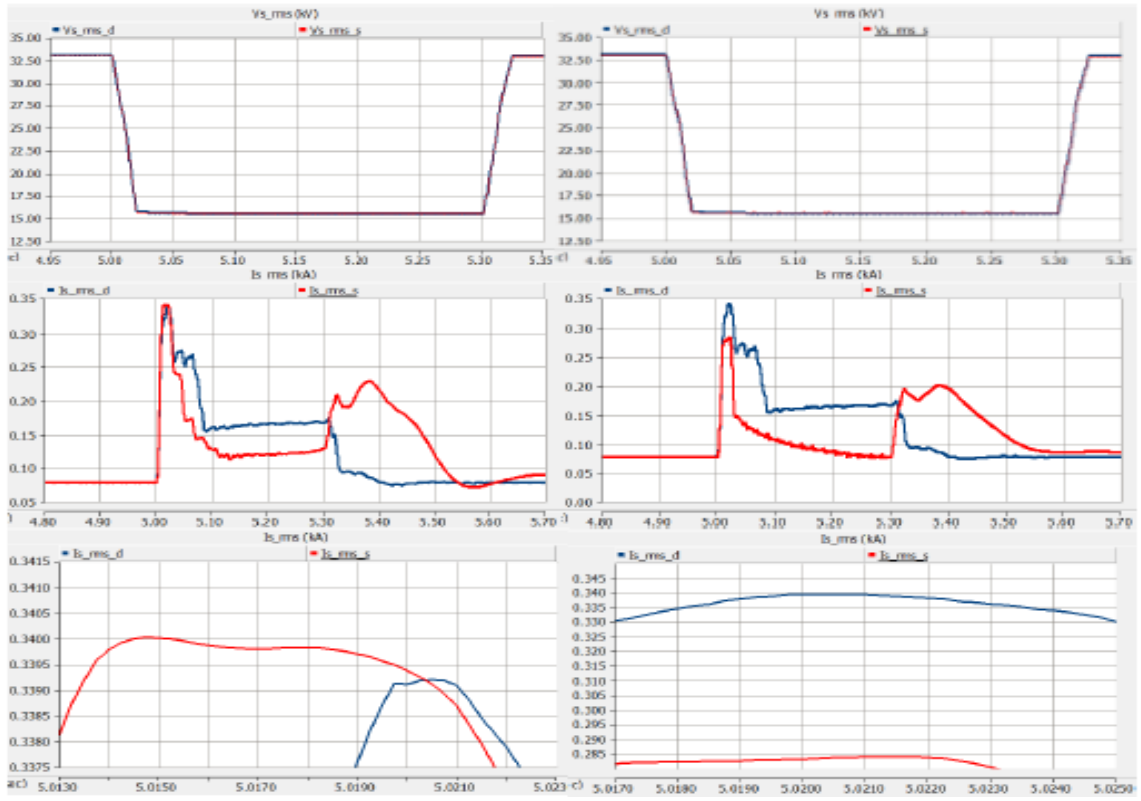


Figure 8.3: Improved type 1 & 2, Case 1 : $Z_f = 10^{-15} \Omega$ & $R_{ex} = 0.125 \Omega$.

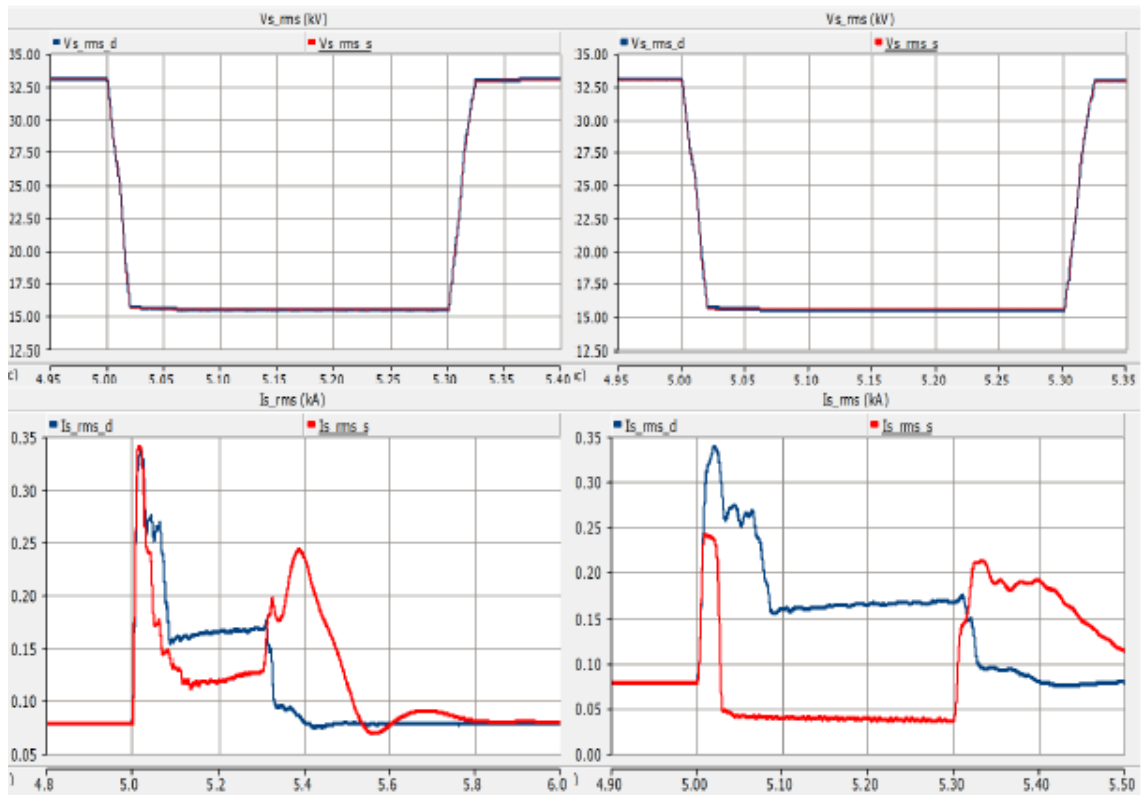


Figure 8.4: Improved type 1 & 2, Case 2 : $Z_f = 10^{-15} \Omega$ & $R_{ex} = 1.25 \Omega$.

8. Simulation of the Detailed and Improved Simplified Models of the DFIG WT, Under SC Faults

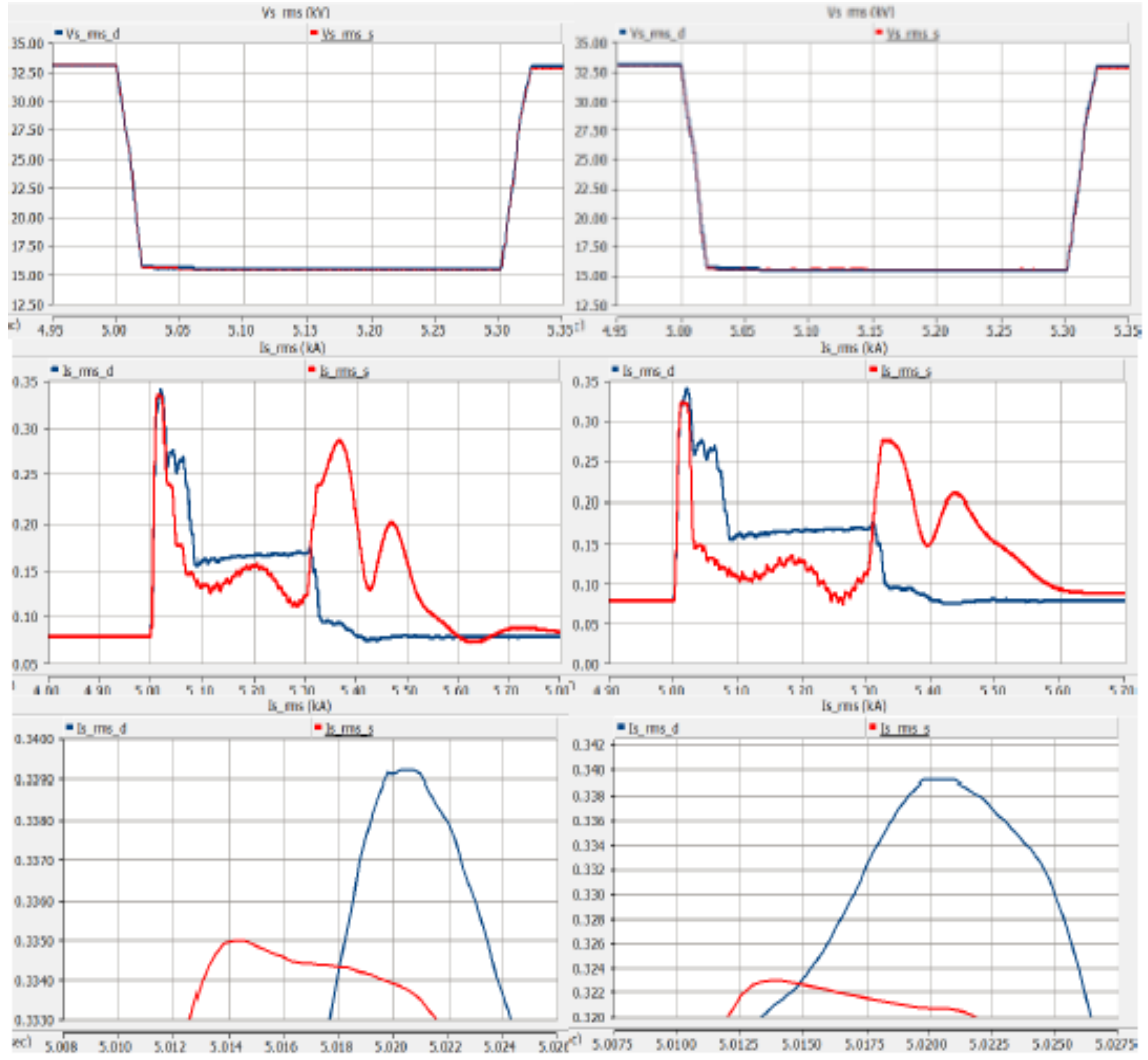


Figure 8.5: Improved type 1 & 2, Case 3 : $Z_f = 10^{-15} \Omega$ & $R_{ex} = 0.00125 \Omega$.

Figures 8.6, 8.7 and 8.8 represent the voltage dip and fault current of improved simplified DFIG types 1 and 2 when fault impedance has the medium amplitude (10^{-5} ohm) with different values of R_{ex} under LLLG SC fault.

8. Simulation of the Detailed and Improved Simplified Models of the DFIG WT,
Under SC Faults

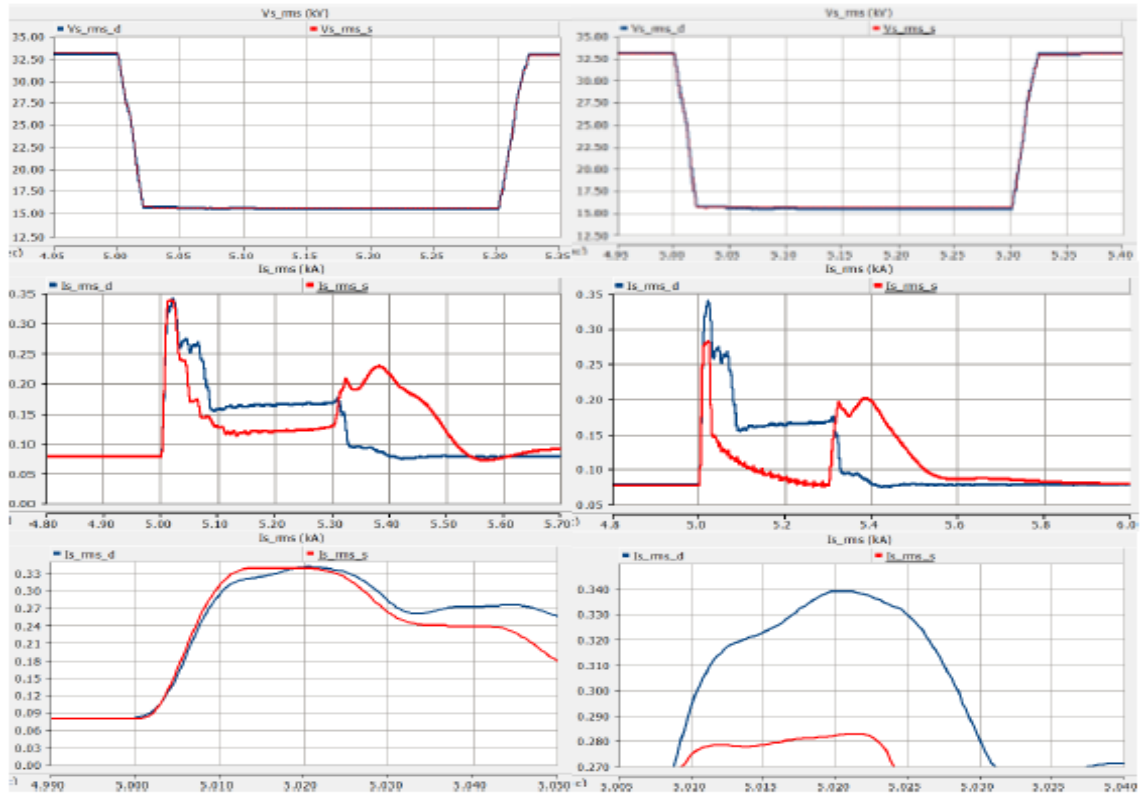


Figure 8.6: Improved type 1 & 2, Case 4 : $Z_f = 10^{-5} \Omega$ & $R_{ex} = 0.125 \Omega$.

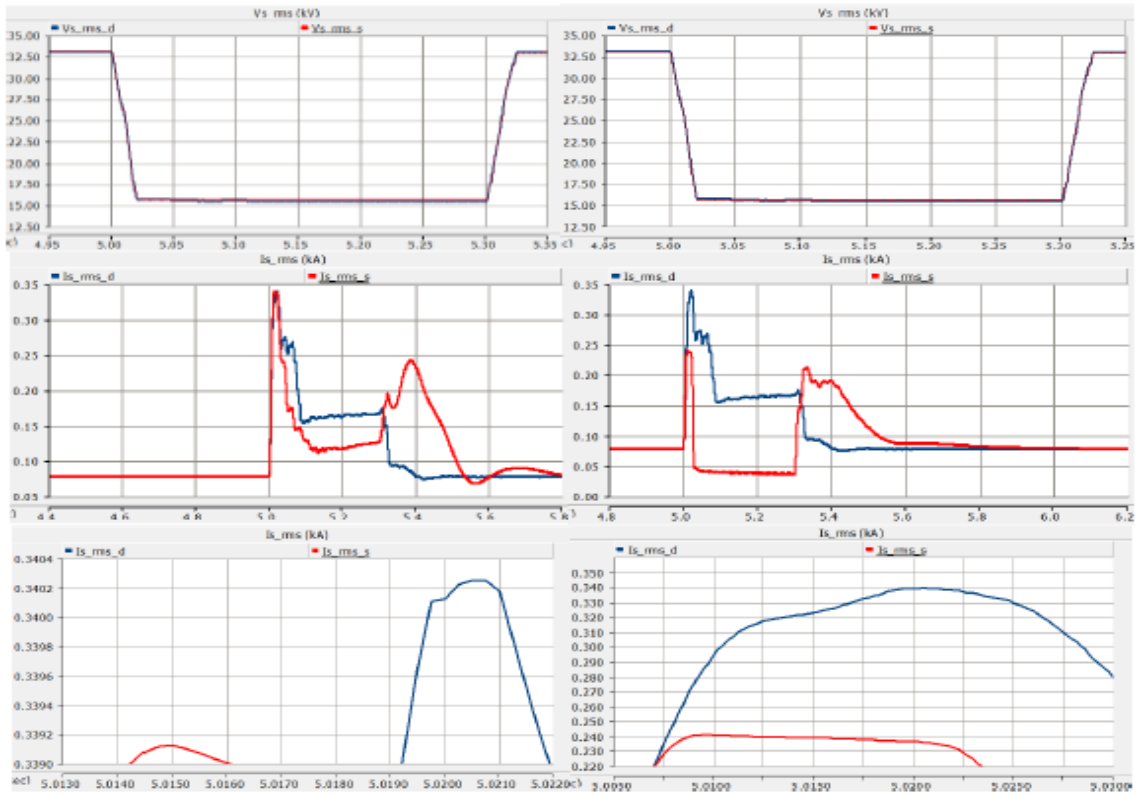


Figure 8.7: Improved type 1 & 2, Case 5 : $Z_f = 10^{-5} \Omega$ & $R_{ex} = 1.25 \Omega$.

8. Simulation of the Detailed and Improved Simplified Models of the DFIG WT, Under SC Faults

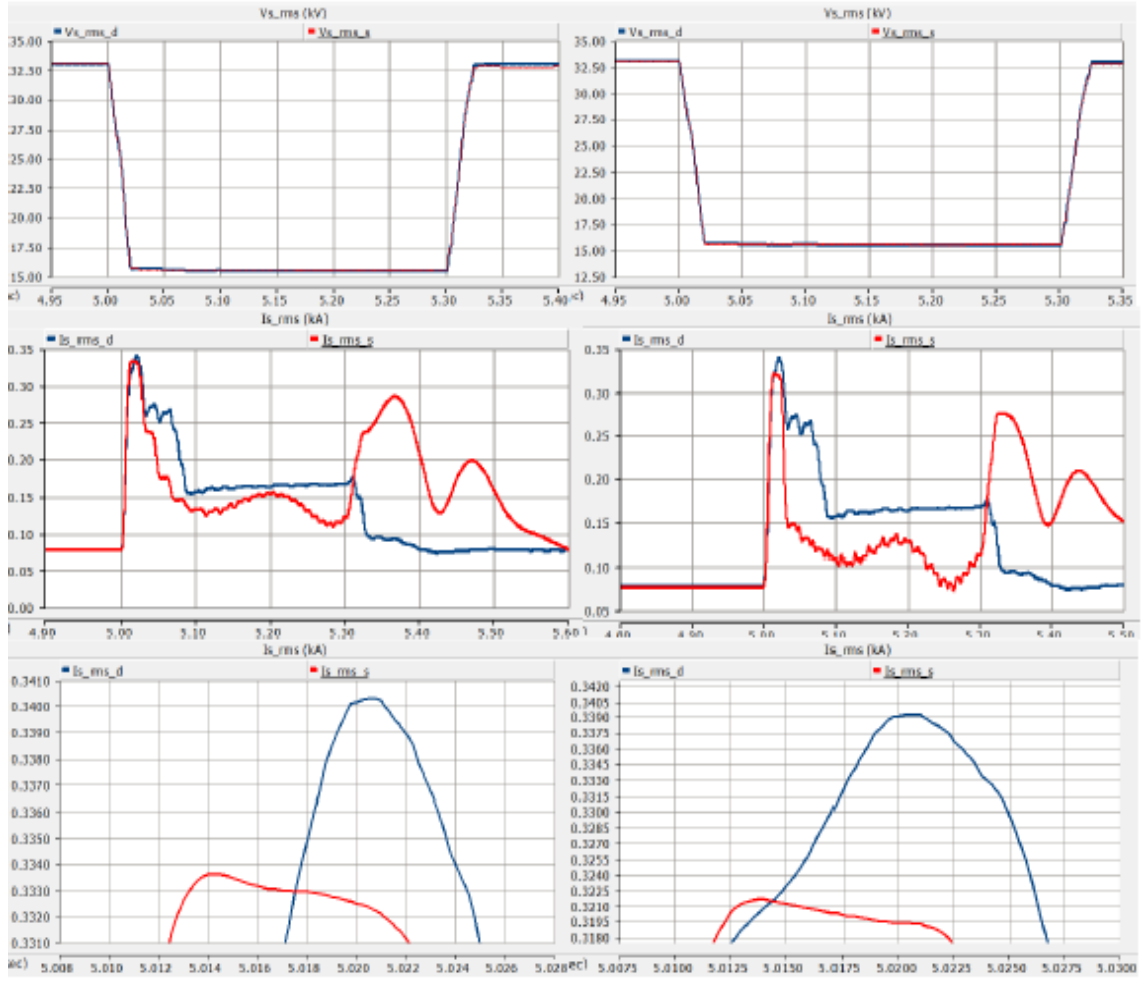


Figure 8.8: Improved type 1 & 2, Case 6 : $Z_f = 10^{-5} \Omega$ & $R_{ex} = 0.00125 \Omega$.

Figures 8.9, 8.10 and 8.11 represent the voltage dip and fault current of improved simplified DFIG types 1 and 2 when fault impedance has the highest amplitude (10^{-2} ohm) with different values of R_{ex} under LLLG SC fault.

8. Simulation of the Detailed and Improved Simplified Models of the DFIG WT,
Under SC Faults

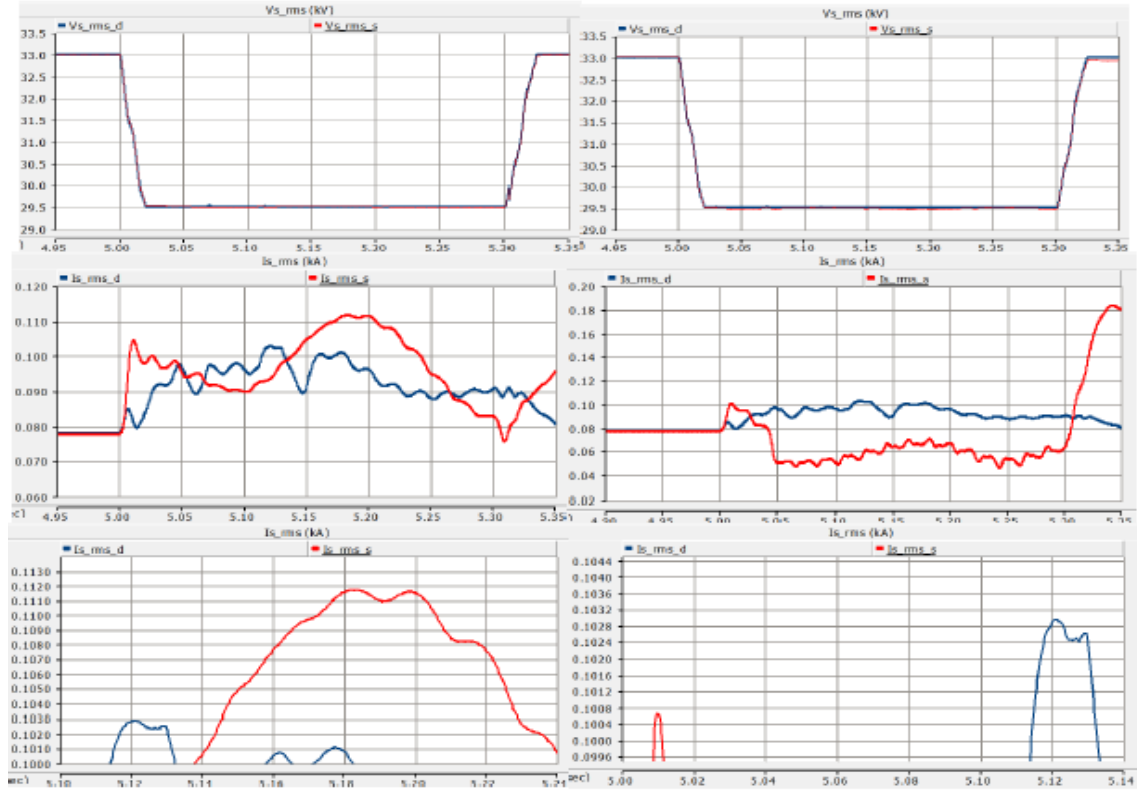


Figure 8.9: Improved type 1 & 2, Case 7 : $Z_f = 10^{-2} \Omega$ & $R_{ex} = 0.125 \Omega$.

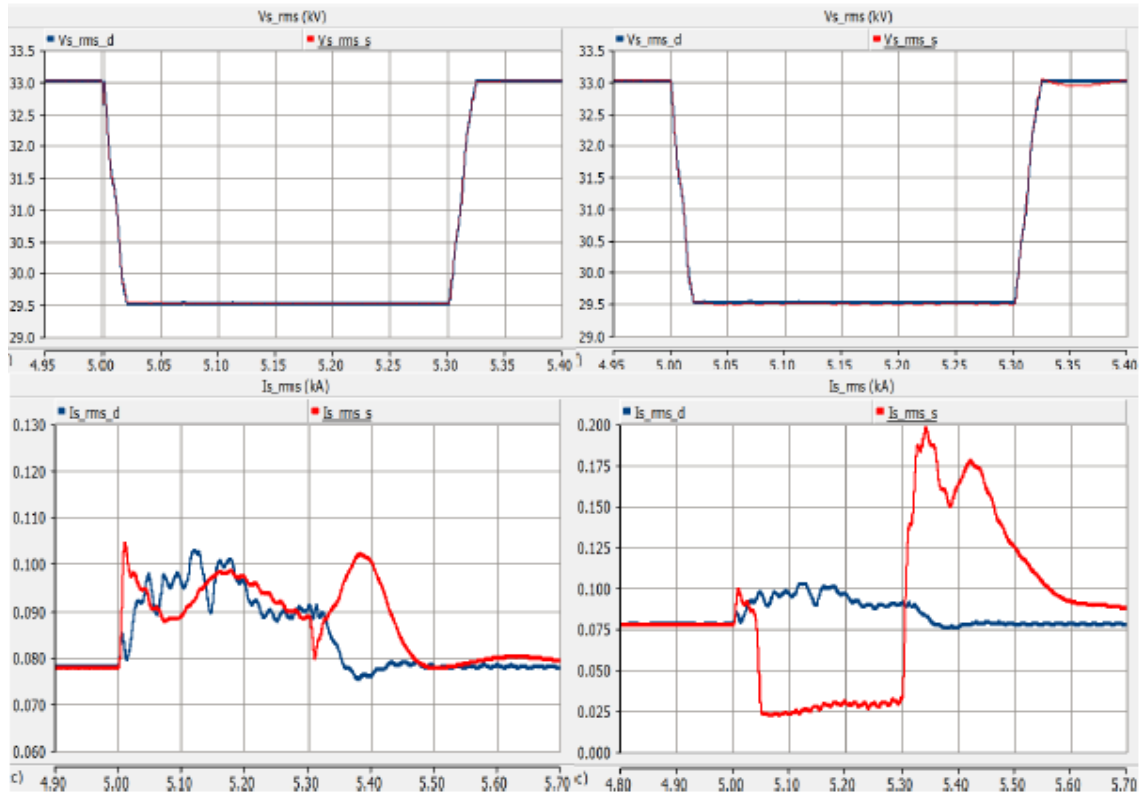


Figure 8.10: Improved type 1 & 2, Case 8 : $Z_f = 10^{-2} \Omega$ & $R_{ex} = 1.25 \Omega$.

8. Simulation of the Detailed and Improved Simplified Models of the DFIG WT, Under SC Faults

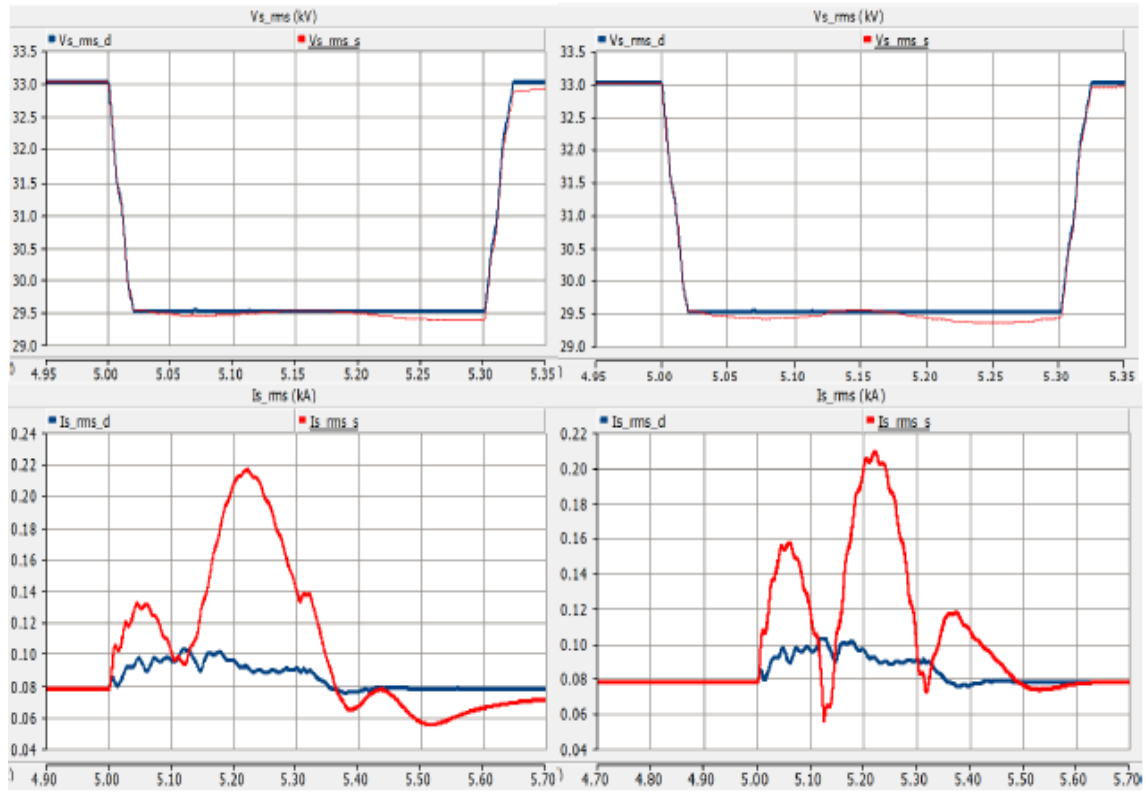


Figure 8.11: Improved type 1 & 2, Case 9 : $Z_f = 10^{-2} \Omega$ & $R_{ex} = 0.00125 \Omega$.

8.0.3 Models Under Unsymmetrical SC Faults

Now, the unsymmetrical SC Fault will be added into the detailed and improved simplified models, which is categorized into types 1 and 2, models of the DFIG WT.

8.0.3.1 Under SLG SC Fault

The results of fault type 1, in the PSCAD/EMTDC software.

8. Simulation of the Detailed and Improved Simplified Models of the DFIG WT, Under SC Faults

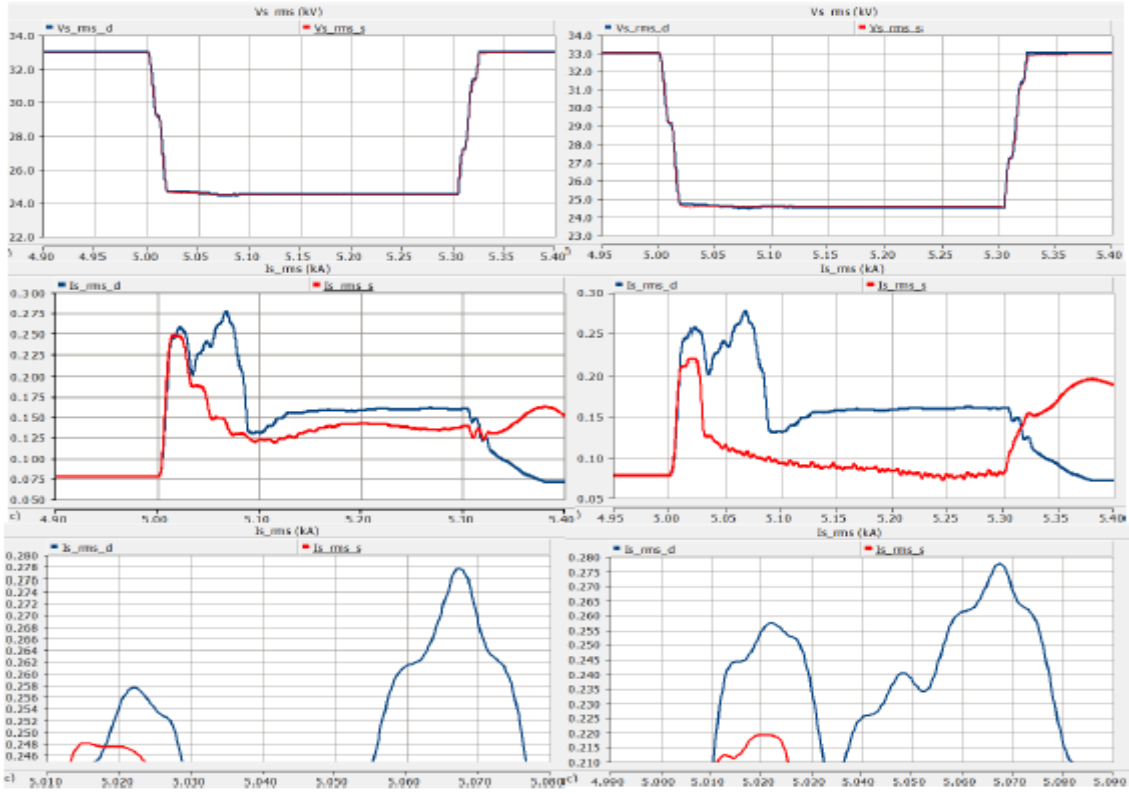


Figure 8.12: Improved type 1 & 2, Case 1 : $Z_f = 10^{-15} \Omega$ & $R_{ex} = 0.125 \Omega$.

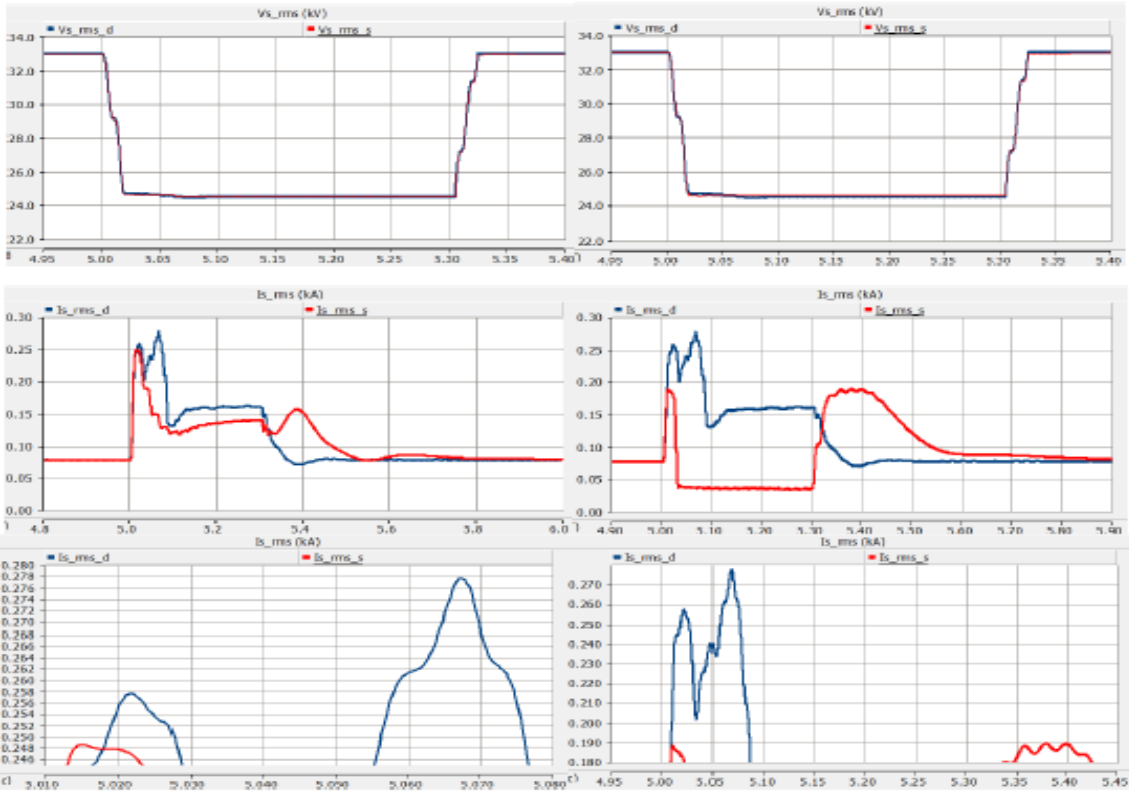


Figure 8.13: Improved type 1 & 2, Case 2 : $Z_f = 10^{-15} \Omega$ & $R_{ex} = 1.25 \Omega$.

8. Simulation of the Detailed and Improved Simplified Models of the DFIG WT, Under SC Faults

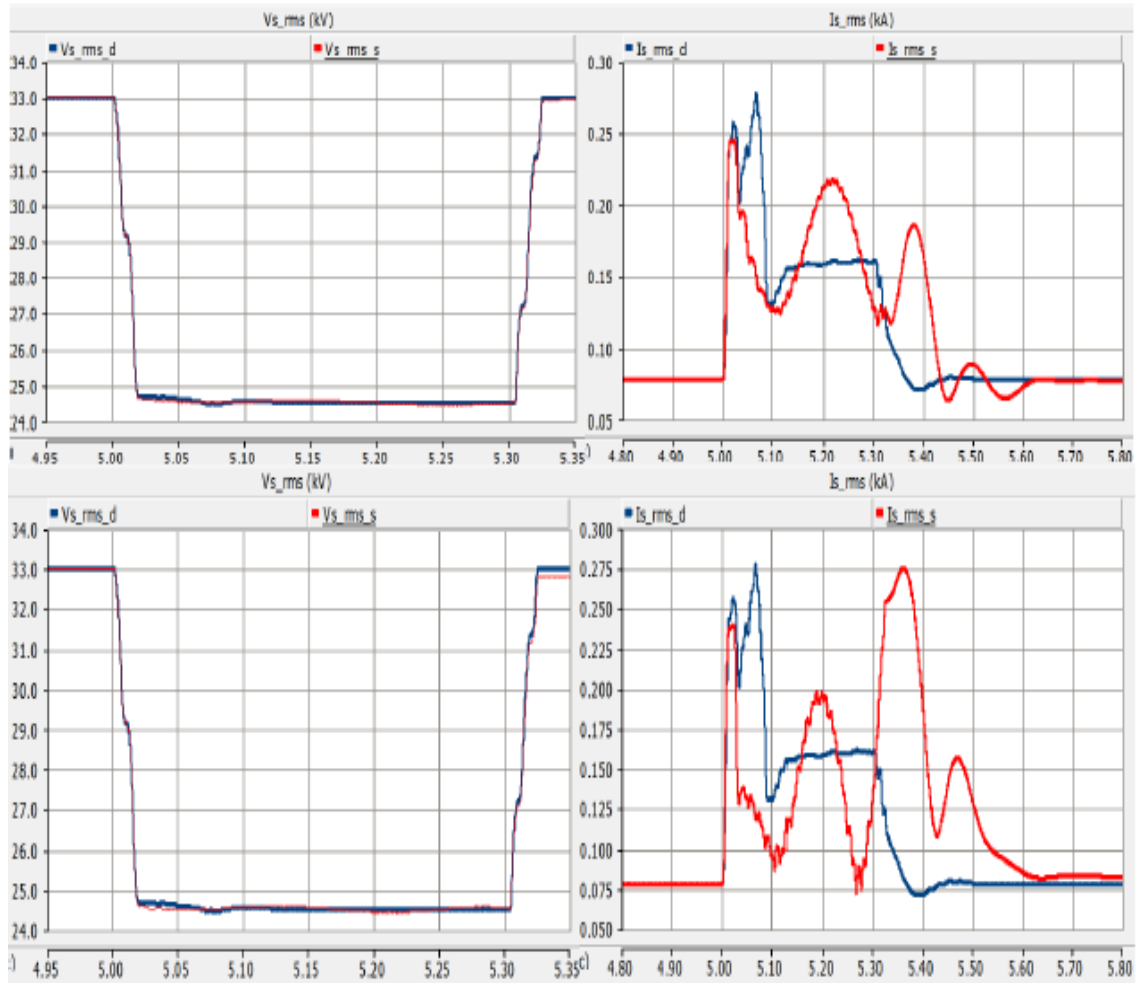


Figure 8.14: Improved type 1 & 2, Case 3 : $Z_f = 10^{-15} \Omega$ & $R_{ex} = 0.00125 \Omega$.

Figures 8.12, 8.13 and 8.14 represent the voltage dip and fault current of improved simplified DFIG types 1 and 2 when fault impedance has the lowest amplitude (10^{-15} ohm) with different values of R_{ex} under SLG SC fault.

8. Simulation of the Detailed and Improved Simplified Models of the DFIG WT, Under SC Faults

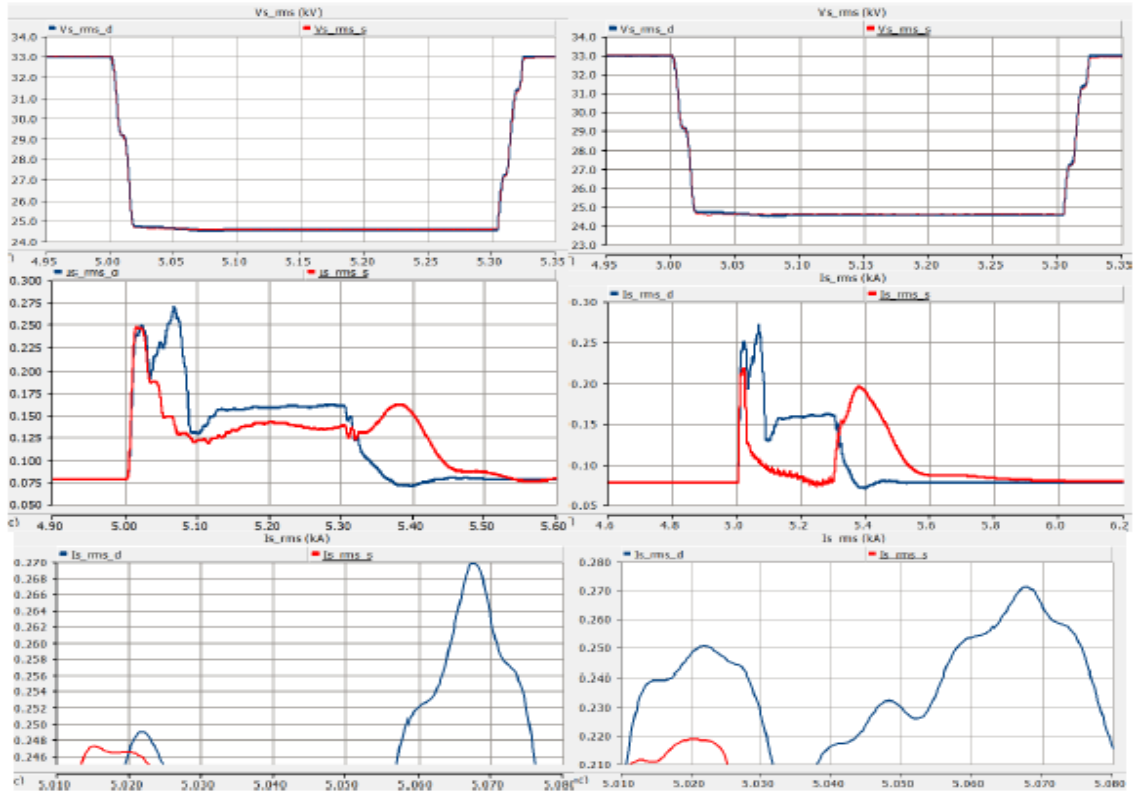


Figure 8.15: Improved type 1 & 2, Case 4 : $Z_f = 10^{-5} \Omega$ & $R_{ex} = 0.125 \Omega$.

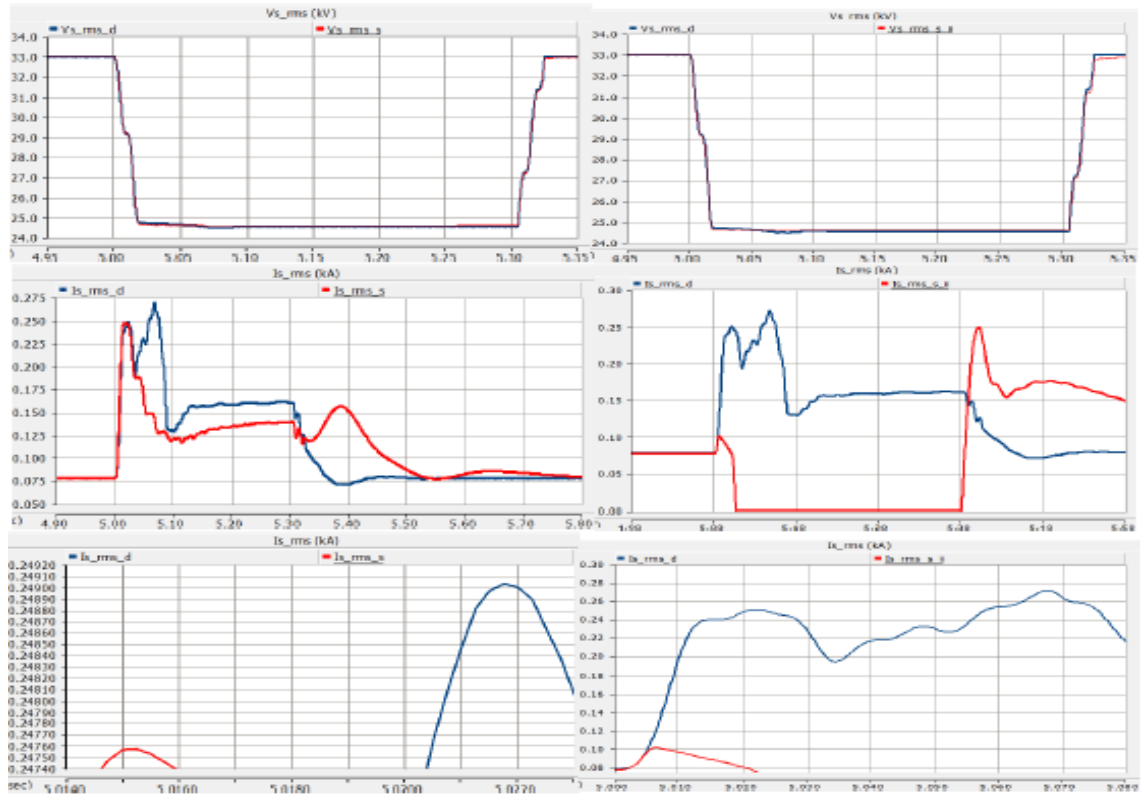


Figure 8.16: Improved type 1 & 2, Case 5 : $Z_f = 10^{-5} \Omega$ & $R_{ex} = 1.25 \Omega$.

8. Simulation of the Detailed and Improved Simplified Models of the DFIG WT, Under SC Faults

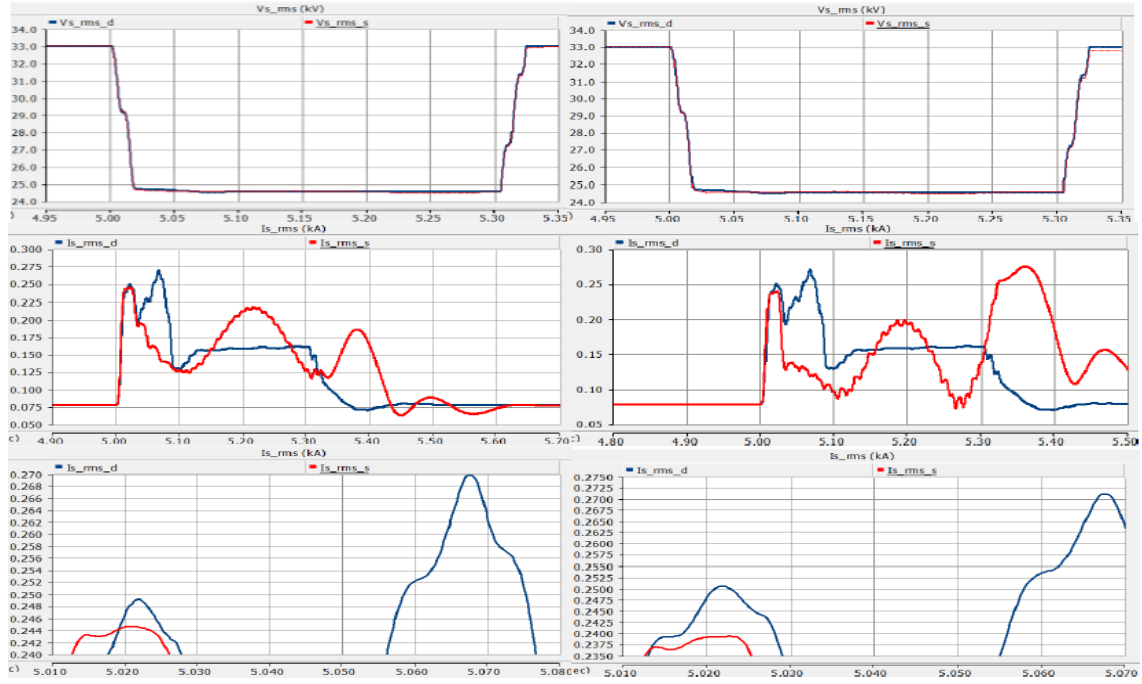


Figure 8.17: Improved type 1 & 2, Case 6 : $Z_f = 10^{-5} \Omega$ & $R_{ex} = 0.00125 \Omega$.

Figures 8.15, 8.16 and 8.17 represent the voltage dip and fault current of improved simplified DFIG types 1 and 2 when fault impedance has the medium amplitude (10^{-5} ohm) with different values of R_{ex} under SLG SC fault.

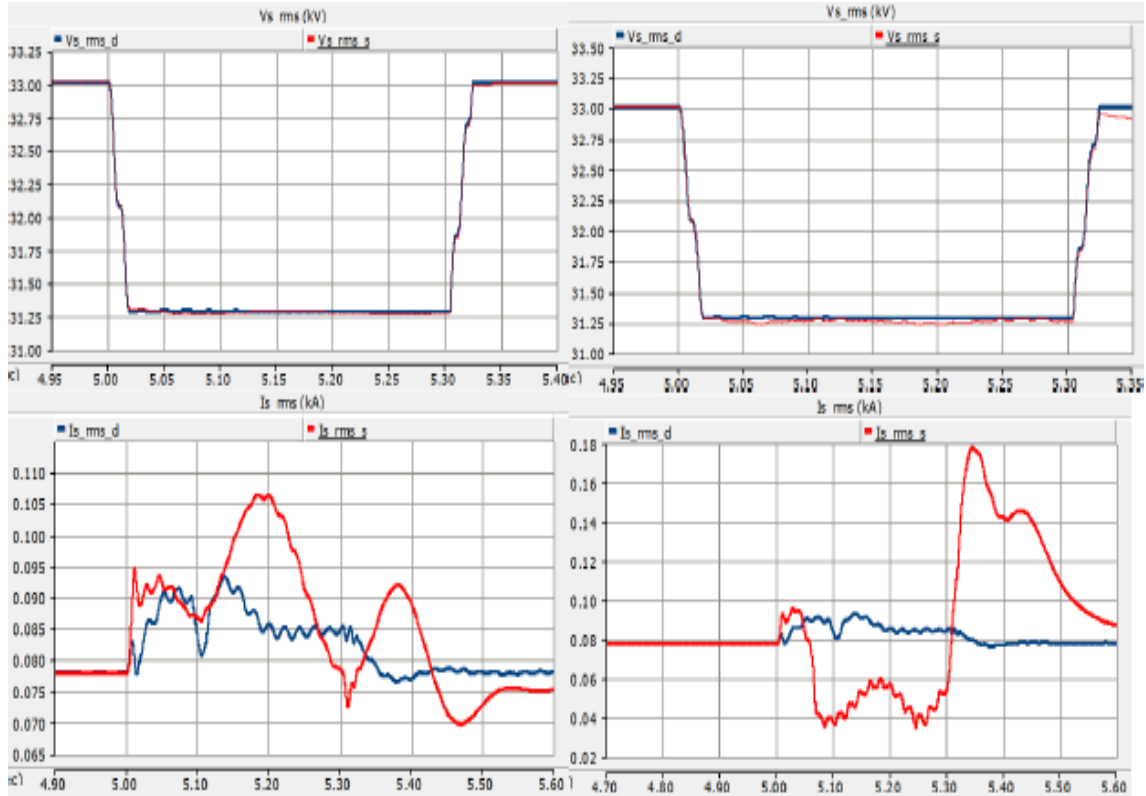


Figure 8.18: Improved type 1 & 2, Case 7 : $Z_f = 10^{-2} \Omega$ & $R_{ex} = 0.125 \Omega$.

8. Simulation of the Detailed and Improved Simplified Models of the DFIG WT,
Under SC Faults

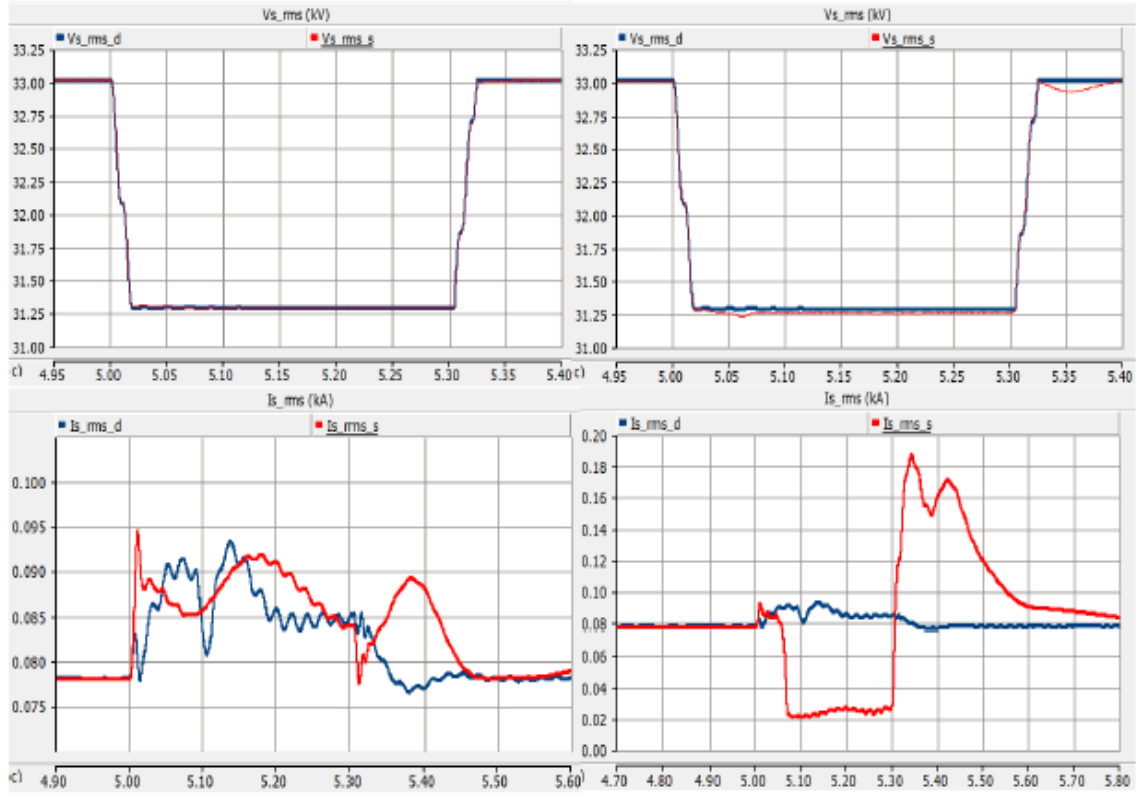


Figure 8.19: Improved type 1 & 2, Case 8 : $Z_f = 10^{-2} \Omega$ & $R_{ex} = 1.25 \Omega$.

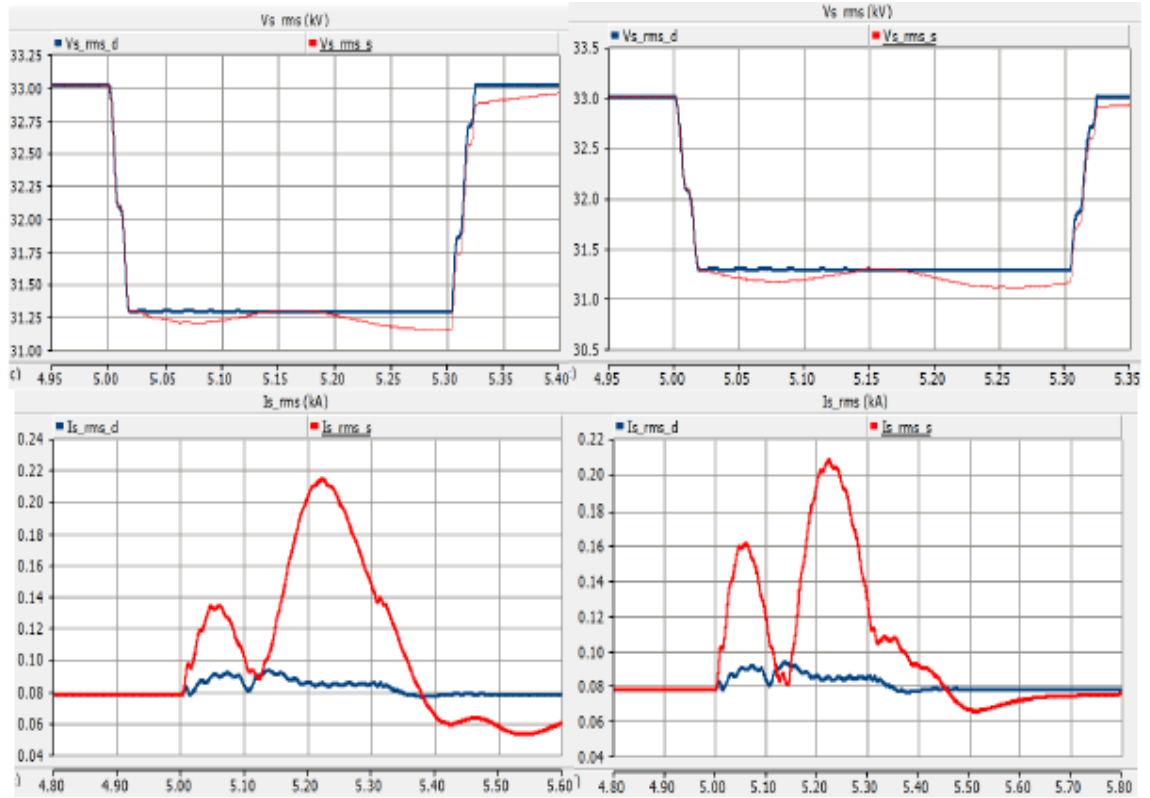


Figure 8.20: Improved type 1 & 2, Case 9 : $Z_f = 10^{-2} \Omega$ & $R_{ex} = 0.00125 \Omega$.

8. Simulation of the Detailed and Improved Simplified Models of the DFIG WT, Under SC Faults

Figures 8.18, 8.19 and 8.20 represent the voltage dip and fault current of improved simplified DFIG types 1 and 2 when fault impedance has the highest amplitude (10^{-5} ohm) with different values of R_{ex} under SLG SC fault.

8.0.3.2 Under LL SC Fault

The results of fault type 3, in the PSCAD/EMTDC software.

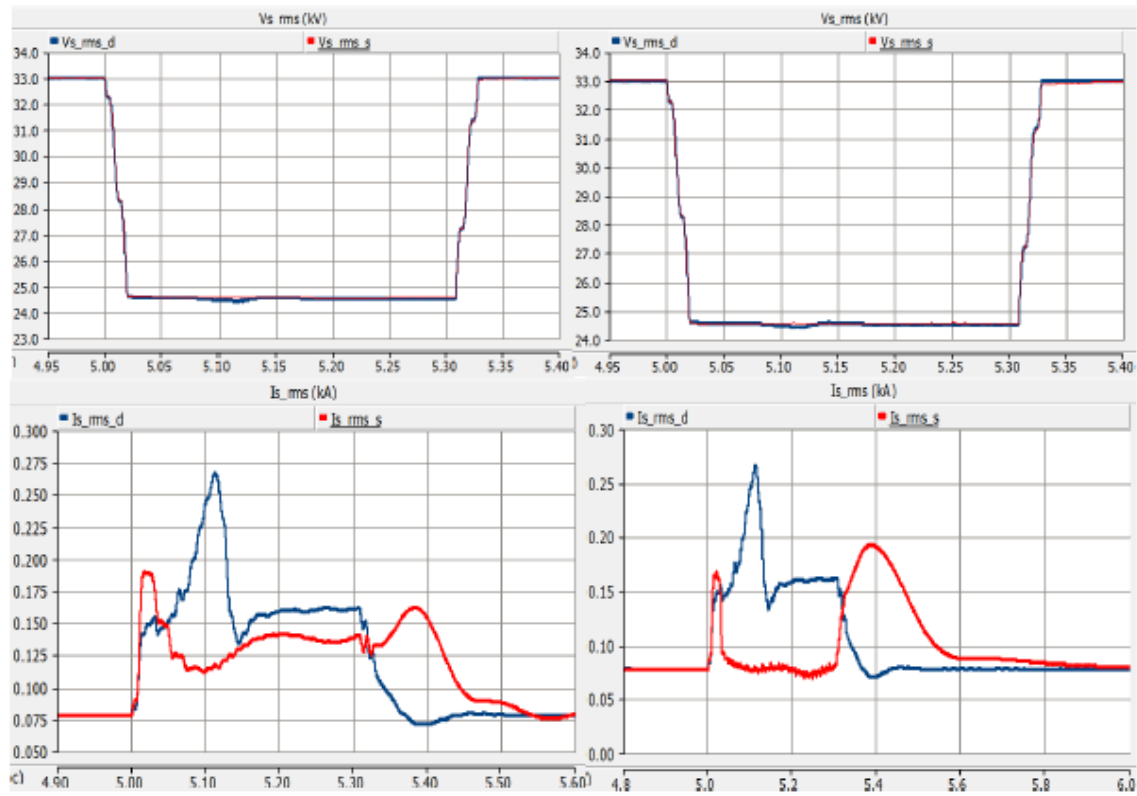


Figure 8.21: Improved type 1 & 2, Case 1 : $Z_f = 10^{-15} \Omega$ & $R_{ex} = 0.125 \Omega$.

8. Simulation of the Detailed and Improved Simplified Models of the DFIG WT,
Under SC Faults

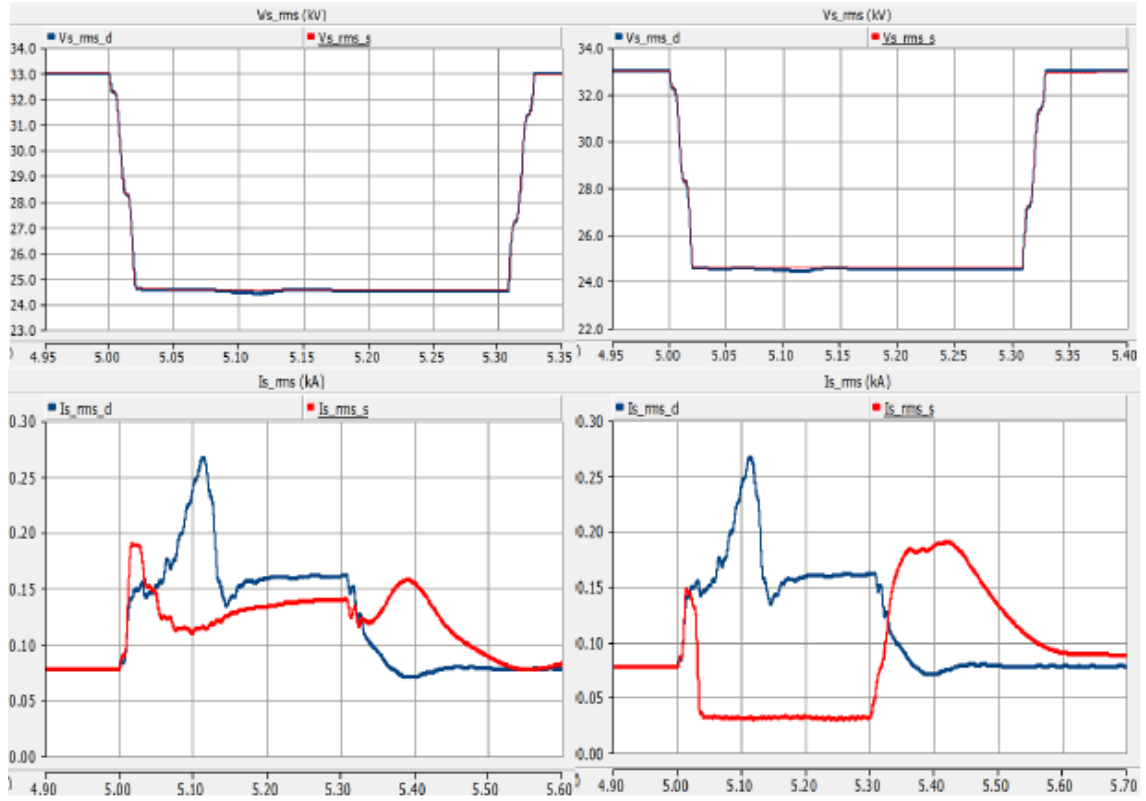


Figure 8.22: Improved type 1 & 2, Case 2 : $Z_f = 10^{-15} \Omega$ & $R_{ex} = 1.25 \Omega$.

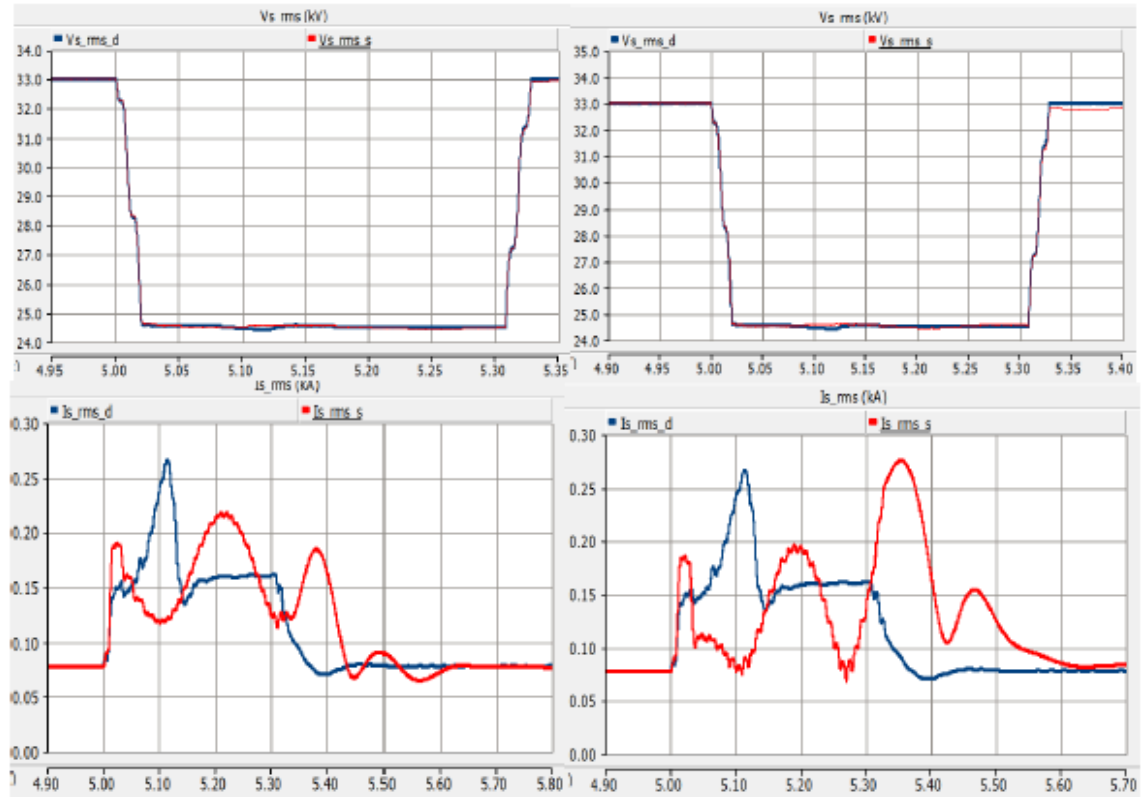


Figure 8.23: Improved type 1 & 2, Case 3 : $Z_f = 10^{-15} \Omega$ & $R_{ex} = 0.00125 \Omega$.

8. Simulation of the Detailed and Improved Simplified Models of the DFIG WT, Under SC Faults

Figures 8.21, 8.22 and 8.23 represent the voltage dip and fault current of improved simplified DFIG types 1 and 2 when fault impedance has the lowest amplitude (10^{-15} ohm) with different values of R_{ex} under LL SC fault.

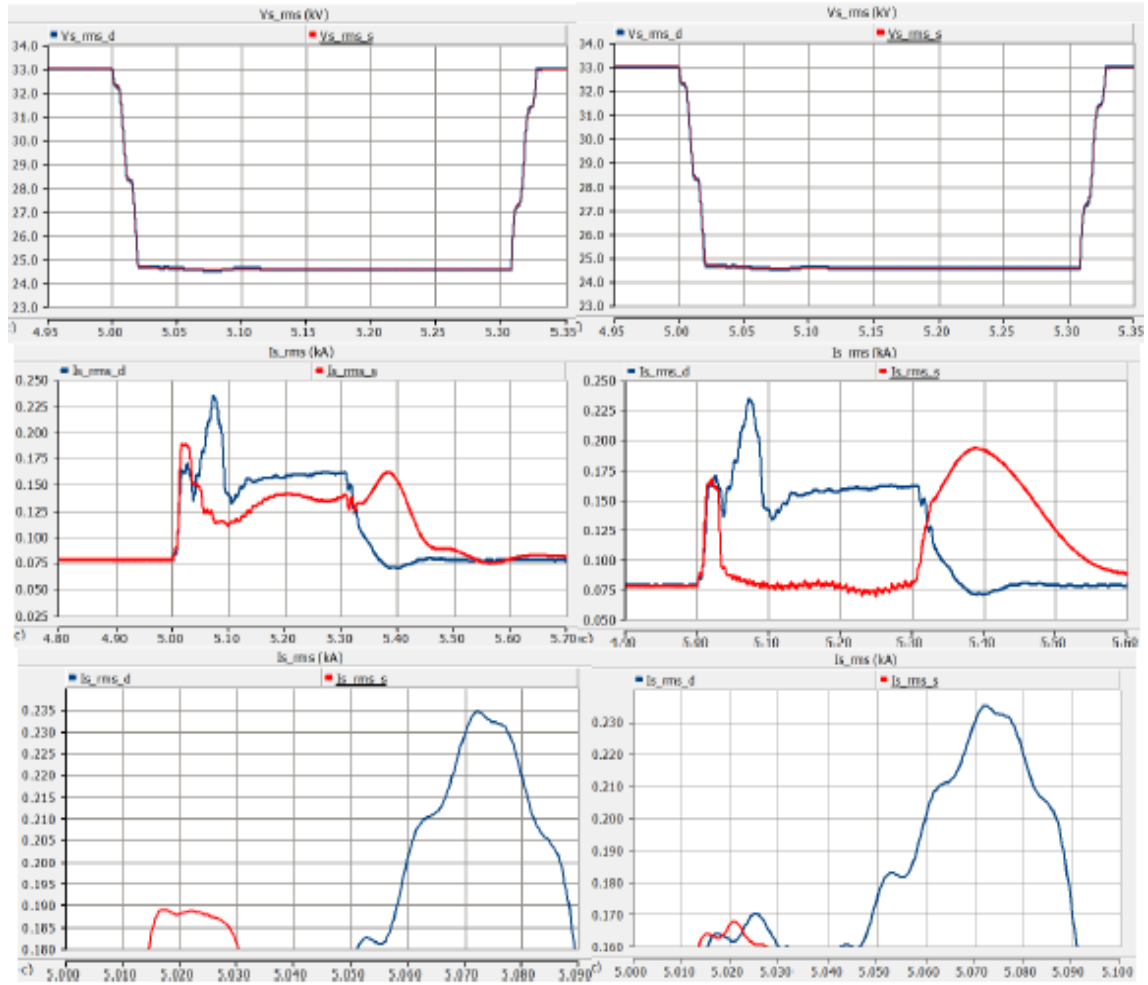


Figure 8.24: Improved type 1 & 2, Case 4 : $Z_f = 10^{-5} \Omega$ & $R_{ex} = 0.125 \Omega$.

8. Simulation of the Detailed and Improved Simplified Models of the DFIG WT,
Under SC Faults

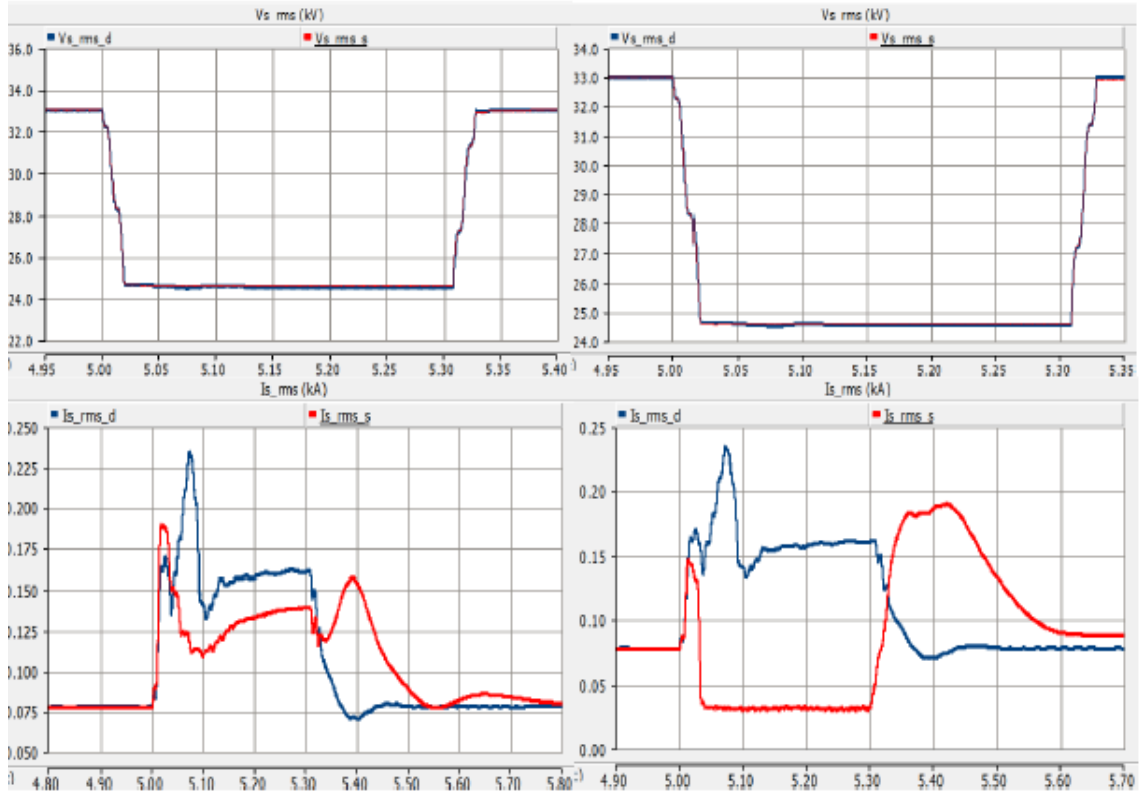


Figure 8.25: Improved type 1 & 2, Case 5 : $Z_f = 10^{-5} \Omega$ & $R_{ex} = 1.25 \Omega$.

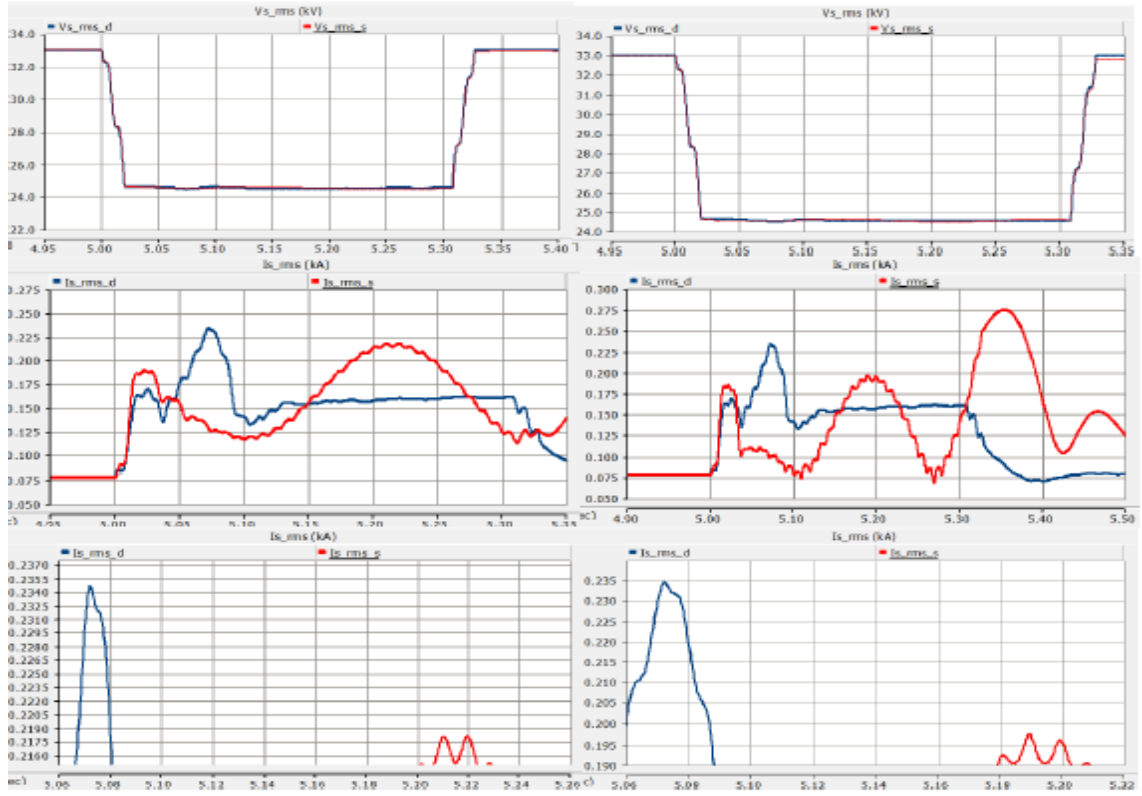


Figure 8.26: Improved type 1 & 2, Case 6 : $Z_f = 10^{-5} \Omega$ & $R_{ex} = 0.00125 \Omega$.

8. Simulation of the Detailed and Improved Simplified Models of the DFIG WT, Under SC Faults

Figures 8.24, 8.25 and 8.26 represent the voltage dip and fault current of improved simplified DFIG types 1 and 2 when fault impedance has the medium amplitude (10^{-5} ohm) with different values of R_{ex} under LL SC fault.

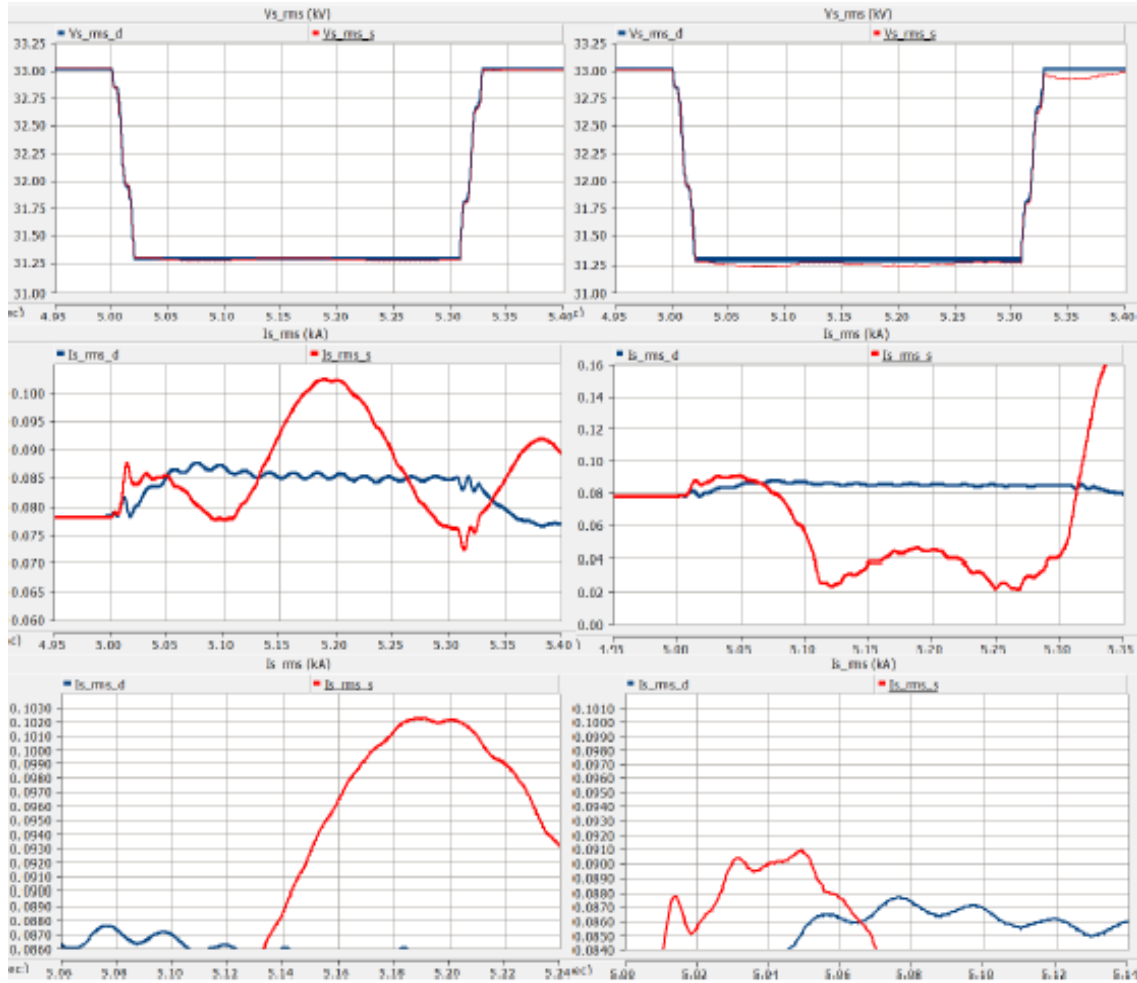


Figure 8.27: Improved type 1 & 2, Case 7 : $Z_f = 10^{-2} \Omega$ & $R_{ex} = 0.125 \Omega$.

8. Simulation of the Detailed and Improved Simplified Models of the DFIG WT,
Under SC Faults

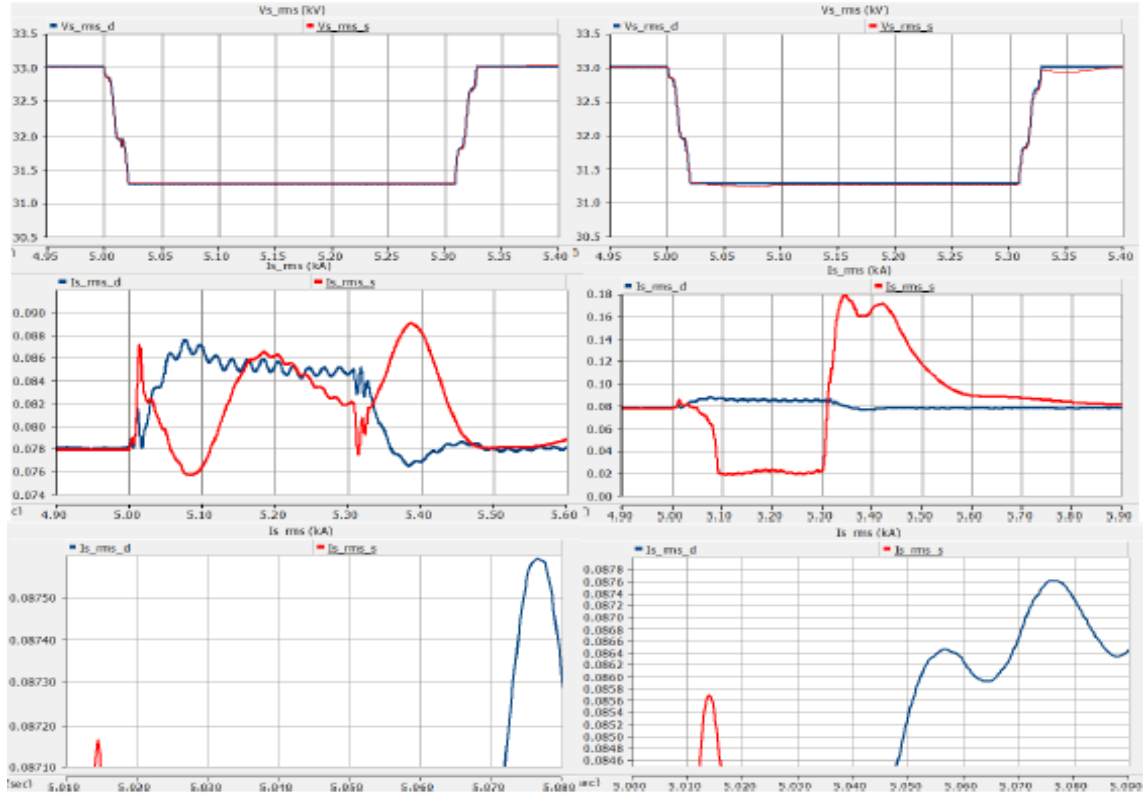


Figure 8.28: Improved type 1 & 2, Case 8 : $Z_f = 10^{-2} \Omega$ & $R_{ex} = 1.25 \Omega$.

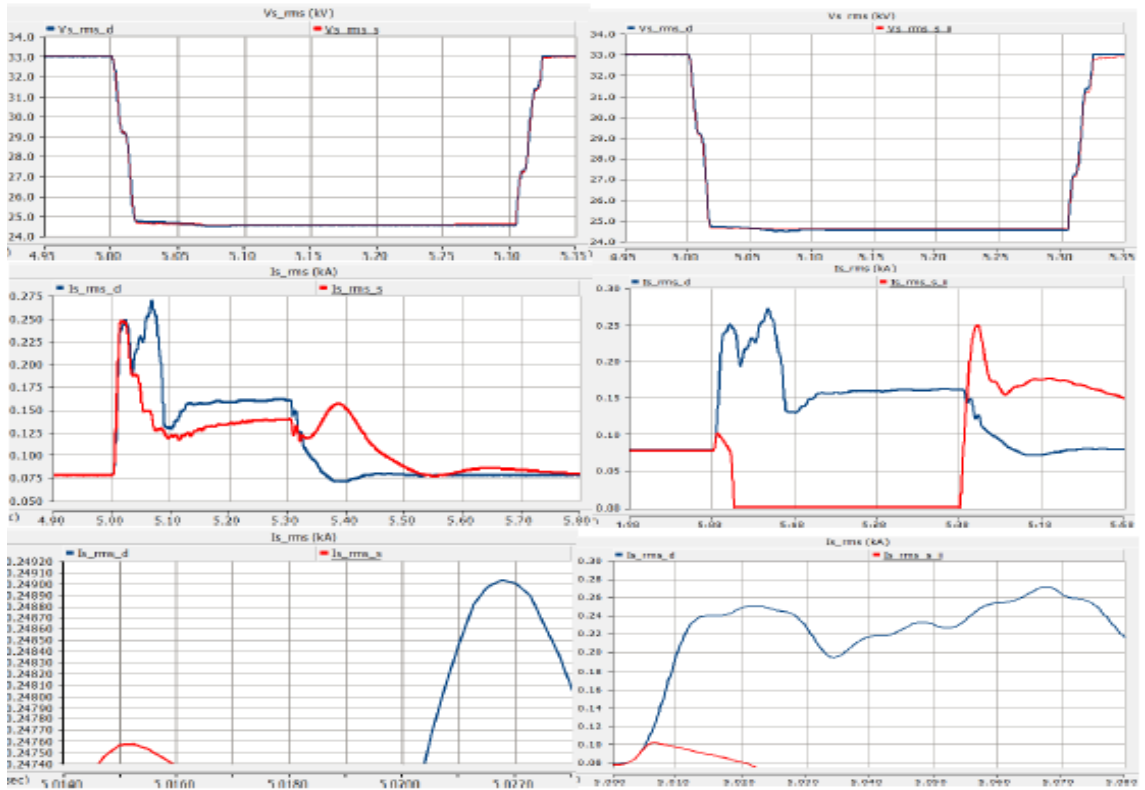


Figure 8.29: Improved type 1 & 2, Case 9 : $Z_f = 10^{-2} \Omega$ & $R_{ex} = 0.00125 \Omega$.

8. Simulation of the Detailed and Improved Simplified Models of the DFIG WT, Under SC Faults

Figures 8.27, 8.28 and 8.29 represent the voltage dip and fault current of improved simplified DFIG types 1 and 2 when fault impedance has the highest amplitude (10^{-2} ohm) with different values of R_{ex} under LL SC fault.

8.0.3.3 Under LLG SC Fault

The results of fault type 2, in the PSCAD/EMTDC software.

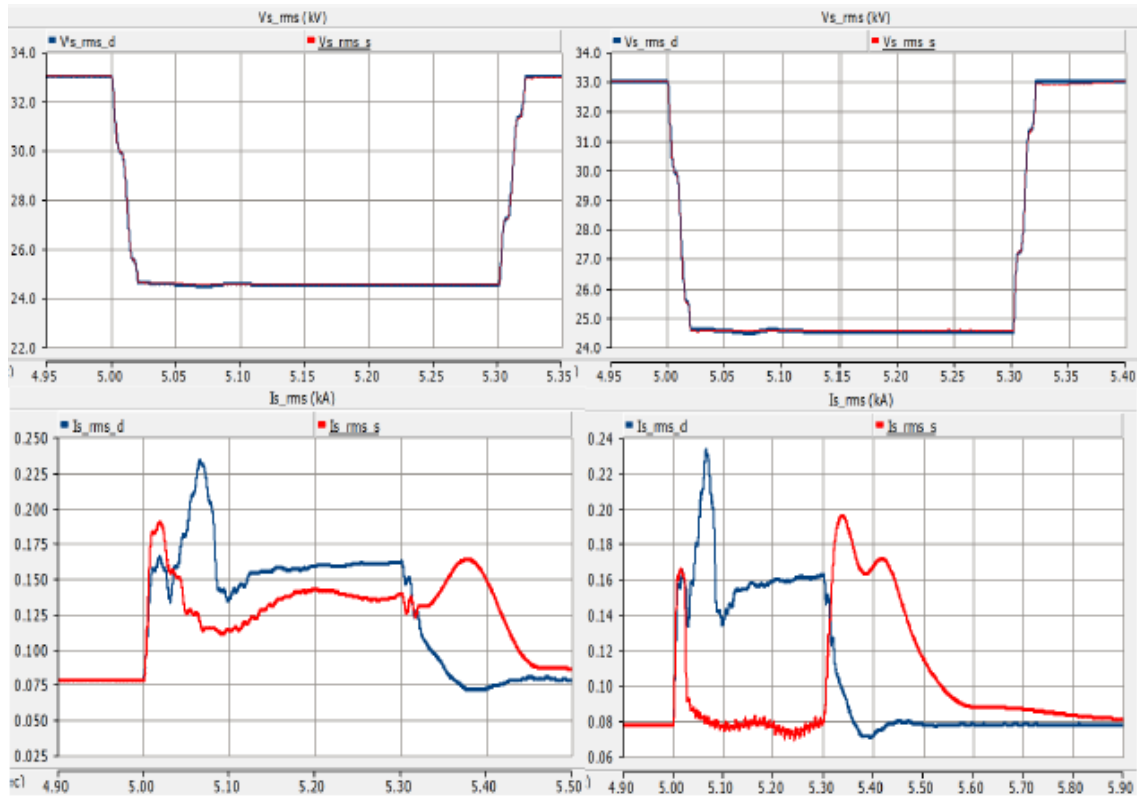


Figure 8.30: Improved type 1 & 2, Case 1 : $Z_f = 10^{-15} \Omega$ & $R_{ex} = 0.125 \Omega$.

8. Simulation of the Detailed and Improved Simplified Models of the DFIG WT,
Under SC Faults

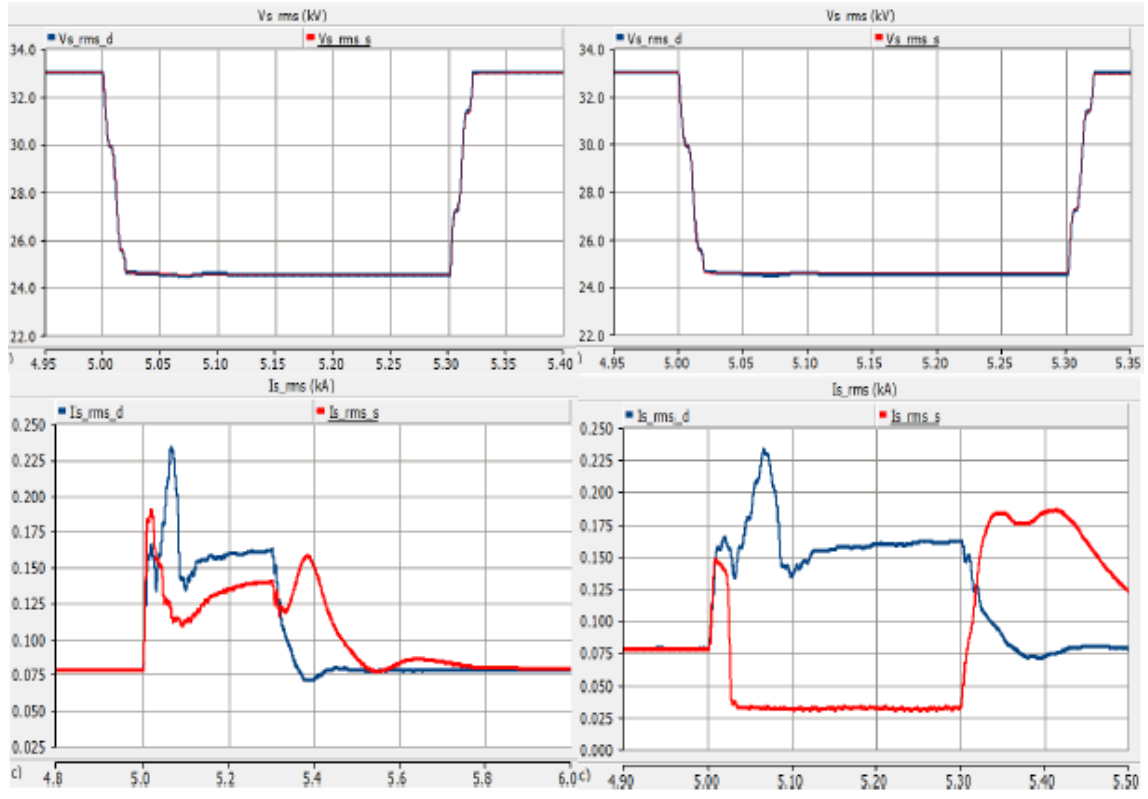


Figure 8.31: Improved type 2 & 2, Case 1 : $Z_f = 10^{-15} \Omega$ & $R_{ex} = 1.25 \Omega$.

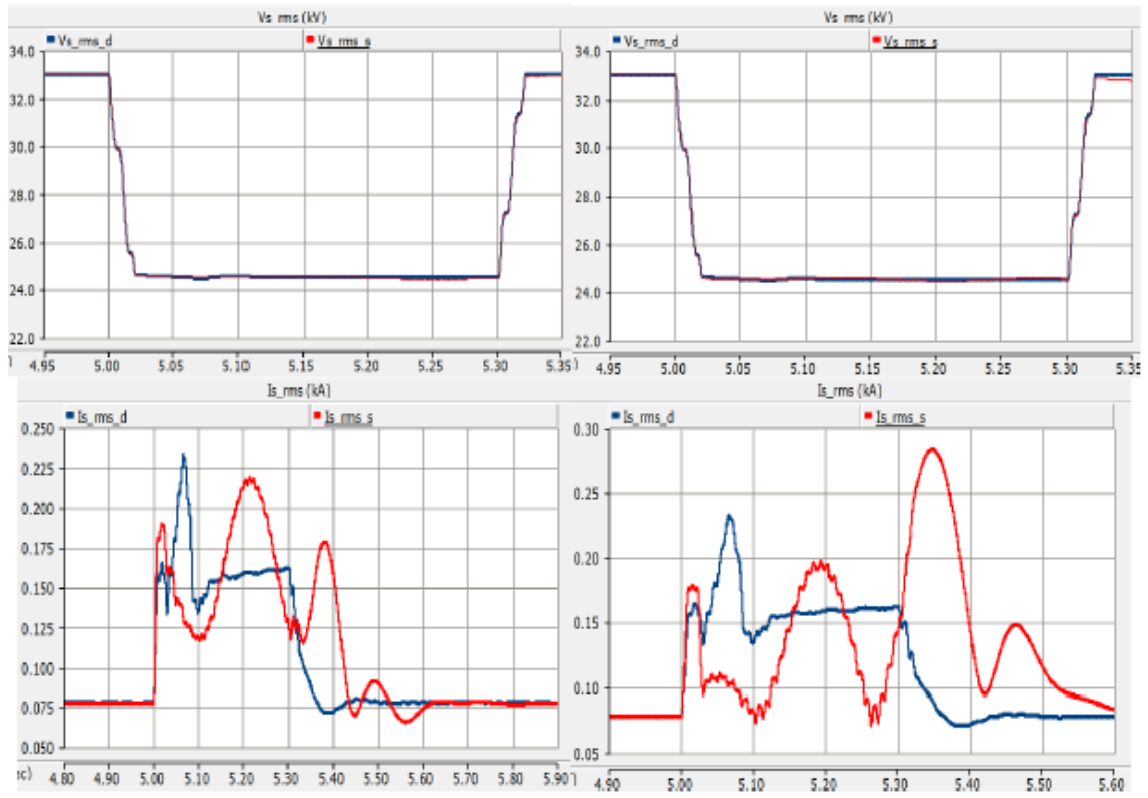


Figure 8.32: Improved type 1 & 2, Case 3 : $Z_f = 10^{-15} \Omega$ & $R_{ex} = 0.00125 \Omega$.

8. Simulation of the Detailed and Improved Simplified Models of the DFIG WT, Under SC Faults

Figures 8.30, 8.31 and 8.32 represent the voltage dip and fault current of improved simplified DFIG types 1 and 2 when fault impedance has the lowest amplitude (10^{-15} ohm) with different values of R_{ex} under LLG SC fault.

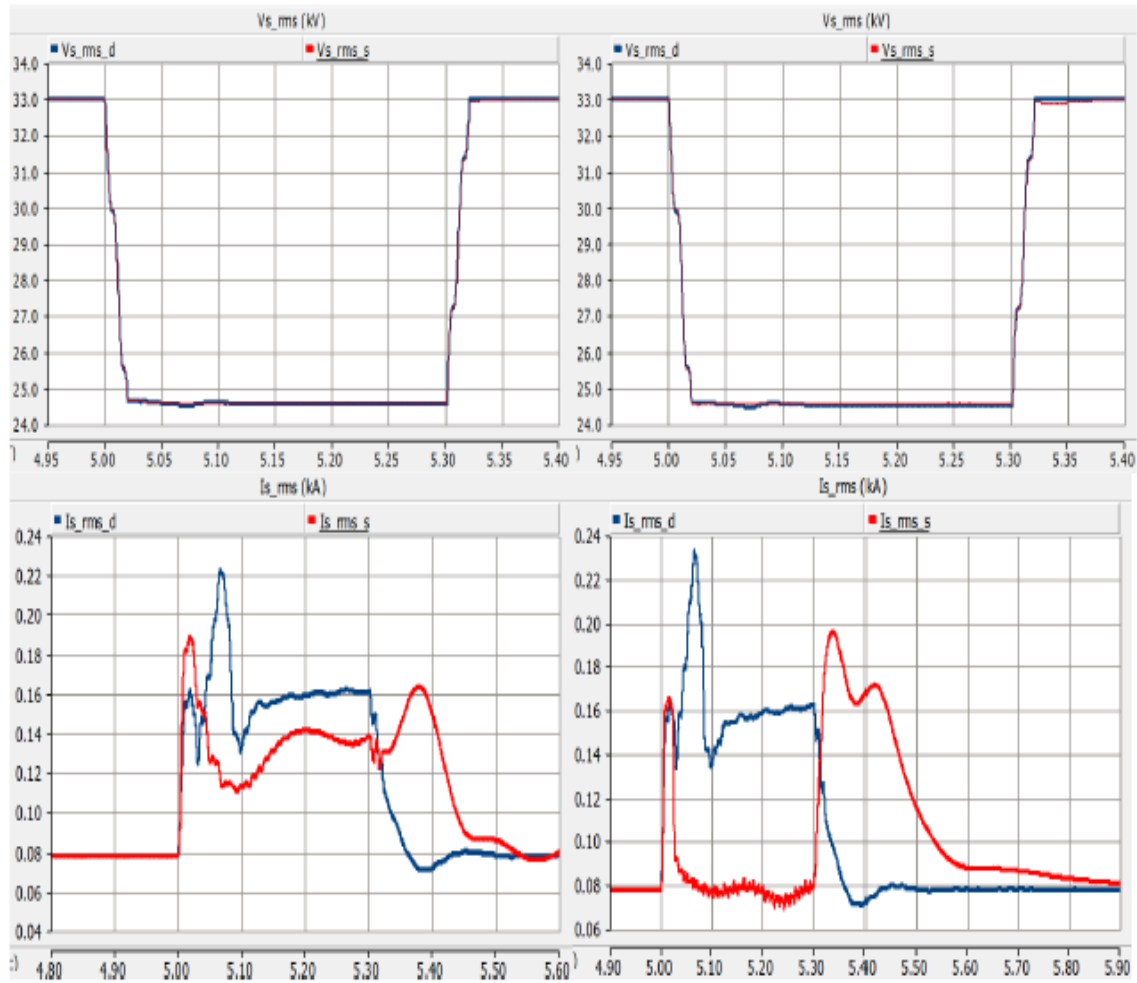


Figure 8.33: Improved type 1 & 2, Case 4 : $Z_f = 10^{-5} \Omega$ & $R_{ex} = 0.125 \Omega$.

8. Simulation of the Detailed and Improved Simplified Models of the DFIG WT,
Under SC Faults

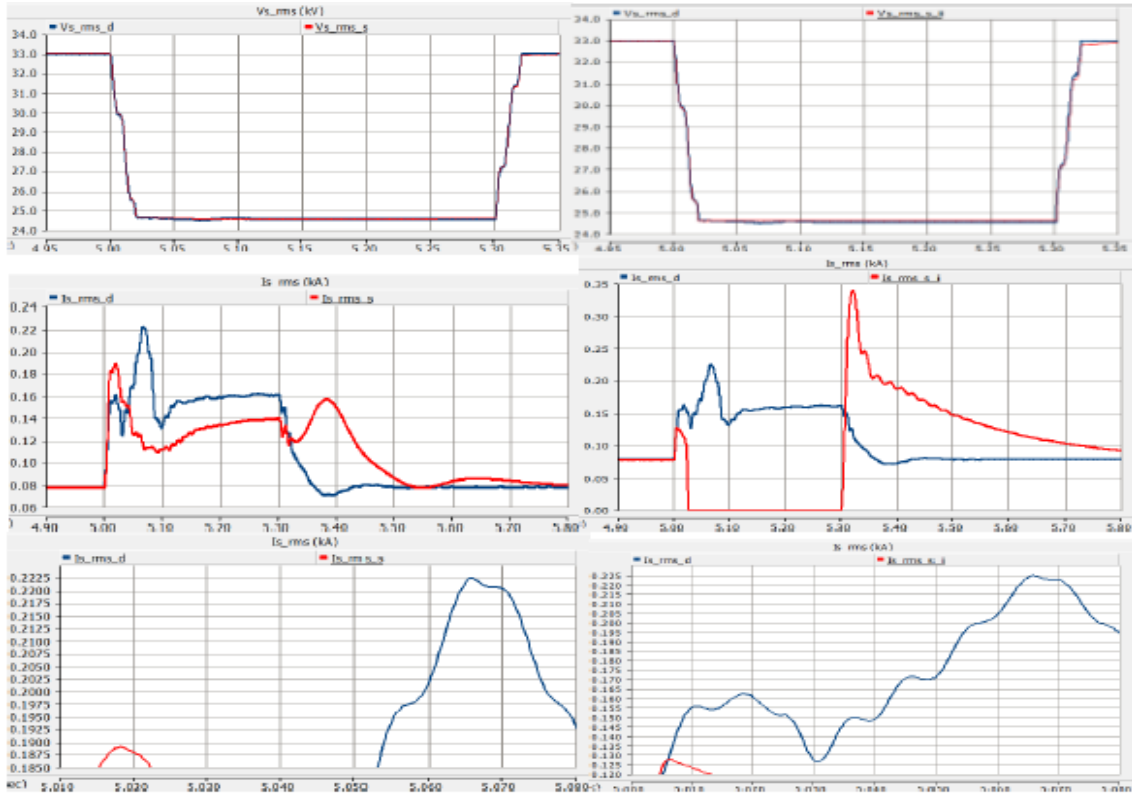


Figure 8.34: Improved type 1 & 2, Case 5 : $Z_f = 10^{-5} \Omega$ & $R_{ex} = 1.25 \Omega$.

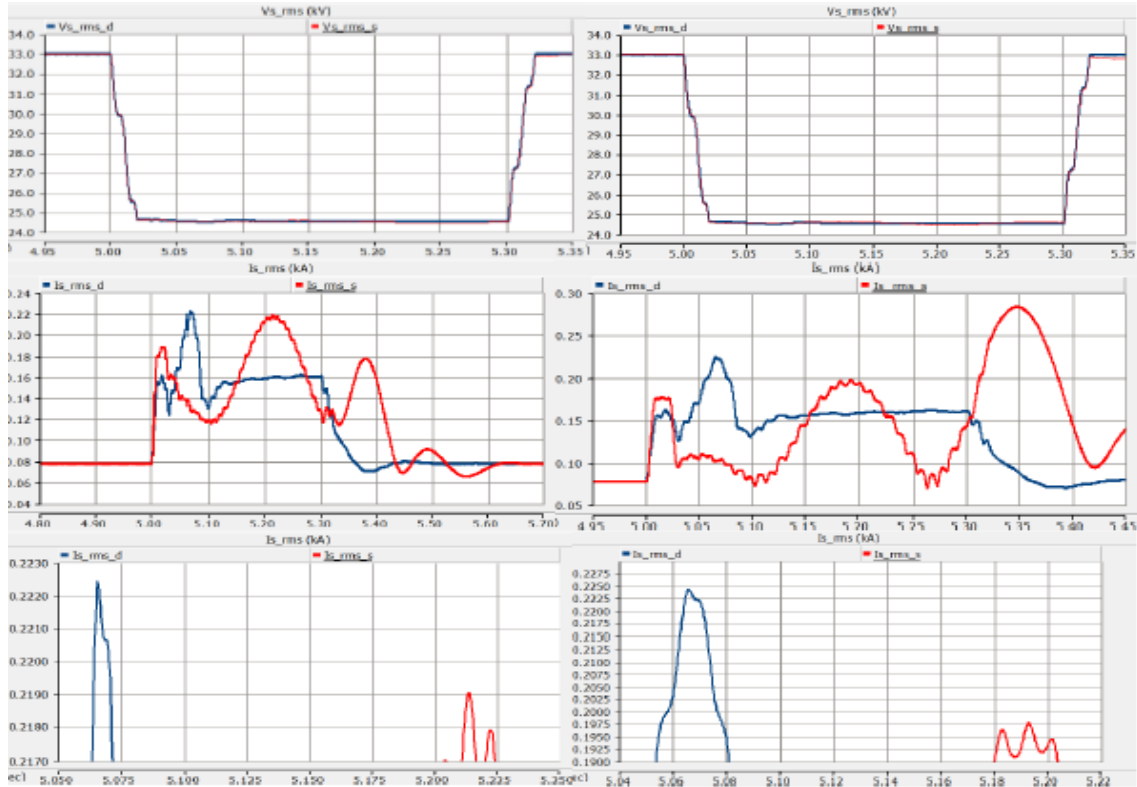


Figure 8.35: Improved type 1 & 2, Case 6 : $Z_f = 10^{-5} \Omega$ & $R_{ex} = 0.00125 \Omega$.

8. Simulation of the Detailed and Improved Simplified Models of the DFIG WT, Under SC Faults

Figures 8.33, 8.34 and 8.35 represent the voltage dip and fault current of improved simplified DFIG types 1 and 2 when fault impedance has the medium amplitude (10^{-5} ohm) with different values of R_{ex} under LLG SC fault.

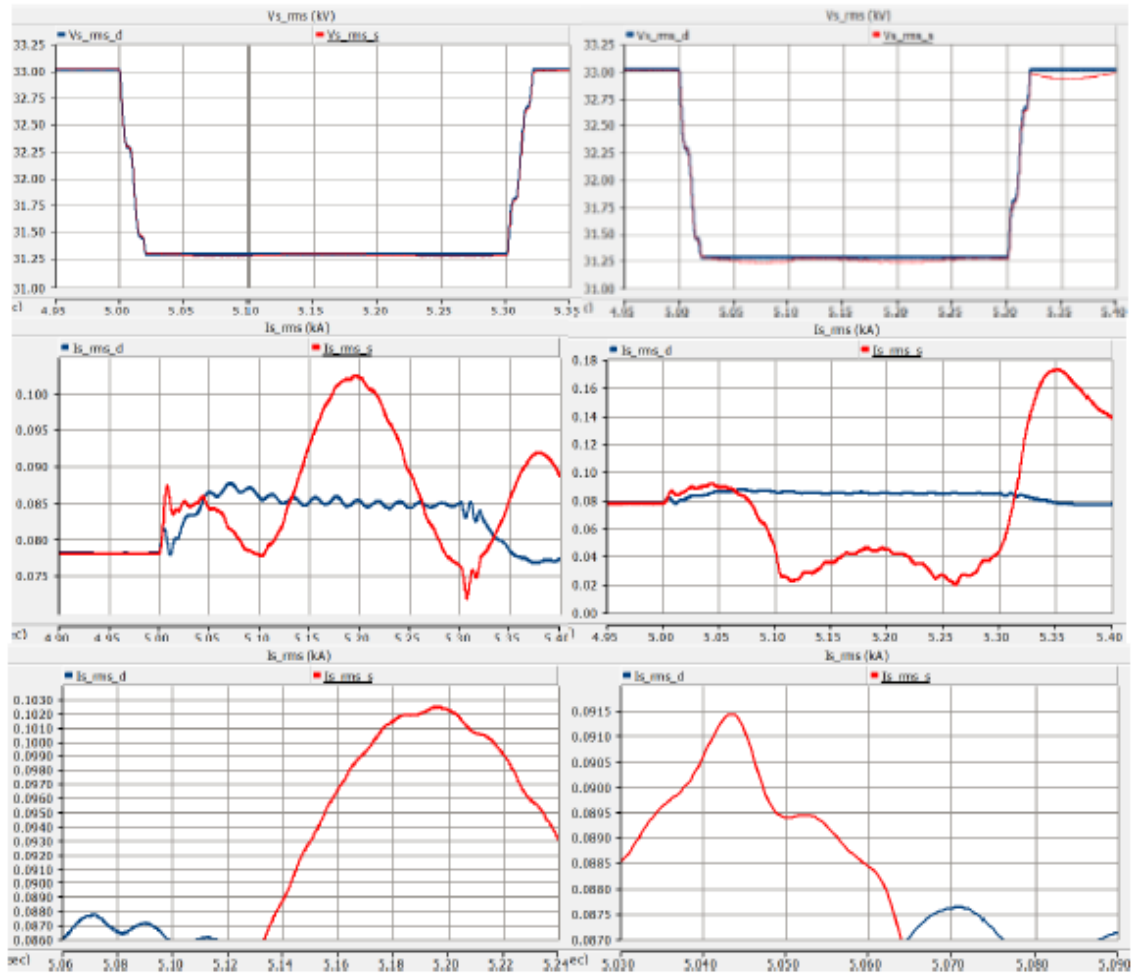


Figure 8.36: Improved type 1 & 2, Case 7 : $Z_f = 10^{-2} \Omega$ & $R_{ex} = 0.125 \Omega$.

8. Simulation of the Detailed and Improved Simplified Models of the DFIG WT,
Under SC Faults

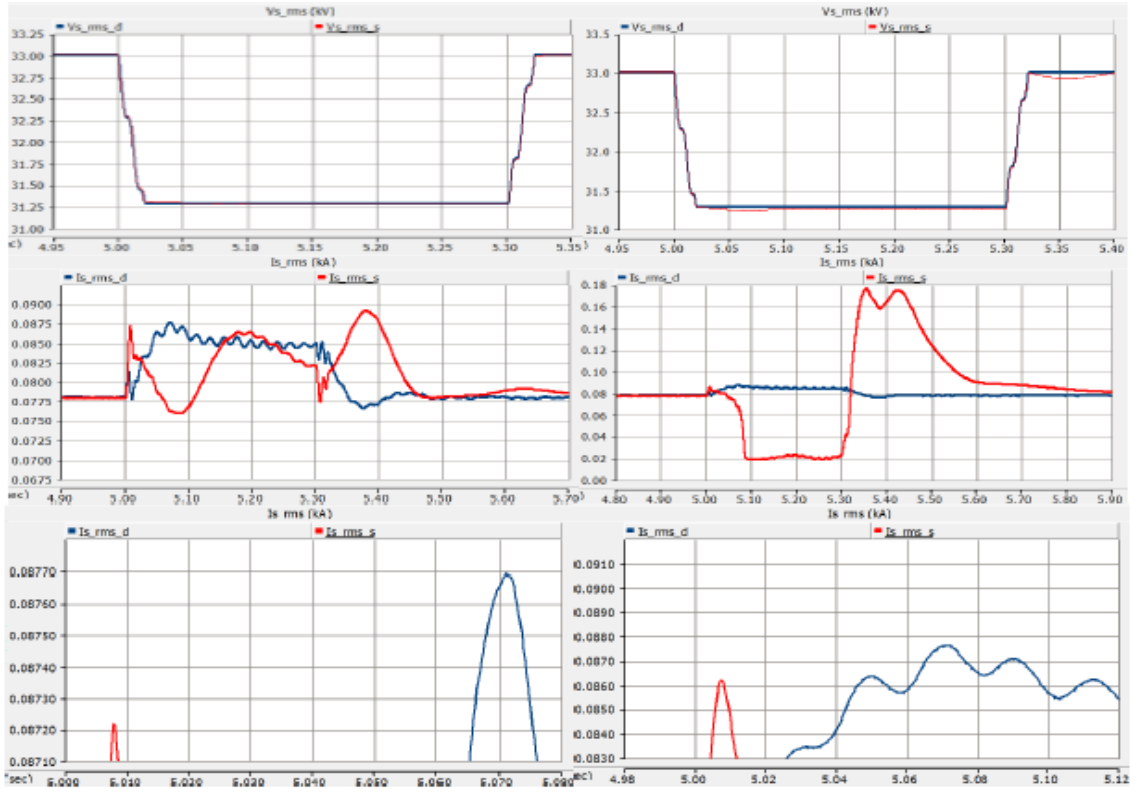


Figure 8.37: Improved type 1 & 2, Case 8 : $Z_f = 10^{-2} \Omega$ & $R_{ex} = 1.25 \Omega$.

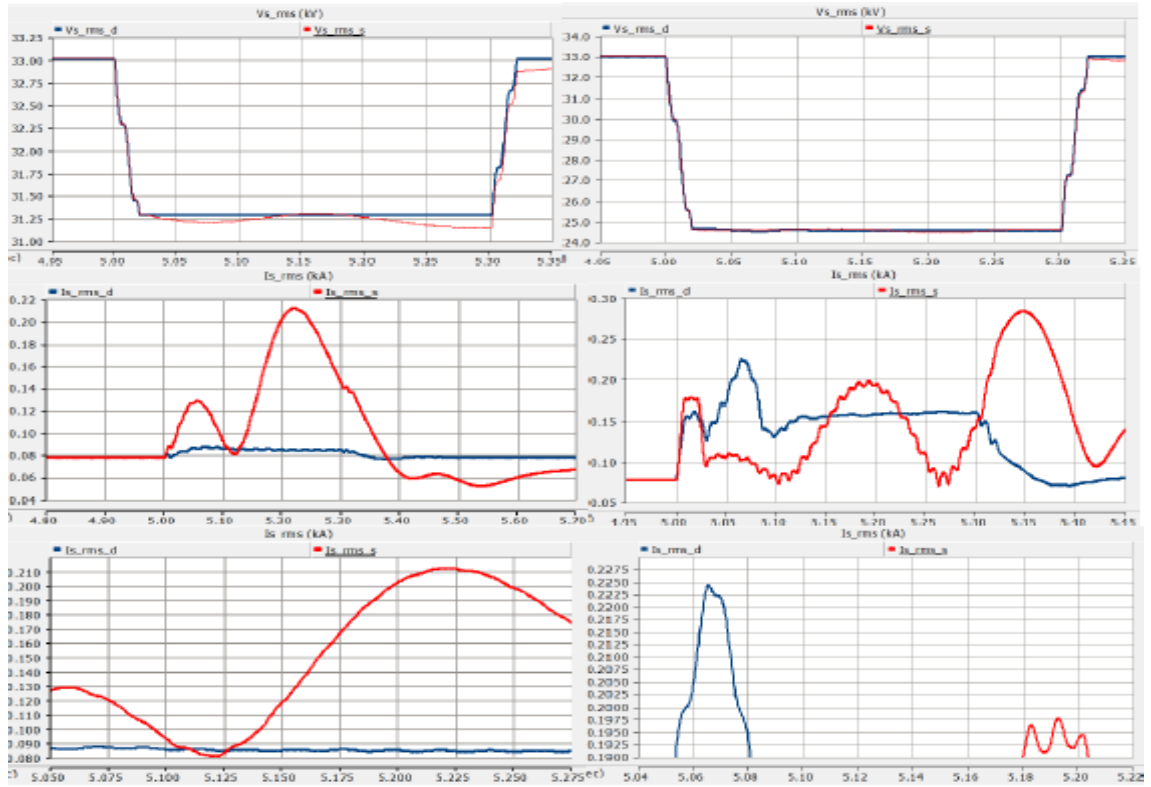


Figure 8.38: Improved type 1 & 2, Case 9 : $Z_f = 10^{-2} \Omega$ & $R_{ex} = 0.00125 \Omega$.

8. Simulation of the Detailed and Improved Simplified Models of the DFIG WT, Under SC Faults

Figures 8.36, 8.37 and 8.38 represent the voltage dip and fault current of improved simplified DFIG types 1 and 2 when fault impedance has the highest amplitude (10^{-2} ohm) with different values of R_{ex} under LLG SC fault.

9

Result

In this section, the results of the detailed, simplified, as well as the two types of improved simplified models will be compared with each other in order to find the best optimal one for each case.

The significant point that should be noticed is two different factors play the key role in terms of the maximum value the fault current. The initial one is the fault type and the second one is the amplitude of the fault impedance.

The maximum current of the fault current in each WTs models under different SC fault types will be compared with each others in this chapter.

9.1 Comparing Detailed and Simplified Models of DFIG WT

The maximum current of the fault currents in the detailed model under different SC fault types will be shown in Table 9.1 .

Table 9.1: Detailed Model of DFIG WT.

Detailed Type	Fault 1	Fault 2	Fault 3	Fault 4
$Z_f = 10^{-15} \Omega$	0.279 kA	0.234 kA	0.267 kA	0.3392 kA
$Z_f = 10^{-5} \Omega$	0.2525 kA	0.286 kA	0.2135 kA	0.339 kA
$Z_f = 10^{-2} \Omega$	0.09340 kA	0.08885 kA	0.0876 kA	0.1031 kA

The values of Table 9.1 should be used as the reference for the I_{fmax} and the other maximum fault currents for the simplified models should be compared with them.

Table 9.2: Simplified Model of DFIG WT.

Simplified Type	Fault 1	Fault 2	Fault 3	Fault 4
$Z_f = 10^{-15} \Omega$	0.249 kA	0.190 kA	0.191 kA	0.3455kA
$Z_f = 10^{-5} \Omega$	0.2478 kA	0.190 kA	0.189 kA	0.339 kA
$Z_f = 10^{-2} \Omega$	0.09455 kA	0.0877 kA	0.0871 kA	0.1044 kA

9.2 Improved Simplified Type 1 with Different Values of R_{ex}

The maximum of the fault currents in improved simplified type 1 with different extra resistance, on the rotor side, under different SC fault types can be noticed in Tables 9.3, 9.4 and 9.5 .

Table 9.3: Improved Simplified Type 1 with $R_{ex} = 0.125 \Omega$.

Simplified Type 1	Fault 1	Fault 2	Fault 3	Fault 4
$Z_f = 10^{-15} \Omega$	0.248 kA	0.190 kA	0.190 kA	0.3400 kA
$Z_f = 10^{-5} \Omega$	0.247 kA	0.189 kA	0.189 kA	0.3400 kA
$Z_f = 10^{-2} \Omega$	0.1065 kA	0.1025 kA	0.1032 kA	0.1118 kA

Table 9.4: Improved Simplified Type 1 with $R_{ex} = 1.25 \Omega$.

Simplified Type 1	Fault 1	Fault 2	Fault 3	Fault 4
$Z_f = 10^{-15} \Omega$	0.249 kA	0.190 kA	0.191 kA	0.3405 kA
$Z_f = 10^{-5} \Omega$	0.2459 kA	0.1878 kA	0.190 kA	0.3391 kA
$Z_f = 10^{-2} \Omega$	0.0946 kA	0.08722 kA	0.08718 kA	0.105 kA

Table 9.5: Improved Simplified Type 1 with $R_{ex} = 0.00125 \Omega$.

Simplified Type 1	Fault 1	Fault 2	Fault 3	Fault 4
$Z_f = 10^{-15} \Omega$	0.245 kA	0.190 kA	0.180 kA	0.3350 kA
$Z_f = 10^{-5} \Omega$	0.245 kA	0.2190 kA	0.2184 kA	0.3337 kA
$Z_f = 10^{-2} \Omega$	0.215 kA	0.202 kA	0.212 kA	0.208 kA

9.3 Improved Simplified Type 2 with Different Values of R_{ex}

The maximum of the fault currents in improved simplified type 2 with different extra resistance, on the rotor side, under different SC fault types can be noticed in Tables 9.6, 9.7 and 9.8 .

Table 9.6: Improved Simplified Type 2 with $R_{ex} = 0.125 \Omega$.

Simplified Type 2	Fault 1	Fault 2	Fault 3	Fault 4
$Z_f = 10^{-15} \Omega$	0.219 kA	0.197 kA	0.170 kA	0.284 kA
$Z_f = 10^{-5} \Omega$	0.219 kA	0.190 kA	0.168 kA	0.285 kA
$Z_f = 10^{-2} \Omega$	0.0961 kA	0.0914 kA	0.0910 kA	0.1030 kA

Table 9.7: Improved Simplified Type 2 with $R_{ex} = 1.25 \Omega$.

Simplified Type 2	Fault 1	Fault 2	Fault 3	Fault 4
$Z_f = 10^{-15} \Omega$	0.190 kA	0.150 kA	0.150 kA	0.245 kA
$Z_f = 10^{-5} \Omega$	0.105 kA	0.127 kA	0.150 kA	0.241 kA
$Z_f = 10^{-2} \Omega$	0.0922 kA	0.0862 kA	0.0857 kA	0.0990 kA

Table 9.8: Improved Simplified Type 2 with $R_{ex} = 0.00125 \Omega$.

Simplified Type 2	Fault 1	Fault 2	Fault 3	Fault 4
$Z_f = 10^{-15} \Omega$	0.230 kA	0.1975 kA	0.175 kA	0.323 kA
$Z_f = 10^{-5} \Omega$	0.2385 kA	0.1975 kA	0.197 kA	0.3217 kA
$Z_f = 10^{-2} \Omega$	0.208 kA	0.1975 kA	0.0774 kA	0.210 kA

9.4 Ultimate Results

As mentioned above, the values of the Table 9.1 should be considered as the reference values and the other tables should be compared with it.

By categorizing the data based on the values of the fault impedance, the below results, which have the closest amplitude of the I_{fmax} to the detailed one during the fault period, will be achieved.

9.4.1 Case 1 : for low value impedance, like $Z_f = 10^{-15} \Omega$

For fault 1, the simplified one and the improved Simplified Type 1 with $R_{ex} = 1.25 \Omega$ ($I_{fmax} = 0.249$ kA) have the best results. For fault 2, the improved simplified type 2 with $R_{ex} = 0.00125 \Omega$ ($I_{fmax} = 0.1975$ kA), has the best ideal behavior. For fault 3, the simplified and improved simplified type 1 with $R_{ex} = 1.25 \Omega$ ($I_{fmax} = 0.191$ kA), have the best behaviors. Finally, for fault 4, the simplified model ($I_{fmax} = 0.3455$ kA) has the best behavior.

9.4.2 Case 2 : for medium value impedance, like $Z_f = 10^{-5} \Omega$

For fault 1, the improved simplified type 1 with $R_{ex} = 1.25 \Omega$ ($I_{fmax} = 0.2495$ kA) has the best ideal behavior. For fault 2 and 3 the improved simplified type 1 with $R_{ex} = 0.00125 \Omega$ ($I_{fmax} = 0.202$ and 0.212 kA, respectively) has the best results. Consequently, the improved simplified type 1 with $R_{ex} = 1.25 \Omega$ and the improved simplified type 2 with $R_{ex} = 0.00125 \Omega$ have the closest results to the detailed values, too. Finally, the improved simplified type 1 with $R_{ex} = 1.25 \Omega$ ($I_{fmax} = 0.210$ kA).

9.4.3 Case 2 : for high value impedance, like $Z_f = 10^{-2} \Omega$

For faults 1, 2, 3 and 4, the improved simplified type 1 with $R_{ex} = 0.125 \Omega$ ($I_{fmax} = 0.1065, 0.1025$ kA, 0.1032 kA and 0.1118 kA, respectively) has the best ideal results.

9.5 Summary of the Results

Ultimately, by comparing the whole results of different types of the simplified DFIG WTs the simplified type has the closest behaviors to the detailed one. The values of the tables 9.1 and 9.2 can prove this claim.

10

Conclusion

The main aim of this project was finding the simplest way of controlling the IG in DFIG WT via the feature of IM which is using passive elements, the external variable resistance. Also, using the capacitor bank in rotor side in order to improve the PF in stator side. For reaching this goal, using the phasor diagram was helpful in order to calculate the amplitude of the capacitor bank, approximately. The significant feature of the simplified model is that its simulation is running much faster in comparison with the detailed model.

As a result, in terms of SC fault analysis in a radial or huge wind park, the simplified type can be used to time saving and reaching the final results.

Ultimately, the final result that will be achieved is that in order to choose the simplified type, for SC fault analysis, two factor play key roles. Initially, the fault type, like being type 1, 2, 3 or 4. Besides, the amplitude of the fault impedance, which can be high or low. So, by considering each of these factors together the optimal simplified type can be chosen.

Due to being the easiest model, the simplified one was the optimal one during the considered simplified models. It has the most close behaviors to the detailed model, which is the reference one, during different types of the faults.

11

Future Work

The investigation of the simplified WT model is a complex task. The focus of this thesis had been on DFIG WT type. Some methods like trying to simplify the DFIG WT based on its dynamic equations had been used previously. But, here the method of controlling directly the rotor side current has been used without controlling the stator current side. The possibility of using some power electronics components in terms of controlling the DFIG in a simpler manner could be used in the future as new methods. Also, these simplified models can be extended in a radial, like a wind park, to analyze its stability during transient.

Consequently, trying to use a varistor (variable resistance) instead of the resistor, which has a fixed-value, to be changed automatically based on the varying of wind speed can be considered as the next future step. Also, this aim demanded specific control methods to tune the varistor values with the wind at different speeds.

Bibliography

- [1] Wind in power 2017, Annual combined onshore and offshore wind energy statistics Published February 2018, EDITORS: Iván Pineda, WindEurope, Pierre Tardieu, WindEurope. Rue d'Arlon 80, 1040 Brussels, Belgium
- [2] Wind Power in Power Systems, Edited by Thomas Ackermann, Royal Institute of Technology Stockholm, Sweden
- [3] <https://www.google.com/url?sa=trct=jq=esrc=ssource=webcd=8cad=rjauact=8ved=2ahUKEwiRlKf-MjcAhXKZpoKHe7XCAAQFjAHegQICRACurl=http>
- [4] <https://www.google.com/url?sa=trct=jq=esrc=ssource=webcd=16cad=rjauact=8ved=2ahUKEwjK5bLv-8jcAhWLiaYKHRl6BII4ChAWMAV6BAgGEAIurl=https>
- [5] <http://easywindenergy.blogspot.com/2013/02/variable-speed-versus-fixed-speed.html>
- [6] Yassine Amirat, Mohamed Benbouzid, Bachir Bensaker, René Wamkeue, Hervé Mangel. The State of the Art of Generators for Wind Energy Conversion Systems. ICEM'06, Sep 2006, Chania, Greece.6pp, 2006. <hal-00527554>
- [7] DFIG versus PMSG for marine current turbine applications S. Benelghali 1*, M. Benbouzid 2† and J.F. Charpentier 3 1 University of Aix-Marseille 3, UMR CNRS 6168 LSIS, 13397 Marseille, France 2 University of Brest, EA 4325 LBMS, 29238 Brest, France 3 French Naval Academy, EA 3634 IRENav, 29240 Brest, France (reçu le 16 Septembre 2011 – accepté le 27 Mars 2012)
- [8] Principles of Electrical Machines and Power Electronics P.C.Sen, 2nd edition, 1997.
- [9] <http://www.vias.org/kimberlyee/img/ee>
- [10] <https://circuitglobe.com/wp-content/uploads/2016/02/Induction-Generator-fig-1.jpg>
- [11] Control of Power Electronic Converters and Variable Speed Drives, Lennart Harnefors, Compendium at Chalmers University of Technology.
- [12] Subsynchronous Resonance in Doubly-Fed Induction Generator Based Wind Farms, Selam Chernet. PhD Thesis, Chalmers University of Technology 2018.
- [13] Comparison of Alternative Equivalent Circuits of Induction Motor with Real Machine Data J. Bradna, J. Bauer, S. Fligl and V. Hlinovsky. 2012.
- [14] LISERRE M., CARDENAS R., MOLINAS M., RODRIGUEZ J., Overview of multi-MW wind turbines and wind parks, IEEE Trans. Ind. Electron., 2011, 58(4), 1081–1095.
- [15] MÜLLER S., DEICKE M., DE DONCKER R., Doubly fed induction generator systems for wind turbines, Ind. Appl. Mag. IEEE, 2002, 8(3), 26–33.

- [16] PANNELL G, ATKINSON D.J.ZAHAWI B., Minimum-threshold crowbar for a fault-ride-through grid-code compliant dfig wind turbine, IEEE Trans. En. Conv., 2010, 25(3), 750–759.
- [17] GENG H., LIU C., YANG G., LVRT capability of DFIG-based WECS under asymmetrical grid fault condition, IEEE Trans. Ind. Electron., 2013, 60(6), 2495–2509.
- [18] D.W. Novotny and T.A. Lipo, Vector Control and Dynamics of AC Drive, 1.edn. Oxford, Oxford University Press, 1996.
- [19] Power System Analysis by Hadi Saadat, Chapter 9. Third Edition
- [20] Grainger, John J. (2003). Power System Analysis. Tata McGraw-Hill. p. 380. ISBN 978-0-07-058515-7.
- [21] <http://nptel.ac.in/courses/108107028/module4/lecture6/lecture6.pdf>
- [22] <https://www.elprocus.com/what-are-the-different-types-of-faults-in-electrical-power-systems/>

A

Appendix

A.1 The Per Unit System

Usually, in power system analysis will be easier to use per unit system (pu) in order to normalize the system variables. The per unit system has significant advantages and simplicity in terms of computational process, in comparison with physical units like volts, ampere, ohm, etc., by removing units and expressing system quantities as dimensionless ratio. Besides, minimizing the computational efforts, actually, the variable quantities such as voltage, current, etc., will be confined to the range between 0 to 1 pu, as long as simplifying the evaluation like eliminating the $\sqrt{3}$ or 3 coefficients in the equations.

It can be defined as:

$$\text{the quantity in pu unit} = \frac{\text{actual quantity}}{\text{the base value of the quantity}} \quad (\text{A.1})$$

The main part of the per unit system calculation is the base value of the quantity. Normally, the base values, like S_{base} , V_{base} and ω_{base} will be chosen and the other principle variables can be calculated easily.

$$I_{base} = \frac{S_{base}}{V_{base}} \quad (\text{A.2})$$

$$Z_{base} = \frac{(V_{base})^2}{S_{base}} \quad (\text{A.3})$$

$$\phi_{base} = \frac{V_{base}}{\omega_{base}} \quad (\text{A.4})$$

$$V^{pu} = \frac{V_{actual}}{V_{base}} \quad (\text{A.5})$$

$$I^{pu} = \frac{I_{actual}}{I_{base}} \quad (\text{A.6})$$

$$\omega^{pu} = \frac{\omega_{actual}}{\omega_{base}} \quad (\text{A.7})$$

$$Z^{pu} = \frac{Z_{actual}}{Z_{base}} \quad (\text{A.8})$$

$$R^{pu} = \frac{R_{actual}}{Z_{base}} \quad (\text{A.9})$$

$$L^{pu} = \frac{X_{actual}}{Z_{base}} = \frac{\omega_{base} \times L_{actual}}{Z_{base}} \quad (\text{A.10})$$

$$t^{pu} = \omega_{base} \times t_{actual} \quad (\text{A.11})$$

B

Appendix

B.1 Transformations for three-phase Systems

B.1.1 Introduction

In this appendix, the necessary transformations from three-phase quantities into vectors in stationary $\alpha\beta$ and rotating dq reference frames and vice versa will be described.

B.1.2 Transformation of three-phase quantities to vectors

A three-phase system constituted by three quantities $V_a(t)$, $V_b(t)$ and $V_c(t)$ can be transformed into a vector $V^{\alpha\beta}(t)$ in a stationary complex reference frame, usually called $\alpha\beta$ -frame, by applying the following transformation:

$$\underline{V}^{\alpha\beta}(t) = V^\alpha(t) + jV^\beta(t) = K_{tran}(V_a(t) + V_b(t)e^{j\frac{2\pi}{3}} + V_c(t)e^{j\frac{4\pi}{3}}) \quad (\text{B.1})$$

The transformation constant K_{tran} can be chosen to be $\sqrt{2/3}$ or $2/3$ to ensure power invariant or amplitude invariant transformation between two systems, respectively. So, the above equation can be expressed in matrix form as:

$$\begin{bmatrix} V^\alpha(t) \\ V^\beta(t) \end{bmatrix} = T_{32} \begin{bmatrix} V_a(t) \\ V_b(t) \\ V_c(t) \end{bmatrix} \quad (\text{B.2})$$

where the matrix T_{32} is given by:

$$T_{32} = K_{tran} \begin{bmatrix} 1 & -1/2 & -1/2 \\ 0 & \sqrt{3}/2 & -\sqrt{3}/2 \end{bmatrix} \quad (\text{B.3})$$

The inverse transformation, assuming no zero-sequence, i.e.

$$V_a(t) + V_b(t) + V_c(t) = 0 \quad (\text{B.4})$$

, is given by the relation:

$$\begin{bmatrix} V_a(t) \\ V_b(t) \\ V_c(t) \end{bmatrix} = T_{32} \begin{bmatrix} V^\alpha(t) \\ V^\beta(t) \end{bmatrix} \quad (\text{B.5})$$

where the matrix T_{23} is given by:

$$T_{32} = \frac{1}{K_{tran}} \begin{bmatrix} 2/3 & 0 \\ -1/3 & 1/\sqrt{3} \\ -1/3 & -1/\sqrt{3} \end{bmatrix} \quad (\text{B.6})$$

B.1.2.1 Transformation between fixed and rotating coordinate systems

For the vector $\underline{V}^{(\alpha\beta)}(t)$ rotating in the $\alpha\beta$ -frame with the angular frequency $\omega(t)$ in the positive (counter-clockwise direction), a dq -frame that rotates in the same direction with the same angular frequency $\omega(t)$ can be defined. The vector $\underline{V}^{(\alpha\beta)}(t)$ will appear as fixed vectors in this rotating reference frame. A projection of the vector $\underline{V}^{(\alpha\beta)}(t)$ on the d -axis and q -axis of the dq -frame gives the components of the vector on the dq -frame as illustrated in the Figure B.1.

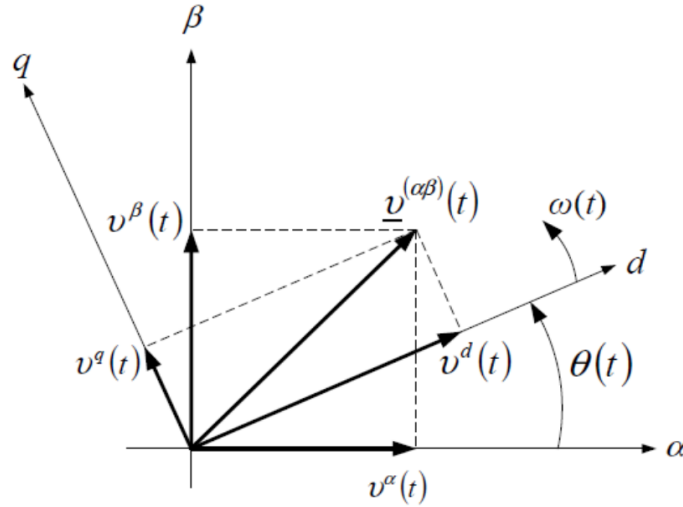


Figure B.1: $\alpha\beta$ and dq vectors frame.

The transformation can be written in vector form as follows:

$$\underline{V}^{(dq)}(t) = V^d + jV^q = \underline{V}^{(\alpha\beta)}(t) + e^{-j\theta(t)} \quad (\text{B.7})$$

with the angle $\theta(t)$ in Figure B.1 given by:

$$\theta(t) = \theta_0 + \int_0^t \omega(\tau) d\tau \quad (\text{B.8})$$

The inverse transformation, from the rotating dq -frame to the fixed $\alpha\beta$ -frame, is provided as:

$$\underline{V}^{(\alpha\beta)}(t) = \underline{V}^{(dq)}(t) e^{j\theta(t)} \quad (\text{B.9})$$

In the matrix form, the transformation between the fixed $\alpha\beta$ -frame and the rotating dq -frame can be written as:

$$\begin{bmatrix} V^d(t) \\ V^q(t) \end{bmatrix} = R(-\theta(t)) \begin{bmatrix} V^\alpha(t) \\ V^\beta(t) \end{bmatrix} \quad (\text{B.10})$$

$$\begin{bmatrix} V^\alpha(t) \\ V^\beta(t) \end{bmatrix} = R(\theta(t)) \begin{bmatrix} V^d(t) \\ V^q(t) \end{bmatrix} \quad (\text{B.11})$$

where the projection matrix is:

$$R(\theta) = \begin{bmatrix} \cos(\theta(t)) & -\sin(\theta(t)) \\ \sin(\theta(t)) & \cos(\theta(t)) \end{bmatrix} \quad (\text{B.12})$$

C

Appendix

C.1 MATLAB Files

C.1.1 m-file

```
1- clc; clear all; close all
2- % the IG parameters
3-
4- S_base = 0.9e6 ; % Nominal power (VA)
5- V_base = 0.69e3 ; % voltage (line-line) (V)
6- fs = 60 ; % frequency (Hz)
7-
8- a = 0.391 ; % stator/rotor turn ratio (N1/N2)
9-
10- J = 6 ; % Angular moment of Inertia (kg.m^2)
11- H = J/2 ; % inertia constant (s)
12- D = 0.0001 ; % mechanical damping (pu)
13- p = 2 ; % pole pairs
14-
15- T_base = S_base/(2*pi*fs/p); % the based torque (N.m)
16-
17- ws = 2*pi*fs ; % synchronous speed (rad/s)
18- Ns = (60*fs)/p ; % synchronous speed (rpm)
19-
20- P_friction = D*(S_base) ; % power of riction factor (W)
21- F = P_friction / (ws) ; % friction factor (N.m.s)
22-
23- Z_base = (V_base)^2/S_base ; % the base impedance (ohm)
24-
25- Lm_pu = 4.5 ; % mutual inductance (pu)
26- Lm_actual =(Lm_pu * Z_base)/ws ; % mutual inductance (H)
27-
28- Rs_pu = 0.0054 ; % stator resistance (pu)
29- Rs_actual = Rs_pu * Z_base ; % stator resistance (ohm)
30- Lls_pu = 0.10 ; % stator leakage inductance (pu)
31- Lls_actual = (Lls_pu * Z_base)/ws ; % stator leakage inductance (H)
32-
33- Rrr_pu = 0.00607 ; % rotor resistance (pu)
34- Rrr_actual = Rrr_pu * Z_base ; % rotor resistance (ohm)
35- Llrr_pu = 0.11 ; % rotor leakage inductance (pu)
36- Llrr_actual = (Llrr_pu * Z_base)/ws ; % rotor leakage inductance (H)
37-
38- Pm = 0 ; % mechanical power (W)
39- Tm = -T_base*0.87; % mechanical input torque (N.m)
```

Figure C.1

